POLITECNICO DI TORINO

College of Chemical and Material Engineering

Master Degree
in Chemical and Sustainable Process Engineering

Master Thesis

Oscillating behaviour of N_2O decomposition over copper-ZSM5 zeolites

Supervisor:

Prof. Samir Bensaid

Co-supervisors:

Prof. Raffaele Pirone

Prof. Marco Piumetti

Candidate:

Maha Maimi

March 2023

Summary in Italian:

Introduzione:

Il protossido di azoto (N_2O), conosciuto anche come gas esilarante, è un gas incolore e non tossico. Fin dalla sua scoperta, avvenuta più di 200 anni fa, è stato ampiamente utilizzato come additivo per carburanti nell'industria automobilistica e come agente di miscelazione e schiumogeno (E942) nell'industria alimentare. N_2O appartiene alla famiglia degli NO_x (ossidi di azoto), specie chimiche altamente inquinanti che originano dai processi di combustione ad alta temperatura. Gli NO_x, insieme ai clorofluorocarburi (CFC), sono la causa principale dell'assottigliamento dello strato di ozono nella stratosfera, fondamentale per la sopravvivenza dell'uomo poiché assorbe le pericolose radiazioni UV del sole. Purtroppo, l'abbattimento del protossido di azoto ha ricevuto scarsa attenzione negli anni '80 e '90, nonostante i suoi effetti negativi sullo strato di ozono. Oltre a ciò, l'N_2O è considerato un gas a effetto serra e la sua influenza sul riscaldamento globale è valutata dal cosiddetto potenziale di riscaldamento globale (GWP). Il GWP del protossido di azoto è 310 e 21 volte più grande dei valori relativi al diossido di carbonio (CO_2) e al metano (CH_4). A causa delle attività antropologiche, il livello di questi tre gas serra è aumentato dal 1850 a ritmi che non erano mai stati osservati negli ultimi 800 000 anni.

Le emissioni antropologiche di protossido di azoto sono dovute principalmente all'agricoltura e alla produzione industriale. L'agricoltura è di gran lunga la principale fonte di emissioni di N_2O e la fonte principale delle emissioni agricole è rappresentata dalle emissioni dirette dal suolo derivanti dall'applicazione di fertilizzanti. Infine, circa il 27% delle restanti emissioni antropologiche proviene dal settore industriale, dove le fonti più importanti sono dovute alla produzione di acido nitrico e acido adipico. L'acido nitrico è la principale materia prima utilizzata per la produzione di esplosivi, fertilizzanti a base di azoto, e altri composti. Durante il processo di sintesi, l'N_2O viene rilasciato come sottoprodotto durante la reazione di ossidazione dell'ammoniaca, catalizzata con il platino. L'acido adipico è un solido cristallino bianco utilizzato principalmente come componente principale del nylon (nylon 6,6), impiegato nella produzione di materie plastiche, tessuti sintetici, lubrificanti, ecc. Il processo di sintesi dell'acido adipico si basa sull'ossidazione di una miscela di chetone e alcol con l'acido nitrico, dove l'N_2O viene prodotto come sottoprodotto. Dato che le attività antropologiche e industriali sono in costante aumento, è necessario trovare metodi efficienti che permettano di controllare e ridurre le emissioni di N_2O.

La decomposizione catalitica dell'N_2O è un metodo efficace per eliminare le emissioni di questo gas, poiché permette di ottenere come prodotti azoto e ossigeno molecolare:

$2N_2O \rightarrow 2N_2 + O_2$

La reazione è esotermica ma limitata dal punto di vista cinetico, per cui la scelta di un catalizzatore è essenziale per promuovere la rottura della molecola. I catalizzatori più comunemente utilizzati per la decomposizione del protossido di azoto sono:

- Ossidi metallici
- Ossidi misti (perovskiti)
- Zeoliti

In particolare, la seguente tesi si concentra sullo studio dell'attività catalitica della zeolite ZSM-5 scambiata con rame (Cu-ZSM-5). La ZSM-5 (Zeolite Socony Mobil-5, brevettata dalla compagnia petrolifera Mobil nel 1975) è una zeolite caratterizzata dalla struttura MFI. L'elevato rapporto Si/Al (che raggiunge l'infinito per la silicalite-1), l'alta stabilità e la forte resistenza agli acidi, combinati con la struttura dei pori, ne fanno un catalizzatore molto attivo e selettivo della forma, soprattutto nella conversione dei mono aromatici. Il gruppo di ricerca guidato da Iwamoto ha scoperto per la prima volta che la zeolite ZSM-5 scambiata con rame (Cu-ZSM-5) è efficace per promuovere la decomposizione di NO (un altro inquinante NO_x). Da allora, numerosi scienziati hanno scoperto che Cu-ZSM-5 ha una maggiore attività nella decomposizione di N_2O rispetto ad altre zeoliti ZSM-5 scambiate con metalli di transizione (M-ZSM-5, dove M = Ni, Mn, Pd, Ce, Zn, Cd). Inoltre, utilizzando la zeolite ZSM-5 scambiata con rame (Cu-ZSM-5) si può osservare un comportamento oscillatorio della decomposizione di N_2O, in condizioni di reazione specifiche.

Nonostante l'ampia ricerca scientifica, alcune questioni cruciali per la comprensione del sistema catalitico Cu-ZSM-5 sono ancora discusse in letteratura. Lo stato di ossidazione del rame in varie condizioni, o l'intera chimica redox del rame nella struttura zeolitica, è una delle questioni più dibattute. La comprensione di questo sistema è fondamentale per definire il tipo di centri di rame presenti nel catalizzatore attivo. Infatti, l'eccellente attività e selettività del Cu-ZSM-5 deriva dalla particolare struttura della matrice della zeolite, che consente la stabilità delle specie polivalenti di rame all'interno dei pori della zeolite. Anche il processo di sintesi è importante, perché può influenzare la composizione strutturale della zeolite e modificare le caratteristiche redox del rame. I due principali metodi di sintesi della Cu-ZSM-5 sono lo scambio ionico e l'impregnazione. È generalmente accettato che la zeolite Cu-ZSM-5 sintetizzata con il metodo dello scambio ionico in eccesso favorisca lo sviluppo di dimeri di rame $[Cu\text{-}O\text{-}Cu]^{2+}$ con ponti di ossigeno extra-lattice (ELO), dove l'ossigeno proviene dalla struttura della zeolite o da gruppi OH strutturali. Inoltre, lo scambio ionico consente anche la formazione di specie di ossido di rame (CuO) distribuite e di singoli ioni Cu^{2+} in posizioni strutturali cationiche. Al contrario, i catalizzatori Cu-ZSM-5 preparati con la procedura dell'impregnazione presentano notevoli differenze nella chimica e nella struttura rispetto ai campioni scambiati. In particolare, nei campioni impregnati è solitamente presente una quantità sostanziale di aggregazione dei cluster di ossido di rame, che si trovano preferibilmente sulla superficie esterna del materiale.

Nel presente lavoro di tesi magistrale sono stati sintetizzati diversi campioni di zeolite Cu-ZSM-5, al fine di studiare l'attività catalitica e l'insorgenza o meno del comportamento oscillatorio nella decomposizione di N_2O. I campioni sono stati sintetizzati cambiando diversi parametri, per valutare gli effetti che questi hanno sull'attività catalitica. I parametri sono:

- Quantità di rame
- Rapporto Si/Al della zeolite – per le sintesi sono state utilizzate tre zeoliti madri con diversi rapporti Si/Al.
- Tipologia di sintesi - scambio ionico o impregnazione

Materiali e metodi:

I catalizzatori sono stati sintetizzati a partire da tre zeoliti madri NH_4-ZSM-5 aventi diversi rapporti Si/Al, mentre come precursore è stato utilizzato l'acetato di rame monoidrato ($Cu(CH_3COO)_2 \bullet H_2O$). Prima di essere impiegate nella sintesi, le zeoliti madri sono state calcinate a 550°C per 5 ore per ottenere la forma protonica della zeolite (H-ZSM-5).

I campioni sintetizzati tramite la procedura dello scambio ionico sono stati preparati miscelando 100 mL di acqua bidistillata, 1 g di H-ZSM-5 con una quantità variabile di precursore. Successivamente, la miscela è stata agitata vigorosamente a temperatura ambiente (RT) per 2 ore. Infine, la zeolite è stata recuperata per centrifugazione e lavata tre volte con acqua bidistillata, per eliminare il precursore non scambiato.

Analogamente ai campioni scambiati, le zeoliti impregnate sono state ottenute miscelando il precursore con 100 mL di acqua bidistillata e 1 g di H-ZSM-5. La soluzione è stata è stata agitata vigorosamente a 80 °C, fino alla completa evaporazione dell'acqua. Successivamente, le zeoliti sono state essiccate in stufa a 60 °C. A differenza del metodo precedente, i campioni impregnati non sono stati sottoposti a lavaggio e centrifugazione. Ne consegue che tutto il precursore di rame introdotto dovrebbe essere completamente presente nel campione, in misura maggiore rispetto ai campioni preparati con scambio ionico.

La nomenclatura dei campioni segue il seguente schema:

ZXX_IMS/SIS_YY_W

Dove:
- XX - rapporto Si/Al della zeolite madre, con valori possibili di 12, 25 o 40.
- IMS/SIS - metodo di sintesi (impregnazione o scambio ionico rispettivamente).
- YY - tipo di precursore di rame utilizzato nella sintesi (Acetato di rame o nitrato di rame).
- W - quantità di precursore in grammi.

Pertanto, è possibile classificare i campioni in base alla percentuale teorica di rame introdotta durante la sintesi (***Tabella 1***).

Tabella 1. Lista dei campioni sintetizzati in base alla quantità teorica di rame e alla molarità della soluzione.

SAMPLE	Theoretical w_{Cu} (%)	M (mmol/L)
Z12_IMS_Ac_0,2	6,4	10
Z12_SIS_Ac_0,2	6,4	10
Z25_IMS_Ac_0,2	6,4	10
Z25_SIS_Ac_0,2	6,4	10
Z40_IMS_Ac_0,2	6,4	10
Z40_SIS_Ac_0,2	6,4	10
Z12_IMS_Ac_0,1	3,2	5
Z12_SIS_Ac_0,1	3,2	5
Z25_IMS_Ac_0,1	3,2	5
Z25_SIS_Ac_0,1	3,2	5
Z40_IMS_Ac_0,1	3,2	5
Z40_SIS_Ac_0,1	3,2	5
Z25_IMS_Ac_0,05	1,6	2,5
Z40_SIS_Ac_0,05	1,6	2,5

La ***Tabella 1*** riporta i campioni sintetizzati e la molarità della soluzione iniziale (indicata come M), basata su un volume di 100 mL.

Come si può notare, sono state utilizzate tre diverse quantità di acetato di rame monoidrato (Ac), per studiare meglio l'effetto della quantità di precursore sul comportamento oscillatorio. Per i campioni con 0,2 e 0,1 g di precursore, sono state utilizzate tutte e tre le zeoliti madri, che stata sintetizzate sia con la tecnica dell'impregnazione che con quella dello scambio ionico. Inoltre, nel tentativo di studiare l'effetto di ogni possibile parametro, sono stati sintetizzati i seguenti campioni:

- Z25_SIS_Ac_0,5: questo campione è stato sintetizzato mediante scambio ionico con un eccesso di precursore (w_{Cu} = 15,9 %).
- Z25_SI50°C_Ac_0,2: durante la procedura di scambio ionico di questo campione, la temperatura è stata mantenuta a 50°C per studiare l'influenza della temperatura sul livello di scambio del Cu.
- Z25_IMS_Nt_0,2: in questo caso è stato utilizzato il nitrato di rame (Nt) come precursore invece dell'acetato di rame.
- NS1_IMS_Ac_0,2: in questo caso la zeolite madre è una silicate porosa con struttura di tipo MFI, sintetizzata in laboratorio. In questa zeolite non è presente alluminio, quindi il rapporto Si/Al tende all'infinito. La zeolite ottenuta è stata impregnata con 0,2 g di acetato di rame monoidrato, secondo il metodo descritto in precedenza.

Tutti i campioni sono stati calcinati in base alla seguente procedura:

1. Atmosfera riducente: il reattore viene riscaldato fino a 550°C con una rampa di 5°/C mentre il catalizzatore viene trattato con un flusso di He di 200 mL/min. Una volta raggiunta la temperatura, queste condizioni vengono mantenute per 2 ore.
2. Atmosfera ossidante: 200 mL/min di una miscela contenente l'1% v/v di O_2 vengono inviati al reattore per 2h a 550°C, al fine di eliminare completamente il residuo organico.

Per i test catalitici è stato utilizzato un reattore tubolare di quarzo con un diametro di 4 mm, il cui letto catalitico è costituito da lana di vetro. Tutte le prove sono state condotte utilizzando 100 mg di zeoliti calcinate, rispettando i seguenti passaggi:

1. Pretrattamento: il reattore è stato riscaldato fino a 550°C con una rampa di 5°/C mentre il catalizzatore è stato trattato facendo fluire un flusso di He di 200 mL/min. Una volta raggiunta la temperatura, queste condizioni sono state mantenute per 2h.
2. Raffreddamento del reattore fino alla temperatura desiderata per il test.
3. Test catalitico, con flusso di 200 mL/min di N_2O, al fine di ottenere una concentrazione di 1000 ppm in He, mantenendo il reattore isotermo per tutta la durata del test.

Infine, i campioni sono stati sottoposti a varie tecniche, per caratterizzarle al meglio le proprietà chimico-fisiche:

- XRD (X-Ray Powder Diffraction) - per determinare la struttura cristallografica.
- TPR (Temperature Programmed Reduction) con H_2 - per analizzare la riducibilità delle specie di rame sui catalizzatori
- Fisisorbimento di N_2 a 77 K - per stimare l'area superficiale dei campioni.
- Spettroscopia FT-IR (Fourier-transform infrared spectroscopy) - per analizzare nel dettaglio le specie di rame e la loro reattività verso la CO.
- EDX (Energy Dispersive X-Ray Analysis) e XRF (X-Ray Fluorescence Analysis) - per stimare la quantità di rame effettivamente presente nei campioni.

Analisi e discussione dei dati:

- ***<u>Risultati caratterizzazione fisico-chimica e morfologica</u>***

- XRD:

Tutte le zeoliti presentano i pattern XRD tipici della struttura zeolitica MFI, con una simmetria ortorombica (segnali 2θ compresi tra 7-9°, 23-25° e uguali 45°), mostrando un alto grado di cristallinità.

Tra tutti i campioni sintetizzati con 0,2 g di precursore (***Figura 1***), è possibile notare che solo quelli preparati con impregnazione presentano un picco a 2θ=38,8°, che corrisponde al piano (111) dell'ossido di rame CuO.

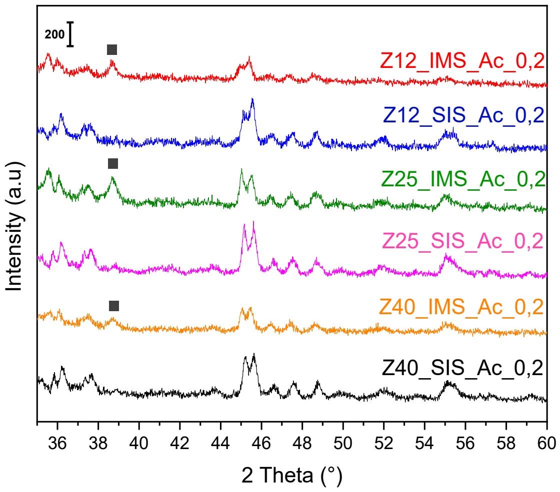

Figura 1. Pattern XRD delle zeoliti sintetizzate con 0,2 g di precursore.

Questa caratteristica è assente nei campioni impregnati preparati con 0,1 g di precursore (***Figura 2***). Ciò potrebbe essere dovuto al fatto che il CuO è presente in questi campioni come particelle piccole e disperse che non possono essere rilevate dallo strumento. Infatti, la XRD è una tecnica sensibile che richiede cristalliti di dimensioni minime prossime ai 5 nm.

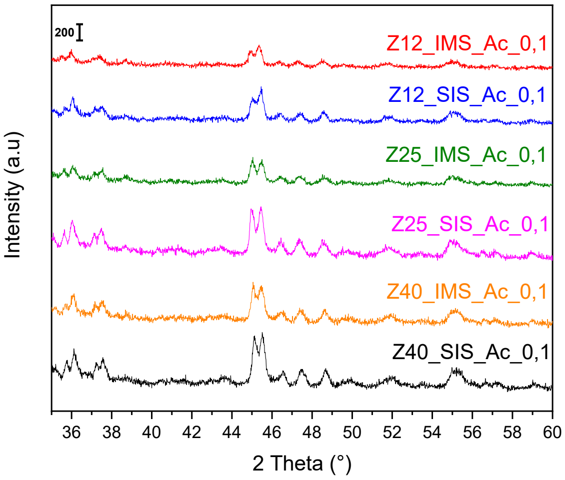

Figura 2. Pattern XRD delle zeoliti sintetizzate con 0,1 g di precursore.

- **TPR:**

L'analisi TPR è stata effettuata introducendo 20 cm^3/min di H_2 al 5% v/v in Ar nel reattore, sottoponendolo a un riscaldamento graduale fino a 800 °C. Prima dell'analisi, ai catalizzatori sono stati applicati due tipi di pretrattamento:

- Pretrattamento riduttivo - un flusso di 20 cm^3/min di gas He è stato inviato all'apparecchiatura, mentre questa veniva riscaldata con una rampa di 10°C/min, fino a raggiungere la temperatura di 550°C.
- Pretrattamento ossidativo - un flusso di 20 cm^3/min di gas O_2 è stato inviato all'apparecchiatura, che è stata riscaldata con una rampa di 10°C/min fino a raggiungere la temperatura di 550°C.

I due tipi di pretrattamento sono stati utilizzati per studiare le possibili variazioni della riducibilità del Cu presente nel catalizzatore.

Per quanto riguarda i campioni pretrattati in He, si può notare che la maggior parte dei campioni impregnati esibisce un picco centrale e ben definito nel range di temperatura tra 250 e 270°C. Questo picco corrisponde al processo di riduzione autocatalitica che coinvolge i cluster di CuO presenti nei canali della zeolite. Invece, i picchi a bassa temperatura (T < 250 °C) sono dovuti alla riduzione di Cu^{2+} a Cu^{+}, mentre a temperatura più elevata (T > 300 °C) si verifica la riduzione di Cu^{+} a Cu^{0}. A titolo di esempio si riporta lo spettro TPR del campione Z25_IMS_Ac_0,2 nella ***Figura 3***:

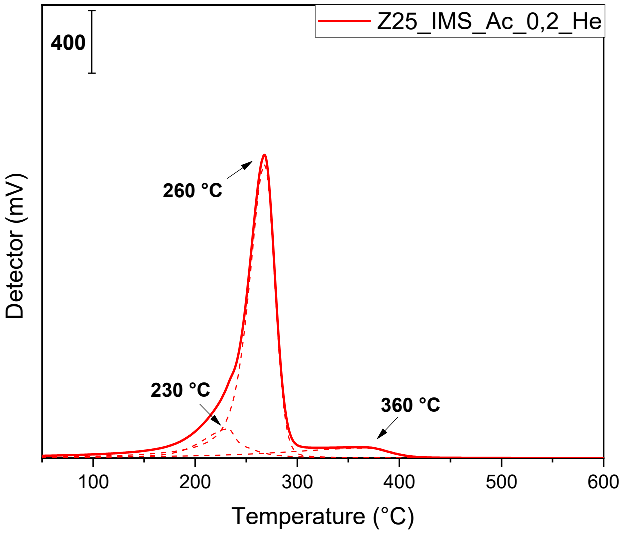

Figura 3. Spettro TPR del campione Z25_IMS_Ac_0,2 pretrattato in He.

Per quanto riguarda i campioni preparati con lo scambio ionico, si può notare come questi esibiscano importanti differenze rispetto agli omologhi impregnati:

- Nei campioni a scambio ionico la riduzione inizia a temperature più basse e termina a temperature più elevate. I picchi a bassa temperatura (< 100 °C) potrebbero essere dovuti alla riduzione dei dimeri di rame $[Cu\text{-}O\text{-}Cu]^{2+}$ con ponti di ossigeno extra-lattice (ELO). Queste specie sono facilmente riducibili grazie alla rimozione dell'ossigeno che funge da ponte. Invece, i picchi ad elevata temperatura sono rappresentativi di una forte interazione tra il metallo e il supporto, che rende le specie meno riducibili.
- Il picco corrispondente alla riduzione dei cluster di CuO è assente, e può essere dovuto a una bassa concentrazione di rame.
- Il numero di picchi è maggiore rispetto ai campioni impregnati.

A titolo di esempio, la ***Figura 4*** rappresenta lo spettro TPR del campione scambiato Z25_SIS_Ac_0,2 pretrattato in He.

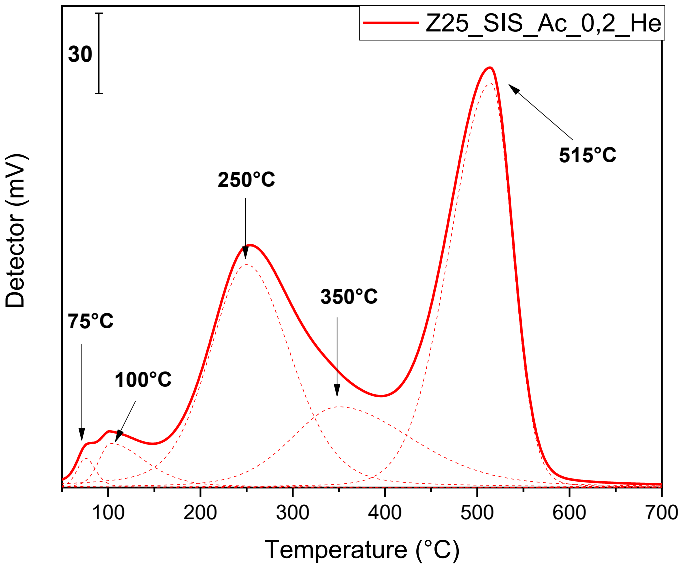

Figura 4. Spettro TPR del campione Z25_SIS_Ac_0,2 pretrattato in He.

Infine, i campioni pretrattati in O_2 presentano spettri simili a quelli descritti precedentemente. Tuttavia, questi campioni presentano due differenze principali rispetto ai corrispondenti campioni pretrattati in He:

- Il pretrattamento ossidante genera spettri con un numero minore di picchi.
- Il pretrattamento ossidante genera spettri caratterizzati da un segnale più elevato (asse y).

Entrambe queste caratteristiche sono attribuite alla maggiore presenza di cluster di CuO, che si formano come conseguenza del pretrattamento ossidante.

- **EDX e XRF:**

Queste tecniche sono state utilizzate per determinare la quantità reale di rame presente nei campioni, al fine di calcolare il consumo di H_2 durante l'analisi TPR. La quantità di Cu è influenzata principalmente dai seguenti parametri:

- Procedura di sintesi: la quantità è significativamente più alta per i campioni impregnati, rispetto a quelli scambiati. Ciò è dovuto al fatto che durante la sintesi dei campioni impregnati, la maggior parte del precursore viene introdotta nella zeolite, grazie all'evaporazione della soluzione, al contrario di quelli scambiati, dove l'eccesso di precursore viene eliminato tramite centrifugazione.
- Rapporto Si/Al: nella maggior parte dei casi, la zeolite con il rapporto Si/Al più basso contiene più precursore rispetto agli altri due campioni. Questo perché la zeolite con rapporto Si/Al pari a 12 contiene più siti di Al, che possono legarsi alle varie specie di rame.

Come si può vedere dalla ***Tabella 2***, il rapporto H_2/Cu per la maggior parte dei campioni impregnati è prossimo a 1, il che significa che c'è stata una riduzione completa delle specie di rame. Inoltre, i valori corrispondenti al pretrattamento con O_2 sono più elevati, poiché questo aumenta lo stato di ossidazione delle specie di rame, da cui ne consegue così una maggiore riduzione. Lo stesso andamento si osserva anche per i valori di %Cu(II).

Tabella 2. Valori dei consumi di H_2 durante l'analisi TPR, basati sul contenuto di Cu rilevato tramite l'analisi EDX.

SAMPLE	Cu (wt%)	Cu (mol)	H_2 consumption (mol)		H_2/Cu ratio		% Cu (II)	
			He	O_2	He	O_2	He	O_2
Z12_IMS_Ac_0,2	6,38	5,0807E-05	4,50219E-05	4,23833E-05	0,8861	0,8342	77,23	66,84
Z25_IMS_Ac_0,2	6,29	4,9694E-05	4,3095E-05	4,67543E-05	0,8672	0,9408	73,44	88,17
Z40_IMS_Ac_0,2	6,86	5,4953E-05	4,01841E-05	4,95195E-05	0,7312	0,9011	46,25	80,22
Z12_SIS_Ac_0,2	2,71	2,1325E-05	2,41481E-05	2,43129E-05	1,1324	1,1401	126,47	128,02
Z25_SIS_Ac_0,2	1,31	1,0329E-05	1,96737E-05	1,46753E-05	1,9047	1,4208	280,94	184,16
Z40_SIS_Ac_0,2	1,49	1,1771E-05	1,38353E-05	1,3416E-05	1,1753	1,1397	135,06	127,94
Z12_IMS_Ac_0,1	4,08	3,2362E-05	2,38572E-05	3,29934E-05	0,7372	1,0195	47,44	103,90
Z25_IMS_Ac_0,1	4,14	3,2968E-05	2,21435E-05	2,50375E-05	0,6717	0,7594	34,33	51,89
Z40_IMS_Ac_0,1	3,63	2,8736E-05	2,12965E-05	3,03084E-05	0,7411	1,0547	48,22	110,94

Si ottengono valori simili utilizzando come base di partenza i contenuti di Cu rilevati tramite l'analisi XRF.

- **FT-IR:**

Per la spettroscopia IR è stato utilizzato il monossido di carbonio (CO) come molecola sonda. Tutti gli spettri sono stati tracciati degassando il CO a partire dalla massima pressione di equilibrio (30 mbar) e arrivando al degasaggio completo. Tutti gli spettri IR sono normalizzati rispetto alla densità superficiale specifica della pastiglia, per permettere un migliore confronto tra i vari spettri. In tutti i campioni analizzati si osserva un assorbimento attribuito alle specie di monocarbonili (Cu^{+}(CO)), a 2156 cm^{-1}. Aumentando la pressione di equilibrio del CO, tali specie vengono gradualmente consumate e contemporaneamente due bande dovute a complessi dicarbonilici iniziano a crescere di intensità. In tutti i campioni, i complessi dicarbonilici possono essere identificati dalle loro lunghezze d'onda a 2177 cm^{-1} e 2150 cm^{-1}, che corrispondono agli stiramenti simmetrici e antisimmetrici del legame C-O rispettivamente.

Oltre alle bande IR dovute alle specie carboniliche, i campioni impregnati Z40_IMS_Ac_0,2, Z40_IMS_Ac_0,1 e Z25_IMS_Ac_0,2 mostrano una spalla evidente nel range 2132-2137 cm^{-1}, che si forma gradualmente attraverso l'adsorbimento di CO. Queste lunghezze d'onda sono attribuite alla formazione di complessi Cu+-CO sulla superficie parzialmente ridotta di alcune particelle di CuO. La presenza di queste specie è supportata anche dalle analisi H2-TPR e XRD per i campioni impregnati. A titolo di esempio, nella ***Figura 5*** si riporta lo spettro IR del campione Z40_IMS_Ac_0,2 nel quale si possono chiaramente osservare i contributi relativi alle specie menzionate precedentemente.

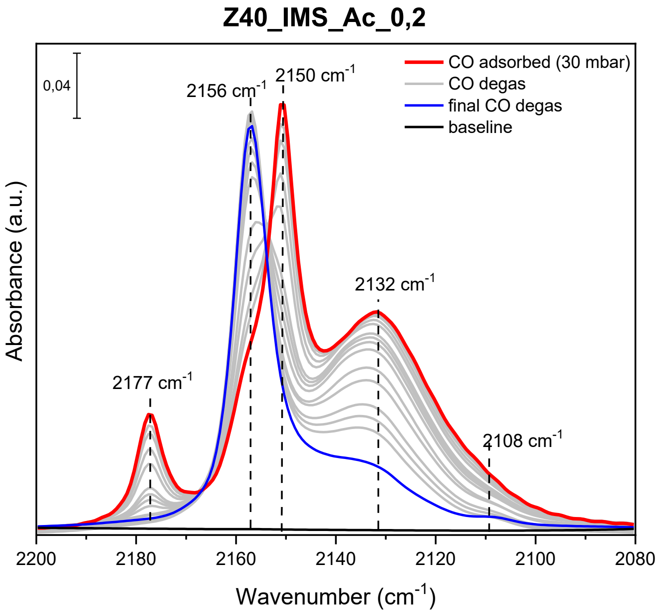

Figura 5. Spettro IR del campione Z40_IMS_Ac_0,2.

- **Fisisorbimento di N_2 a 77 K:**

Attraverso questa analisi si è riuscita a calcolare l'area superficiale di ciascun campione, tramite il metodo BET.

Tabella 3. Valori delle aree superficiali dei campioni calcolate tramite il metodo BET.

SAMPLE	S_{BET} (m^2/g)	SAMPLE	S_{BET} (m^2/g)
Z12_IMS_Ac_0,2	261	**Z12_IMS_Ac_0,1**	297
Z25_IMS_Ac_0,2	324	**Z25_IMS_Ac_0,1**	325
Z40_IMS_Ac_0,2	328	**Z40_IMS_Ac_0,1**	331
Z12_SIS_Ac_0,2	279	**Z12_SIS_Ac_0,1**	311
Z25_SIS_Ac_0,2	361	**Z25_SIS_Ac_0,1**	362
Z40_SIS_Ac_0,2	359	**Z40_SIS_Ac_0,1**	308
Z25_IMS_Ac_0,05	349	**Z25_SI50°C_Ac_0,2**	381
Z40_IMS_Ac_0,05	374	**NS1_IMS_Ac_0,2**	355
Z25_SIS_Ac_0,5	398	**Z25_IMS_Nt_0,2**	322

La maggior parte dei valori riportati nella ***Tabella 3*** sono prossimi a 363 m^2/g, che è l'area superficiale media della zeolite commerciale. L'area superficiale diminuisce all'aumentare della quantità di rame nel campione. In particolare, questo fenomeno è più evidente per le zeoliti impregnate, in cui la maggior parte del precursore è stata introdotta nella struttura, grazie alla procedura di sintesi. Inoltre, i valori dell'area superficiale sono minimi per i campioni con il rapporto Si/Al più basso, e questo potrebbe essere dovuto alla presenza di più siti di Al nella struttura. Infatti, l'area più bassa appartiene a Z12_IMS_Ac_0,2, che è un campione impregnato sintetizzato con la più alta quantità di precursore e caratterizzato dal più basso rapporto Si/Al.

- ***Risultati test catalitici***

Tutte le prove catalitiche sono state eseguite a 400°C, con un flusso entrante avente concentrazione di N_2O uguale a 1000 ppm. Per osservare l'effetto della temperatura, sono state eseguite prove a 375°C e a 350°C per i campioni che mostravano un comportamento oscillante e/o una buona attività catalitica.

Per quanto riguarda i campioni preparati con lo scambio ionico, nessuno di essi presentava il comportamento oscillatorio (***Figura 6***). Inoltre, l'attività catalitica risulta essere significativamente bassa anche a 400°C, che è la temperatura più alta utilizzata per i test catalitici. La conversione più alta (5%) è stata raggiunta per il campione scambiato Z25_SIS_Ac_0,5, che è stato sintetizzato con la maggior quantità di precursore.

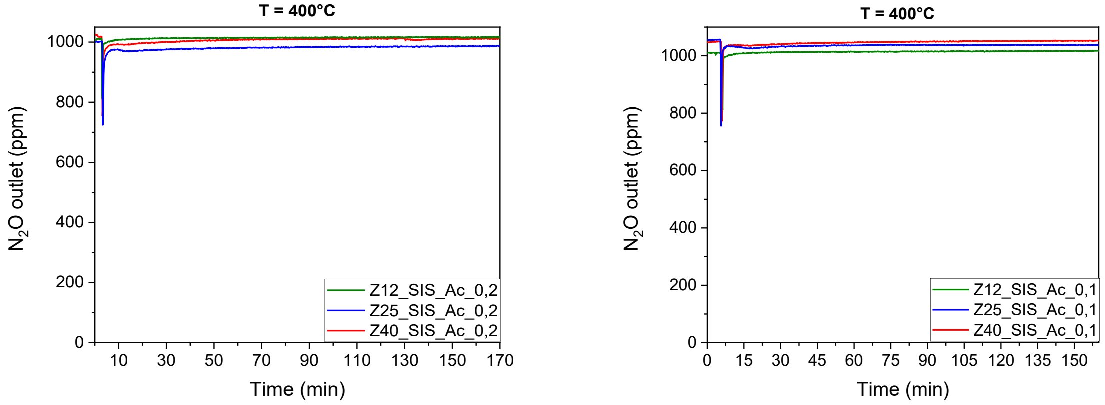

Figura 6. Concentrazione in uscita di N_2O durante i test catalitici per i campioni preparati con scambio ionico sintetizzati con: (i) 0,2 g di precursore (a sinistra), (ii) 0,1 g di precursore (a destra).

Al contrario, alcuni dei campioni impregnati presentano il comportamento opposto. Ad esempio, il campione Z40_IMS_Ac_0,2 presenta oscillazioni a 400°C, perciò il suo comportamento è stato studiato anche a 375°C e 350°C. La ***Figura 7*** rivela che a 375°C e 400°C si verificano oscillazioni nella curva di decomposizione di N_2O all'uscita del reattore. Si può osservare inoltre che la frequenza delle oscillazioni diminuisce con la temperatura, mentre il loro periodo aumenta. Inoltre, le oscillazioni a 375°C appaiono più regolari di quelle a temperature più elevate. A 350 °C non si osserva alcuna oscillazione, e questo potrebbe essere dovuto probabilmente a una durata dell'isoterma troppo breve. In corrispondenza della temperatura a cui si verificano le oscillazioni, è possibile osservare un picco di concentrazione di N_2O nella fase transitoria, più pronunciato a 375 °C. Questo fenomeno può essere correlato allo stato iniziale di riduzione del rame nel catalizzatore, indotto dal pretrattamento con elio.

Oltre a ciò, le oscillazioni di N_2O sono accompagnate anche dalle oscillazioni dell'O_2 prodotto e dei sottoprodotti NO e NO_2, che appaiono sotto forma di picchi, piuttosto che di vere e proprie oscillazioni. Il picco di produzione di O_2, NO e NO_2 si verifica sempre all'inizio del periodo di massima attività del catalizzatore nella decomposizione di N_2O. Infatti, la concentrazione del protossido di azoto non convertito è al suo minimo quando le produzioni di O_2, N_2O e NO raggiungono il massimo.

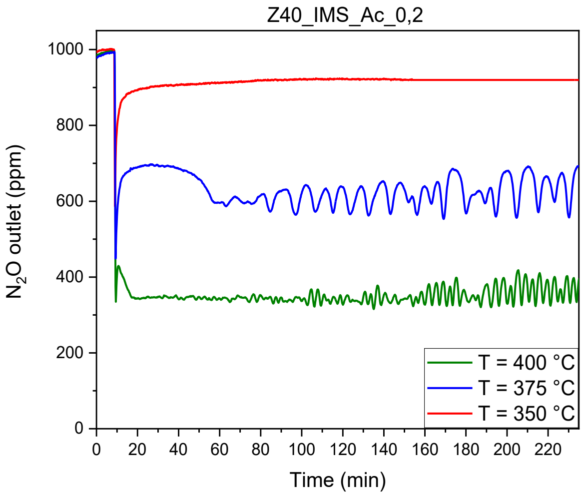

Figura 7. Concentrazione in uscita di N_2O durante i test catalitici di Z40_IMS_Ac_0,2.

Confrontando le curve relative ai campioni sintetizzati con 0,2 g di precursore (***Figura 8***), si nota come Z25_IMS_Ac_0,2 sia il campione caratterizzato dalle oscillazioni più regolari, mentre la zeolite con il rapporto Si/Al più basso non presenti oscillazioni a nessuna delle temperature. Inoltre, la conversione è maggiore per la zeolite con rapporto Si/Al più alto.

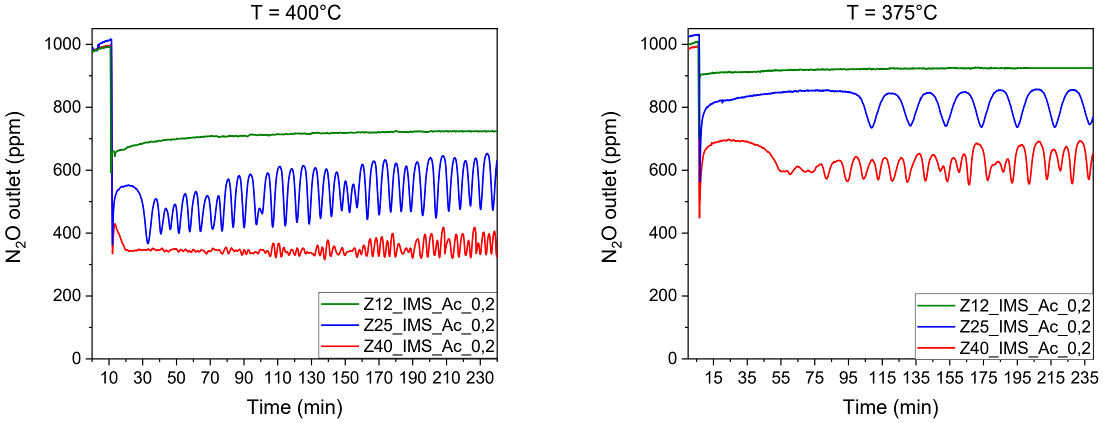

Figura 8. Confronto tra i campioni preparati con impregnazione sintetizzati con 0,2 g di precursore a 400°C (a sinistra) e a 375°C (a destra).

I test catalitici hanno rilevato che le zeoliti impregnate con il rapporto Si/Al intermedio (uguale a 25) sono quelle che presentano sempre oscillazioni regolari, anche quando la quantità di precursore è minima (0,05 g). Lo stesso non si può dire per le zeoliti con il rapporto Si/Al più alto (uguale a 40), che presentano oscillazioni regolari solo quando la quantità di precursore è massima, come si può vedere dalla ***Figura 9***.

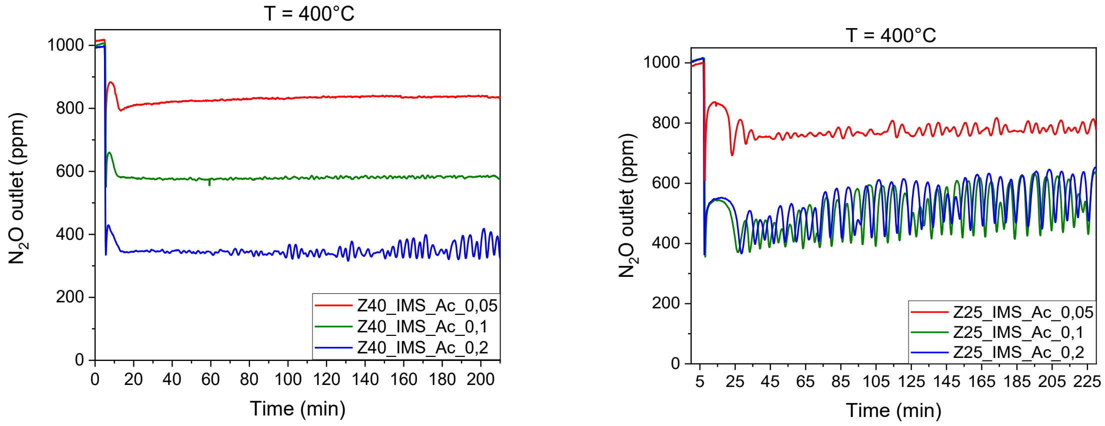

Figura 9. Confronto tra i campioni preparati con impregnazione, sintetizzati con diverse quantità di precursore aventi rapporto Si/Al uguale a 40 (a sinistra) e a 25 (a destra).

Infine, è stata analizzata l'attività catalitica del campione NS1_IMS_Ac_0,2, per studiare l'effetto della zeolite. La struttura originale di questo campione è una zeolite microporosa di silicalite-1 con struttura di tipo MFI e rapporto Si/Al = infinito, che è stata impregnata con 0,2 g di acetato di rame. Di conseguenza, tutto il rame introdotto viene depositato sotto forma di particelle di CuO e non viene scambiato a causa dell'assenza di siti di Al. Al contrario, le zeoliti con il rapporto Si/Al più basso (=12) sono quelle caratterizzate dal maggior numero di siti di Al, che permettono a questi campioni di scambiare più specie di rame rispetto alle altre zeoliti. Come si può notare dalla ***Figura 10***, oltre a non presentare oscillazioni, il campione non converte il gas in ingresso.

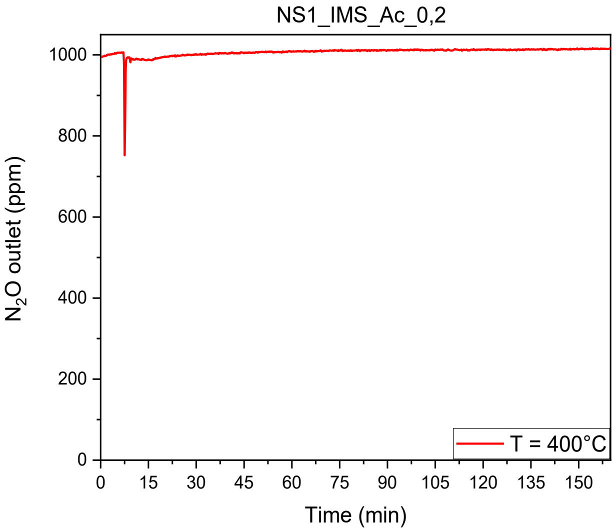

Figura 10. Concentrazione in uscita di N_2O durante il test catalitico di NS1_IMS_Ac_0,2.

Conclusioni:

Questo lavoro di tesi magistrale è stato dedicato allo studio dell'attività catalitica e del comportamento oscillatorio relativo alla decomposizione di N_2O su Cu-ZSM-5. Sono stati sintetizzati diversi catalizzatori attraverso il metodo dello scambio ionico o dell'impregnazione, partendo da zeoliti con tre diversi rapporti Si/Al.

I test catalitici hanno rivelato che i campioni scambiati presentano una bassa attività catalitica e nessun comportamento oscillatorio, a differenza di quelli impregnati. I test di caratterizzazione hanno contribuito a far luce sulle differenze tra i campioni impregnati e quelli scambiati. In primo luogo, sia EDX che XRF hanno mostrato che i campioni impregnati presentano un contenuto di rame significativamente più elevato rispetto a quelli scambiati. Un'altra differenza tra i campioni scambiati e quelli impregnati è la presenza di cluster di ossido di rame (CuO). L'analisi H_2-TPR ha rivelato la presenza di picchi nell'intervallo 250-270°C solo per i campioni impregnati, attribuiti alla riduzione dei cluster di CuO. La spettroscopia IR ha rivelato la presenza di specie dicarboniliche e monocarboniliche per tutti i campioni. Tuttavia, solo i campioni impregnati con il più alto rapporto Si/Al (cioè quelli che presentano le oscillazioni) sono caratterizzati da una spalla attribuita alle particelle di CuO, mentre nessuna zeolite con Si/Al più basso presenta questa caratteristica.

In conclusione, le zeoliti con rapporto Si/Al intermedio (uguale a 25), che hanno sempre esibito un comportamento oscillatorio, presentano le seguenti caratteristiche:

- Un rapporto Si/Al ottimale che ha permesso l'introduzione di ioni e varie specie di rame nella struttura. Una diminuzione del rapporto Si/Al della zeolite porta a un aumento del numero di siti di scambio ionico e, di conseguenza, al raggiungimento della concentrazione massima di ioni Cu^{2+} isolati nella struttura.
- L'abbondanza di cluster di CuO presenti sulle zeoliti, dimostrata dall'analisi TPR, XRD e FTIR.
- Gli spettri FTIR presentano un punto isosbestico ben definito, che potrebbe indicare l'omogeneità delle specie di rame nella struttura.

Come spiegato in precedenza, il rapporto Si/Al è un fattore importante che può determinare il verificarsi del fenomeno oscillatorio. Il fatto che le zeoliti con un rapporto Si/Al intermedio presentino oscillazioni così evidente può essere dovuto alla sinergia e alla coesistenza delle specie di rame e dei cluster di CuO, che potrebbero favorire la presenza dei fenomeni oscillatori.

TABLE OF CONTENTS

LIST OF FIGURES

LIST OF TABLES

1 Introduction

1.1 N_2O and the environmental problem

Nitrous oxide (N_2O), also referred to as laughing gas, is a colourless, non-toxic gas. Since its discovery more than 200 years ago, it has been widely used as a fuel additive in automotive industry, and as a mixing and foaming agent (E942) in the food industry. Besides that, due to the anaesthetic and analgesic properties of nitrous oxide it is extensively utilized in dental, emergency, and anaesthetic practices. [1]

Due to the significant increases in N_2O emissions during the last century, N_2O is the major contributor to stratospheric ozone destruction and the third most important human greenhouse gas. Due to the anthropogenic activities, atmospheric N_2O concentrations have seen an unprecedented, alarming yearly growth rate of between 0.2% and 0.3% during the past century. [2]. It is also predicted that for every doubling of the atmospheric concentration of N_2O, the earth's temperature would increase by 0.3K. [3] In addition to being a greenhouse gas, N_2O is also part of the NO_x family.

1.1.1 The nitrogen oxides (NO_x) family and the ozone layer

Nitrogen oxides (NO_x) are a particularly interesting and significant family of air pollution-causing chemicals, which originate from high-temperature combustion processes. The family of NO_x compounds and their properties are listed in ***Table 1.1*** [4]

Table 1.1 Nitrogen Oxides (NO_x) [4]

Formula	**Name**	**Properties**
N_2O	Nitrous oxide	Colourless gas
NO	Nitric oxide	Water soluble
N_2O_2	Dinitrogen dioxide	Colourless gas
N_2O_3	Dinitrogen trioxide	Slightly water soluble
NO_2	Nitrogen dioxide	Black solid, water soluble, decomposes in water
N_2O_4	Dinitrogen tetroxide	Red-brown gas, very water soluble, decomposes in water
N_2O_5	Dinitrogen pentoxide	White solid, very water soluble, decomposes in water

From all possible origins, nearly half of the nitrogen oxides emissions are produced by mobile sources, because of the combustion at high temperatures, as it is shown in ***Figure 1.1***. A significant amount of NO_x is produced from the anthropogenic sources, such industrial boilers, incinerators, gas turbines, and diesel engines. Biogenic sources of NO_x are mainly due to the combustion in forest fires and to the extreme heat in vicinity of lightning bolts, which transforms O_2 and N_2 present in the air into NO and NO_2. [5]

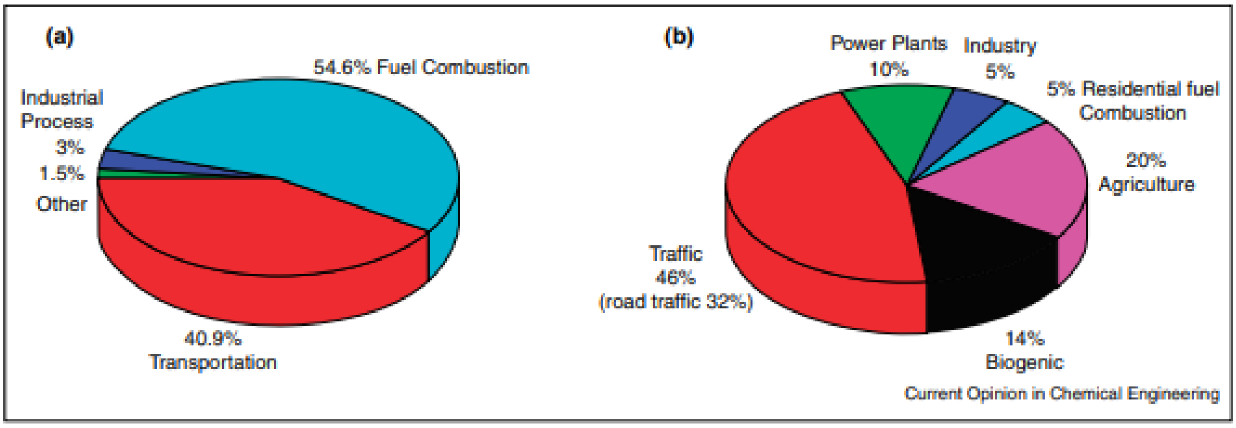

Figure 1.1 Nitrogen oxide emissions by source category in (a) the United States and (b) European Countries. [5]

There are three ways in which NOx are formed in the combustion processes [4]:

1) **Thermal NO_x:** it represents most of the NO_x produced during the combustion and it's formed when nitrogen and oxygen from the combustion air mix with one another at high temperatures. Above a flame temperature of 1300°C, NO_x production often speeds up significantly. Therefore, the molar concentrations of nitrogen and oxygen as well as the combustion temperature regulate the concentration of "thermal NO_x."
2) **Fuel NO_x:** it's created when oxygen in the combustion air reacts with nitrogen that is present in the fuel. Gaseous fuels rarely cause this issue. However, in oils with high levels of nitrogen compounds, fuel NO_x can make up as much as 50% of the total NO_x emissions.
3) **Prompt NO_x:** it's a minor source of NO_x formation and it results from the quick reactivity of air nitrogen with hydrocarbon radicals.

NO_x, along with fully halogenated chlorofluorocarbons (CFCs), are the main cause of the ozone layer's depletion in the stratosphere. The stratosphere is the second layer of the atmospheric envelope and it's crucial for human survival since it contains the ozone layer, which absorbs dangerous UV radiation from the sun, protecting the biological world. For the past forty years, there has been concern regarding the anthropogenic chemical disruptions of the ozone layer. The early research from the 1970s initially defined that the biggest contributions of the emissions caused by NO_x radicals were due to potential increases in supersonic aircraft flying activities in the stratosphere. Later, from around 1974, the attention shifted to chlorine radicals from rocket exhaust and CFCs. Chlorine-induced ozone depletion received most of the attention in the literature as the production of chlorinated compounds was rapidly rising during the 1970s and 1980s.
Due to the effectiveness of the Montreal Protocol (signed in 1987), their production has significantly declined, and the measurements show that atmospheric chlorine levels are progressively diminishing. [6]

Unfortunately, the abatement of nitrous oxide (along with methane and carbon dioxide) has received very small recognition during the 1980s and 1990s, regardless of its negative effect on the ozone layer. Lately, attention has once again been drawn to the impacts of these gases due to the concerns regarding the long-term recovery of the ozone layer. Nitrous oxide shares many similarities with the CFCs: both CFCs and N_2O are relatively stable in the troposphere (where they are emitted) and are transported to the stratosphere where they produce active chemicals that destroy stratospheric ozone through chlorine (or nitrogen oxide) catalysed processes.[7]
Ozone is produced via the breaking of O_2 by light (photolysis) to give oxygen atoms, followed

by the reaction of O atoms with molecular O_2. This process occurs in the stratosphere, where N_2O can react with highly energetic oxygen atoms ($O(^1D)$), thus leading to the production of NO_x [6]:

$$N_2O + O(^1D) \rightarrow 2NO \tag{1.1}$$

Crutzen and Johnson identified the following catalytic cycle, through which nitrogen oxides destroy ozone (O_3) [7]:

$$NO + O_3 \rightarrow NO_2 + O_2 \tag{1.2}$$

$$NO_2 + O_3 \rightarrow NO + O_2 \tag{1.3}$$

$$\text{Net: } O_3 + O \rightarrow 2O_2 \tag{1.4}$$

Reaction ***(1.4)*** represents the dominant catalytic ozone loss cycle in the extra polar regions and it's essential for quantifying the stratospheric ozone budget. Before NO_x are removed from the stratosphere, gas phase catalytic reactions of NO_x through the catalytic cycle mentioned above can destroy millions of ozone molecules. As was observed and documented in the early 1970s, a tiny amount of NO_x can consequently result in a significant reduction in ozone abundance.[6] As it can be seen from ***Figure 1.2***, N_2O emissions are currently the most important ozone-depleting emission, while the contributions of CFCs and halons to ozone layer destruction are expected to continue declining [3]. These evaluations are based on the ODP (Ozone Depleting Potential), which is a parameter used to quantify the relative ozone-depleting abilities of chemicals. It compares the amount of stratospheric ozone destroyed by a unit mass of a chemical released at the Earth's surface to the amount destroyed by a unit mass of CFC-11, which has an ODP of 1.0. In particular, the ODP of N_2O has been calculated to be about 0.017 by Ravishankara, et al. [7] The ODP weighted emissions reported in the graph are calculated by multiplying the ODP of the specific gas by the amount of its emissions. By looking at the predicted values, N_2O is expected to remain the dominant ozone-layer-depleting agent. More concerningly, unless countries come up with mitigation plans, anthropogenic N_2O emissions are expected to increase quickly and practically double by 2050.

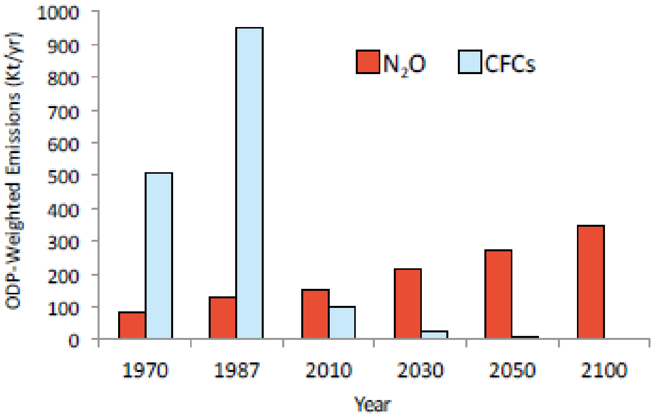

Figure 1.2 ODP-Weighted emissions of anthropogenic N_2O and the sum of CFC-11, CFC-12 and CFC-13 for 6 different years. Included is 1987, the year around which CFC emissions peaked, and the Montreal Protocol was signed. [3]

1.1.2 N_2O as greenhouse gas

Beside its role in the stratospheric ozone layer depletion N_2O is also regarded as a greenhouse gas; and therefore its influence on the global warming is evaluated by so called Global Warming Potential (GWP). The use of GWP was established to enable comparisons between the effects of various gases on global warming. In more detail, it is a measurement of the amount of energy that 1 ton of a gas will absorb over a certain amount of time in comparison to 1 ton of carbon dioxide (CO_2). The larger the GWP, the more that a given gas warms the Earth compared to CO_2 over a time period, which is typically 100 years. In the case of nitrous oxide, it has a global warming potential 310 and 21 times greater than CO_2 and CH_4 respectively. [8]
As it can be seen from the ***Figure 1.3***, the most important GHGs (Green House Gases) are represented by CO_2, CH_4 and N_2O.

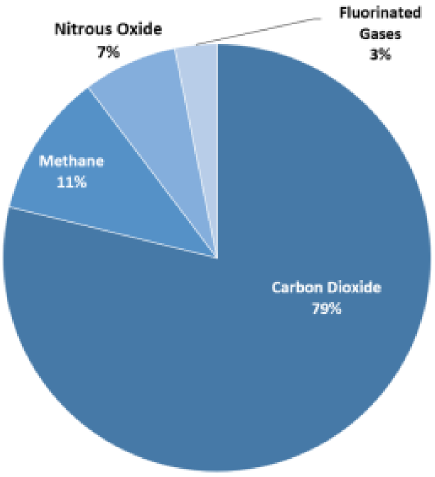

Figure 1.3 Repartition of the total GHGs emissions in the USA (2020). Percentages may not add up to 100% due to independent rounding. [9]

Because of human activities, the level of these three greenhouse gases have been rising since 1850 at rates that haven't been observed in at least the last 800,000 years. As it can be noted from ***Figure 1.4***, atmospheric concentrations have been rising, with annual averages for carbon dioxide (CO_2), methane (CH_4), and nitrous oxide (N_2O) reaching 410 parts per million (ppm), 1866 parts per million (ppb), and 332 ppb, respectively, in 2019. [10]

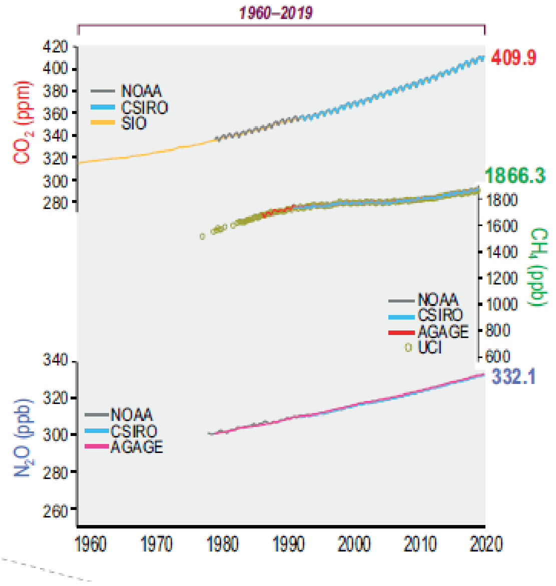

Figure 1.4 Trends of N_2O, CH_4 and CO_2 concentrations from 1960 to 2019. [10]

Moreover, N_2O has a long atmospheric lifetime currently estimated to be approximately 120 years, which leads to important consequences. First of all, since released N_2O builds up in the atmosphere over several decades, the majority of the natural and man-made N_2O emissions from the previous 50 years are still present in the atmosphere today. The removal of N_2O from the atmosphere would take several centuries, even if all emissions were stopped right away. Additionally, due to its prolonged lifetime, N_2O is uniformly mixed in the lower atmosphere, which along with the diffuse character of the N_2O emissions makes it difficult to identify the specific sources of N_2O using atmospheric monitoring. [3]

Overall, N_2O is the third most prevalent greenhouse gas after carbon dioxide and methane. Considering the global elimination of CFCs and other ozone depleting compounds, N_2O is also the biggest hazard to the stratospheric ozone layer. However, despite increasing recognition of N_2O's significant contributions to these urgent concerns, it has received little political attention. There are a variety of reasons why, including the challenge of monitoring agricultural emissions, and the total lack of mitigation techniques and technologies (due to the costs of mitigation in comparison to other sources of GHG emissions).

1.2 Sources of N_2O emissions

The estimation of the total worldwide N_2O emissions from 2007 to 2016 with their respective uncertainties is presented in the ***Figure 1.5***.

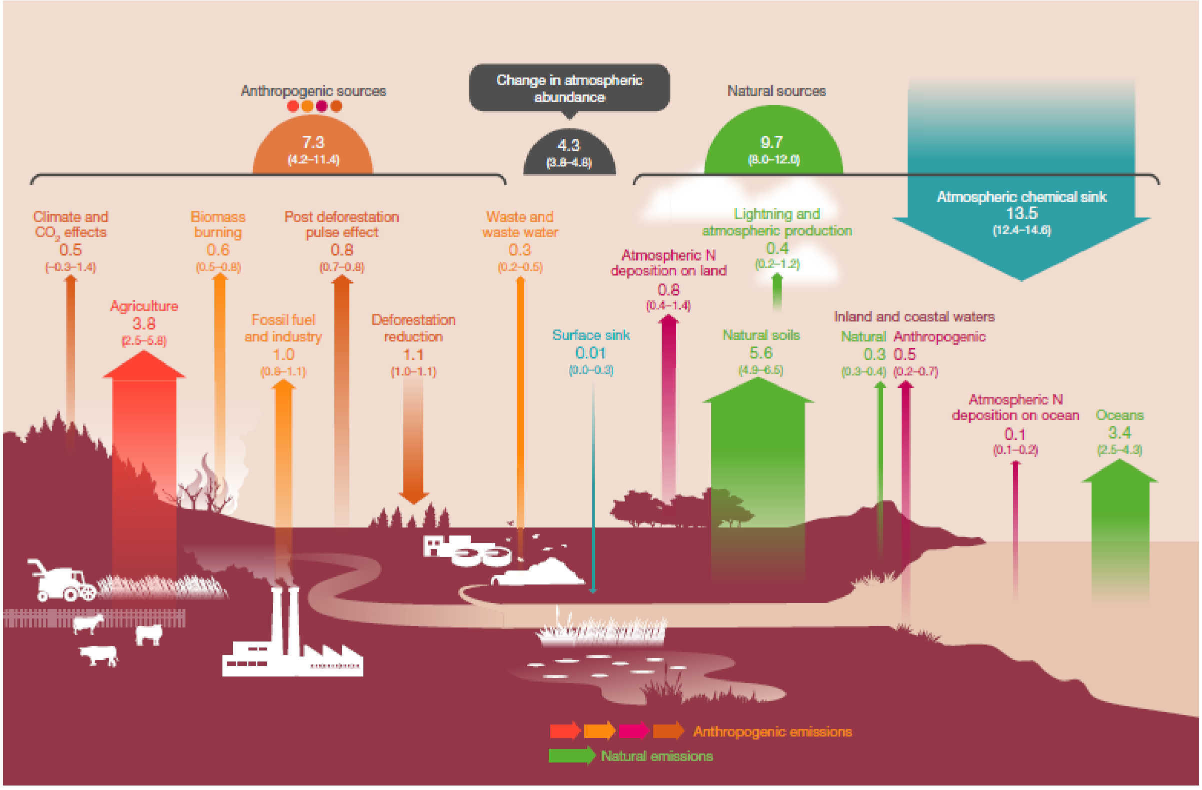

Figure 1.5 N_2O emissions. The coloured arrows represent N_2O fluxes (in Tg N/yr) for 2007–2016 as follows: red, direct emissions from nitrogen additions in the agricultural sector; orange, emissions from other direct anthropogenic sources; maroon, indirect emissions from anthropogenic nitrogen additions; brown, perturbed fluxes from changes in climate; green, emissions from natural sources.[11]

The unit used to describe the emissions of N_2O is Teragrams N_2O-N/yr (Tg N/yr), meaning teragrams (10^{12} grams) of nitrous oxide in equivalent nitrogen units per year. It's possible to distinguish three main contributions[11]:

1) **Atmospheric sink:** N_2O in the atmosphere can be decomposed in N_2 and O_2 either via photolysis or by reacting with electronically excited atomic oxygen ($O(^1D)$)

   $$N_2O + O(^1D) \rightarrow N_2 + O_2 \qquad (1.5)$$

   The global calculated N_2O emissions due to this phenomenon are around 13.5 Tg N/yr.

2) **Natural sources:** they account around 57% of total emissions (9.7 Tg N/yr). Biological production of N_2O is mostly performed by fungi and certain classes of bacteria, including those living in soils and in the oceans, being a part of their respiratory processes. [12] In these environments, the microorganisms produce most of the nitrous oxide, primarily as an intermediate during both nitrification (the oxidation of ammonium to nitrate) and denitrification (the reduction of nitrate to nitrogen gas). Since these emissions are compensated by the decomposition of N_2O occurring in the atmosphere, they do not contribute to the growth of nitrous oxide emissions. [11]

3) **Anthropogenic sources:** they make up for, on average, 43% of the total N_2O emission (7.3 Tg N/yr), with nitrogen contributions in agriculture and other sectors making up about 52% and 18% of the direct and indirect emissions, respectively. Agriculture is by far the main source of N_2O emissions that result from human activity. The main source of the increase in the agricultural emissions is direct soil emissions from fertilizer application, followed by a slight but noticeable increase in emissions from livestock manure and aquaculture. [11] Wastewater treatment is another source of anthropological emissions (0.3 Tg N/yr), where N_2O can be produced by microorganisms during the nitrification and denitrification processes. Finally, about 27% of the remaining human-caused emissions comes from other anthropogenic sources, such as fossil fuel use and industry (approximately 13%), and only 3% from perturbed fluxes brought on by changes in the climate, CO_2 levels, or land use. Anthropogenic emissions are the main reason leading to the accumulation of nitrous oxide in the atmosphere.

The geographical distribution of nitrous oxide anthropogenic emissions levels is represented in ***Figure 1.6***. East Asia has the most overall anthropogenic emissions in ten terrestrial regions, followed by North America, Africa and Europe. From 1980 to 2016, European and Russian N_2O fluxes fell by a total of 0.6 Tg N/yr. While the decline in Russia is attributed to the failure of the agricultural cooperative system after 1990, the decline in Europe is assigned to efficient emissions abatement in industry as well as agricultural programs. In the other regions, emissions increased by a total of 2.9 Tg N/yr: 1,34% of the increase was attributable to East Asia, 18% to Africa, 18% to South Asia, 13% to South America, and 6% to North America. In tropical and sub-tropical areas, N_2O natural soil emissions are around 50% higher than the global value, due to the excess nitrogen present in many lowlands. [11]

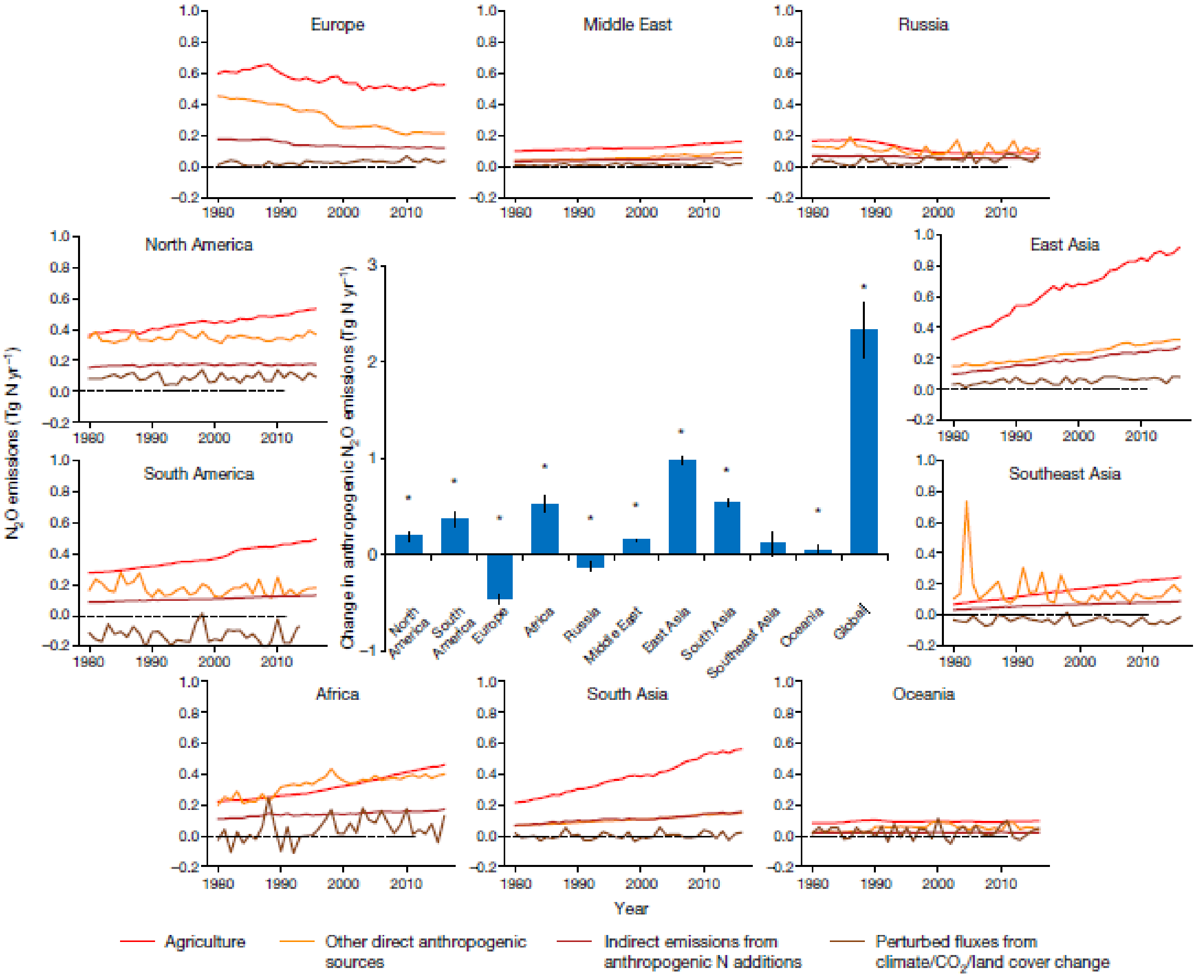

Figure 1.6 Ensembles of regional anthropogenic N_2O emissions over the period 1980–2016. The bar chart in the centre shows the accumulated changes in regional and global N_2O emissions during the study period of 1980–2016. All regions except Oceania show a significant increasing or decreasing trend in the estimated N_2O emissions during the study period. [11]

1.2.1 Industrial sources of N_2O

The two major industrial sources of nitrous oxide emission are nitric and adipic acid productions as well as emissions from stationary and mobile combustion sources. In 2013 the adipic acid and nitric acid industries alone accounted for about 5% of global gross anthropogenic N_2O emissions. [13] Therefore, nitric and adipic acid production facilities are thought to be the major industrial sources of N_2O emissions, with adipic acid sites often releasing tail gas emissions with higher N_2O concentrations (20–40 v/v%) than nitric acid facilities (around 300–3500 ppm). [8]

- Nitric acid is the main raw material used in the fabrication of explosives, nitrogen-based fertilizers, adipic acid, and other products. In this process, N_2O is released as a by-product during the Pt-catalysed ammonia oxidation process. The amount of N_2O produced is influenced by the oxidizing unit's combustion parameters, catalyst type, and age. The following reactions are thought to be the cause of N_2O generation at nitric acid plants [13]:

$$2NH_3 + 2O_2 \rightarrow N_2O + 3H_2O \qquad (1.6)$$

$$2NH_3 + 8NO \rightarrow 5N_2O + 3H_2O \qquad (1.7)$$

$$4NH_3 + 4NO + 3O_2 \rightarrow 4N_2O + 6H_2O \tag{1.8}$$

- Adipic acid ($(CH_2)_4(COOH)_2$) is a white crystalline solid used primarily as the main constituent of nylon (nylon 6,6), which is employed in the manufacturing of plastics, synthetic textiles, lubricants, etc. The production of adipic acid accounted for the majority of industrial N_2O emissions in 1990. The synthesis process of adipic acid is based on the oxidation of a ketone-alcohol mixture with nitric acid, where N_2O is produced as a by-product [13]:

$$(CH_2)_5CO + (CH_2)CHOH + HNO_3 \rightarrow (CH_2)_4(COOH)_2 + N_2O + H_2O \tag{1.9}$$

- Stationary sources of N_2O are represented by public and industrial power plants, together with other combustion processes employing fossil or biofuels as energy carriers. The high-temperature oxidation of nitrogen, which can be found in the atmosphere or in fossil fuels, produces N_2O. The properties of the fuel, the combustion temperature, and the abatement technology all have a significant impact on how much N_2O is generated during fossil fuel burning. [13]

- The principal mobile sources of nitrous oxide emissions are three-way catalytic converters (TWCs), which are used all over the world to concurrently reduce nitrogen oxides, carbon monoxide (CO), and hydrocarbon emissions. The reactions occurring in TWCs produce N_2O as a by-product. The driving cycle, the TWC operating temperature, composition, and aging all have a significant impact on the amount of N_2O emitted by the transportation sector. Additionally, catalyst deactivation and higher quantities of sulphur in the fuel also result in an overall increase in N_2O emissions. [13]

1.3 Mitigation strategies

With the increasing levels of environmental pollution, it is of the highest importance to find the efficient ways to control N_2O emissions and develop efficient N_2O treatment methods as quickly as possible.

Although N_2O emissions from agriculture are inextricably linked to the cycling of nitrogen and the production of food, there are many mitigation strategies in the agricultural industry possessing the high potential of implementation, as schematically represented in ***Figure 1.7*** [3]:

- Increasing the effectiveness of nitrogen utilization in crop and livestock production. When it comes to crop production, it's possible to increase both crop yield and nitrogen use efficiency by combining properly factors such as plant breeding, irrigation, pest control and drainage management.
- Using management techniques and technology to reduce the percentage of input nitrogen emitted as N_2O

As an example, it should be mentioned the so-called Nitrates Directive [14], an agricultural policy that promoted optimization and reduction of fertilizer use as well as water protection legislation. It put into effect between 1990 and 2010, which resulted in a 21% drop in N_2O emissions from agricultural soils in Europe. [3]

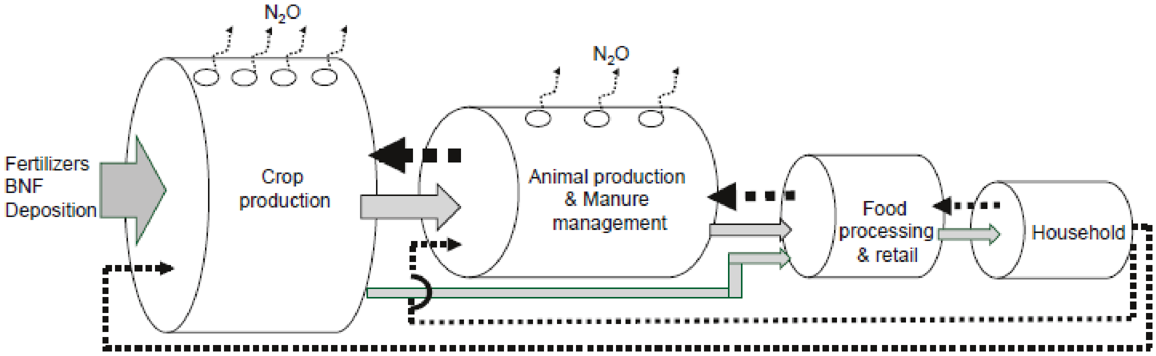

Figure 1.7 A food system approach for reducing N_2O emissions in the production, processing, and consumption of food. The cylinders represent 'N_2O-leaky' compartments of the food system. The large grey arrow at the left indicates 'new' nitrogen inputs via fertilizers, biological nitrogen fixation (BNF) and atmospheric deposition. Smaller grey arrows indicate the flow of nitrogen in food and feed from production to consumption in households. Dashed black arrows indicate recycled nitrogen in manure, residues and wastes. [3]

An effective reduction of N_2O emissions in the chemical industry was accomplished in the European Union's nitric acid facilities resulted in the depletion of industrial nitrous oxide emissions, being reduced from 11% to 3%.

Examples of successful approach to the N_2O mitigation that can be mentioned are the selective catalytic reduction (SCR) and non-selective catalytic reduction (NSCR) processes, both of which are extensively used in the US nitric acid business. By employing more effective oxidation conditions with lower reaction temperatures, progress has recently been made in lowering the amount of N_2O generated during the NH_3 oxidation process. As an alternative, the use of an iron zeolite catalyst can be proposed, that could lead to the reduction N_2O and NO_x emissions in nitric acid facilities. [3]

In the adipic acid industry, catalytic breakdown and thermal destruction are the two most frequently employed methods for reducing N_2O emissions, since they turn N_2O into elementary oxygen and nitrogen elements. By employing these processes, some nations such as the US have managed to decrease significantly their N_2O emissions over the past 20 years (***Figure 1.8***). In particular, N_2O emission decrease is generally thought to have improved from about 32% in 1990 to about 90% for the manufacturing of adipic acid.

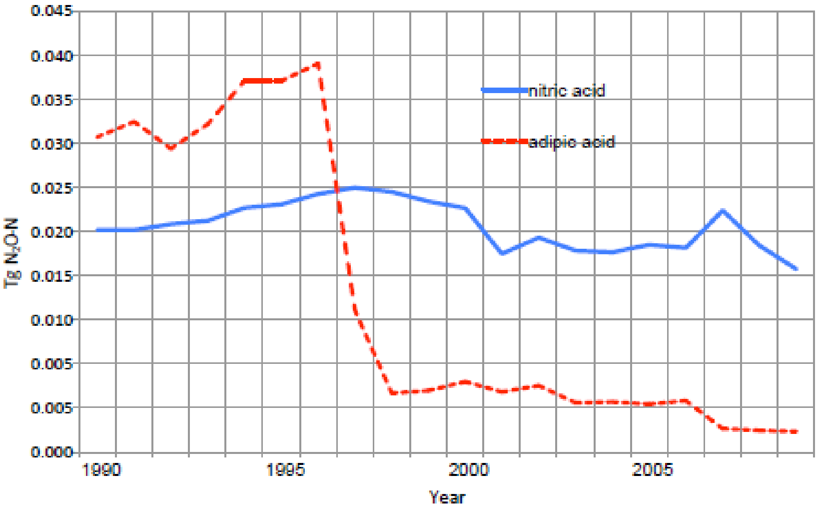

Figure 1.8 US nitrous oxide emissions from nitric acid and adipic acid production. [15]

1.4 Purpose of the thesis

In the present Master Thesis work different samples of Cu-ZSM-5 zeolite have been synthetized in order to observe their effect on the conversion and the isothermal oscillatory behaviour of N_2O decomposition. As it is described in ***Chapter 3***, the samples have been synthetized by changing different parameters, to evaluate the effects they have on the catalytic activity. The parameters are:

- Copper loading
- The Si/Al ratio of the zeolite - three parents zeolites having different Si/Al ratios have been used in the synthesis
- Preparation technique - ion-exchange or impregnation

First, isothermal catalytic tests have been performed for each sample, in order to evaluate its catalytical activity, the effect of temperature and the presence of the oscillatory behaviour. In addition to this, physical and chemical caracterizations have been conducted to better evaluate the copper species present on the catalysts and their properties. The techniques include:

- XRD (X-Ray Powder Diffraction) - to determine the cristallographic structure
- TPR (Temperature Programmed Reduction) with H_2 – to analyze the reducibility of the copper species on the catalysts
- N_2 physisorption at 77 K – to estimate the superficial area and the physisorption isotherms
- FT-IR (Fourier-transform infrared spectroscopy) spectroscopy – to analyse better the copper speices and their reactivity towards CO
- EDX (Energy Dispersive X-Ray Analysis) and XRF (X-Ray Fluorescence Analysis) – to estimate the quantity of copper effectively present in the samples

The results of both the characterization techniques and the catalytic tests are described in ***Chapter 4***, while ***Chapter 5*** reports the conclusions.

2 Cu-ZSM-5: State of the art

2.1 Zeolites and the MFI structure

The origin of the word “zeolite” derives from the combination of the Greek words "zeo" (boil) and "lithos" (stone) which, when merged together, give rise to the English term "zeolite," which means "boiling stones". This name was given to the new class of compounds in 1756 by Swedish mineralogist Axel Fredrik Cronstedt, who also discovered them. He noticed that when this mineral was heated, steam was generated along with water evaporation, giving the impression that the zeolite was boiling.[16] High void volumes produced by heating or dehydrating zeolites give them their so-called "molecular sieve" and adsorbent capabilities. Molecules bigger than the pore size are rejected by molecular sieves, which only permit molecules of a specific size (equal to, or less than, the pore size) to pass through entrance channels. Zeolites are microporous, meaning that the size of their pores are usually below 13 Angstroms [1.3 nm] in diameter. [16] Therefore, they can act as microreactors in which a variety of "green" chemical reactions, such as oxidations and other valuable processes that can be carried out with a smaller environmental impact. Volcanic activity is responsible for the majority of naturally occurring zeolites. Magma, or molten rock within the ground, flows out as lava along with gases, dust, and dense ash when volcanoes erupt. Hot lava, seawater, and sea salt interact causing processes that over the course of thousands of years have produced zeolites. [17]

These are a some of the most significant applications for zeolites [16]:

- They are commonly used as a builder in detergents, removing and encapsulating Ca^{2+} and Mg^{2+}, therefore helping to soften the water.
- Cation-exchange into zeolites is an efficient method for removing harmful heavy metal cations from the environment, such as Pb^{2+}, Cd^{2+}, and Zn^{2+}.
- Zeolites that have been H^+ exchanged are utilized as solid acid catalysts in the petrochemical sector. Every year, about 300,000 tonnes of synthetic zeolites are produced for this purpose.
- Catalytic converters filled with zeolites are widely used for the removal of NO_x emissions from vehicles.
- The presence of pores of specific shape and dimensions gives zeolites the possibility to selectively sort molecules basing on their sizes and forms. This phenomenon is called molecular sieving effect, making zeolites extremely effective drying agents for the elimination of water vapor from other solvents. [18]
- Hydrocarbon sieving: zeolites can selectively separate linear n-alkanes, which are essential to manufacture detergents, from branched alkanes due to the different diffusivity of these molecules through zeolites’ channels.
- Zeolites are also helpful in environmental decontamination techniques since they can adsorb effectively positively charged pollutants such as heavy metals. This is due to many properties such as their surface acidity, their framework structure and their large superficial area.
- Molecular sieves: small pore zeolites preferentially absorb small polar molecules, such as water, making them extremely effective drying agents for eliminating water vapor from other solvents. Zeolites also function as shape-selective catalysts with high selectivity and yields in reactions. There are three types of reactor selectivity, which depend on the size and the shape of the pores (***Figure 2.1***):

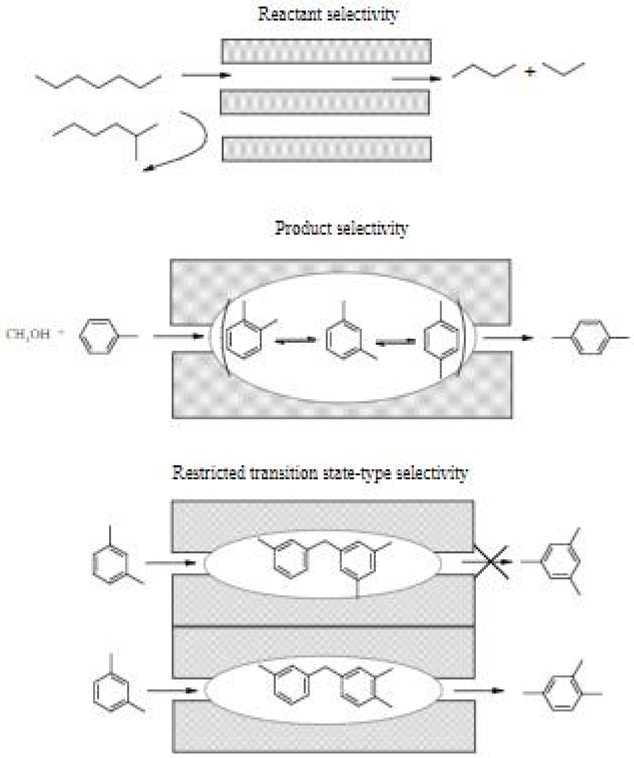

Figure 2.1 Schematic representation of the three types of shape selectivity. [19]

1. **Reactant selectivity**: only the molecules having a diameter small enough to enter the pores can pass through the zeolite.
2. **Product selectivity**: the products that are small enough in relation to the pore size can diffuse more or less quickly and leave the zeolite structure.
3. **Restricted transition state-type selectivity**: some reactions are blocked by the zeolite because the corresponding transition state would require more space than available in the pores.

Zeolites are defined as aluminosilicates constituted by tetrahedra structures (TO_4, where T = Si, Al) which are connected to each other's by O atoms (***Figure 2.2***). [19]

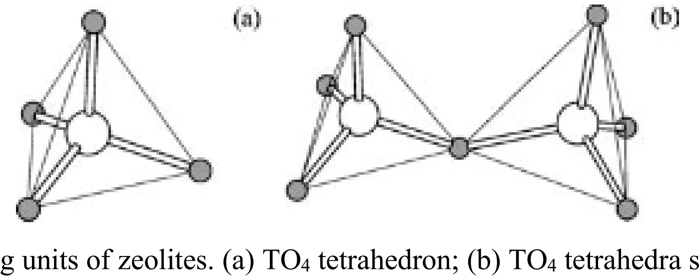

Figure 2.2 Building units of zeolites. (a) TO_4 tetrahedron; (b) TO_4 tetrahedra sharing a common oxygen vertex. [17]

Formally, the Si cation's 4^+ charge and the oxygen anion's 2^- charge result in neutral tetrahedra. As a result, a framework made entirely of Si-O tetrahedra is neutral and can only have acidic qualities due to structural defects. Al^{3+} may replace a Si^{4+}cation, changing the formal charge of the tetrahedron from neutral to negative. [19]

Figure 2.3 represents a zeolite framework where counterions, which are often alkaline or alkaline earth metals like Na^+, K^+, or $Ca^{2+,}$ balance the resulting negative sites.

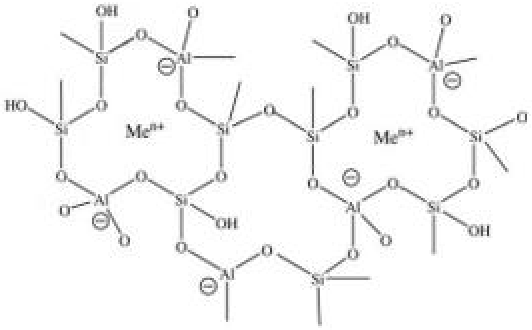

Figure 2.3 A two-dimensional representation of the framework structure of zeolites, were Me^{n+} represents extra framework cations [20]

This property plays an important role in the catalytic activity of zeolites, which are defined by the nature of the extra cation used to compensate the net charge. Depending on the type of the cation there could be present:

- Brønsted acid sites (BASs) - when H+ protons are used to the charge compensation. In the IUPAC Gold Book, a Brønsted acid is defined as "a molecular entity capable of donating a hydron (proton) to a base or the corresponding chemical species". [21]
- Lewis acid sites (LASs) - when the counterion is an alkaline or alkaline earth metal centre, Lewis acid is defined as "species with a vacant orbital that can accept a pair of electrons". [22]

A simplified empirical formula for an aluminosilicate zeolite is [23]:

$$Mn^{n+}_{x/n}Al_xSi_{1-x}O_2 \cdot \gamma X$$

where M^{n+} represents inorganic or organic cations and X are included or adsorbed species. Typically, primary building units (PBUs) and secondary building units (SBUs) are used to classify the crystal structures of zeolites. The $(SiO_4)^{4-}$ and $(AlO_4)^{5-}$ tetrahedra are the PBUs: these come together to form the SBUs, a spatial arrangement of simple geometric structures, by exchanging oxygens with nearby tetrahedra. The SBUs can be single rings, double rings, polyhedra, or even more complicated units. These different SBU configurations can be joined together in a variety of ways to create a special system of channels and cages.

Figure 2.4 shows the kinds of SBUs that have been found to occur in tetrahedral frameworks.

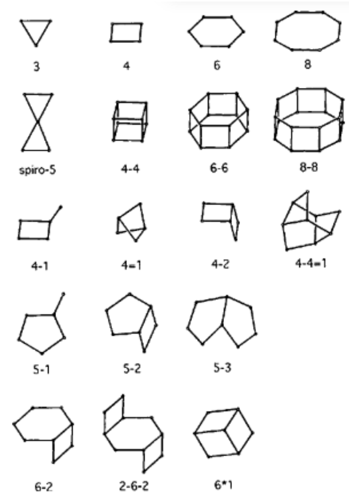

Figure 2.4 Examples of Secondary Unit Buildings (SBUs) that can be found in the zeolite's structure

Zeolites may also contain other structural elements such as cancrinite cages, and alpha cavities in addition to the PBUs and SBUs mentioned above. These are called CBUs, or composite building units. Rings are the most common example of CBUs, whose dimensions determine the pore's size of the zeolite (***Figure 2.5*)**. The diameters of the pore openings are approximately 3.8 Å in small pore, 5.6 Å in medium pore and 7.3 Å in large pore zeolites, respectively.[23]

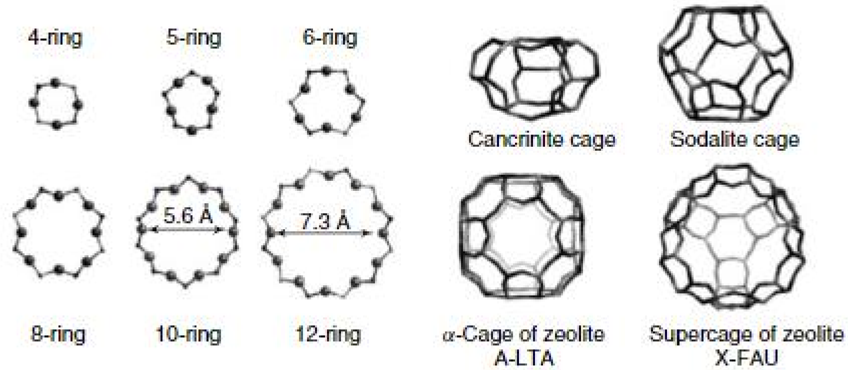

Figure 2.5 Examples of rings and cages (CBUs) frequently found in zeolite structures.[23]

For instance, the MFI framework (***Figure 2.6***), which will be studied more thoroughly in this thesis, is built connecting 5 silicate chains, forming the so called pentasil building units. The assembling of the latter forms a system of two-dimensional 10-member rings (10-MR) forming sinusoidal channels along a-axis which are interconnected with straight channels along the b-axis. Along the c-axis a tortuous pore path is formed. The pore diameter range in the MFI structure is around 5 Å (angstroms). [17]

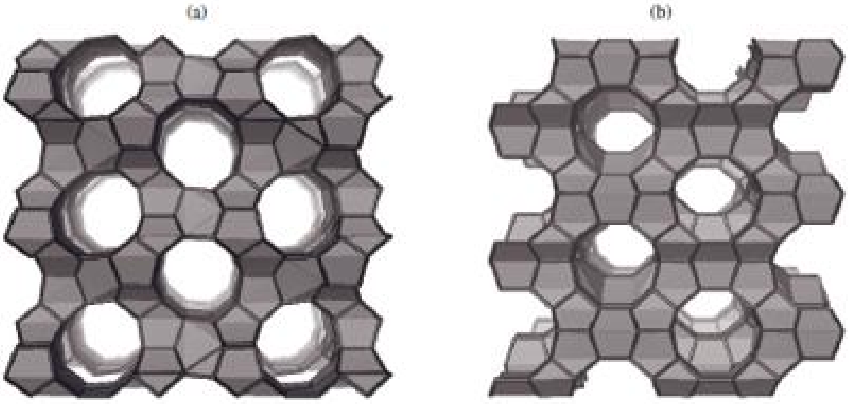

Figure 2.6 MFI framework views: (a) down the straight ten-ring channel system, (b) down the zig-zag ten-ring channel system. [23]

ZSM-5 (Zeolite Socony Mobil-5, patented by Mobil oil company in 1975) is a high silica zeolite with a MFI framework structure. It is synthesized by using tetra propylammonium (TPA+) cations as SDAs (organic templates). Its high Si/Al ratio (reaching infinite for silicalite-1) and high stability and strong acid strength, combined with the pore structure, make it a very active and shape-selective catalyst, especially in the conversion of monoaromatics. [23] ZSM-5 catalysts' characteristics can be influenced by several factors, such as the type of synthesis and the crystallization conditions. The "methanol to gasoline" (MTG) process was made possible thank to the introduction of H-ZSM-5: it's a process which transforms methanol into hydrocarbon mixtures to be used in internal combustion engines. H-ZSM-5 is also widely used to supply the polyester industry with pure para-xylene, which diffuses out of the micropores of ZSM-5 10,000 times faster than the other two xylene isomers do. The para-xylene is then oxidised to terephthalic acid, which is converted into esterified glycols, used to create synthetic polyester fabrics for the fashion industry. [16]

Iwamoto and colleagues first discovered that Cu-ZSM-5 (Cu-exchanged ZSM-5 zeolite) is effective for promoting the decomposition of NO (another NO_x pollutant). Since then, numerous scientists have investigated the use of various metal cation-exchanged zeolites in the catalytic decomposition of N_2O. It was discovered that Cu-ZSM-5 has greater activity in the decomposition of N_2O than other transition metal exchanged ZSM-5 zeolite (M-ZSM-5, where M = Ni, Mn, Pd, Ce, Zn, Cd). One of the system's key characteristics is the exchanged copper's redox property, which is crucial to the $DeNO_x$ reaction.
Unfortunately, Cu-ZSM-5 cannot be used in real-world applications due to at least two difficult limitations: it significantly deactivates in the presence of water and cannot withstand the presence of sulphur compounds. In any case, the Cu exchanged ZSM-5 continues to serve as a model catalyst for the development of new, more resilient systems as well as an explanation of the unique characteristics that make it so interesting and active in $DeNO_x$ processes. [24]
Methane to methanol conversion is another important field in which the contribution of Cu-ZSM-5 has proven to be of value. The current method for producing industrial methanol includes first steam reforming methane to create syngas, a mixture of H_2 and CO, which is then further reacted over a catalyst made of copper, zinc oxide, and alumina at high temperatures and pressures to produce methanol. The creation of strong catalysts that can selectively oxidize the robust C–H bond of methane (104 kcal/mol) to methanol in a single step, under mild conditions, is essential to the development of a more effective method of converting methane into methanol. However, it has been recently shown that Cu-ZSM-5 can convert methane to methanol with a low activation energy (Ea = 15.7 kcal/mol) and a high selectivity (>98%) at a relatively low temperature (< 100 °C) and atmospheric pressure. [25]

2.2 Decomposition of N_2O

The catalytic decomposition of N_2O is a direct exothermic reaction, which is kinetically limited, so the selection of a suitable catalyst is essential to promote the break-up of the molecule. The N-O bond thermal fission activation energy is around 250-270 kJ/mol, and temperatures above 900 K are necessary to achieve detectable conversions ***(2.1)***:

$$2N_2O \rightarrow 2N_2 + O_2 \qquad (\Delta_r H^0(298K) = -163 \text{ kJ/mol}) \tag{2.1}$$

The main catalytic action may result from charge donation into the antibonding orbitals, weakening the N-O bond and lowering the activation energy and reaction temperature.[26]
Over oxidic catalyst (being the most studied type of catalyst) the reaction happens by first adsorbing N_2O, then oxidizing the active sites (*), and then recombining to remove the deposited oxygen (***Eqs.(2.2)-(2.4)***). Under conditions of decomposition, the adsorption ***(Eq.(2.2))*** and desorption ***(Eq.(2.4))*** are typically assumed to be in quasi-equilibrium:

$$N_2O + * \overset{K_{N2O}}{\longleftrightarrow} N_2O \tag{2.2}$$

$$N_2O^* \overset{k}{\rightarrow} N_2 + O^* \tag{2.3}$$

$$2O^* \underset{K_{O2}}{\longleftrightarrow} O_2 + 2^* \tag{2.4}$$

For steady-state conditions and assuming a constant number of active sites, this results in the rate equation ***(2.5),*** where r_{N2O} is the conversion rate of N_2O (mol/s g_{cat}) and N_T is the active site concentration (mol/g_{cat}). [27]

$$r_{N2O} = \frac{kN_T K_{N2O} p_{N2O}}{1 + K_{N2O} p_{N2O} + \sqrt{K_{O2} p_{O2}}} \tag{2.5}$$

Most commonly used catalysts for nitrous oxide decomposition are:

- Metal oxides
- Mixed oxides (perovskites)
- Zeolites

Ion-exchanged transition metal zeolites demonstrated to have a significant activity in the nitrous oxide decomposition reaction. Because of its thermostability, Co-ZSM-5 is the most desirable ZSM-5 catalyst due to its high activity, whereas Fe- and Cu-ZSM-5 have been proven to be deactivated in hydrothermal conditions.

Moreover, under specific reaction conditions, the oscillating behaviour of N_2O decomposition is observed by using Cu-ZSM-5 as a catalyst.

Turek et al. and Ciambelli et al., two different research teams, reported the oscillation of N_2O as a monomolecular reaction over Cu-ZSM-5 catalysts in the middle of the 1990s. [28], [29] Both groups came to the conclusion that an exchange level greater than 100% is necessary to generate isothermal oscillations during N_2O decomposition. They also showed the impact of the temperature of the reaction and the pre-treatment of the catalyst on the oscillation pattern and the N_2O conversion.

2.2.1 Ciambelli et al.'s mechanism

For this research, over exchanged Cu-ZSM-5 zeolites were prepared by performing ion-exchange of H-ZSM-5 zeolite (Si/Al=80) with copper acetate aqueous solution for 2 h at 50°C. The exchange level is approximately 640% (Cu/Al=3.2), while the 100% exchange level corresponds to the atomic ratio Cu/Al=0.5.

The test was run at 344 °C using Cu-ZSM-5 (200-300 µm particle size) that had been pre-reduced in flowing He for two hours at 550 °C. The stream fed to the reactor is a mixture of N_2O and He, in order to reach an initial concentration of 600 ppm for N_2O. After roughly one hour from the start of the run, it appears that N_2O and O_2 concentrations start to oscillate in a regular way. [28]

The oscillations of oxygen have the same frequency and were out of phase with the reactant's oscillations, as shown in ***Figure 2.7***. Additionally, during the transitory phase, the system showed a one-hour long peak in N_2O concentration and a steady value for O_2 outlet concentration (~200 ppm) during the first 30 minutes.

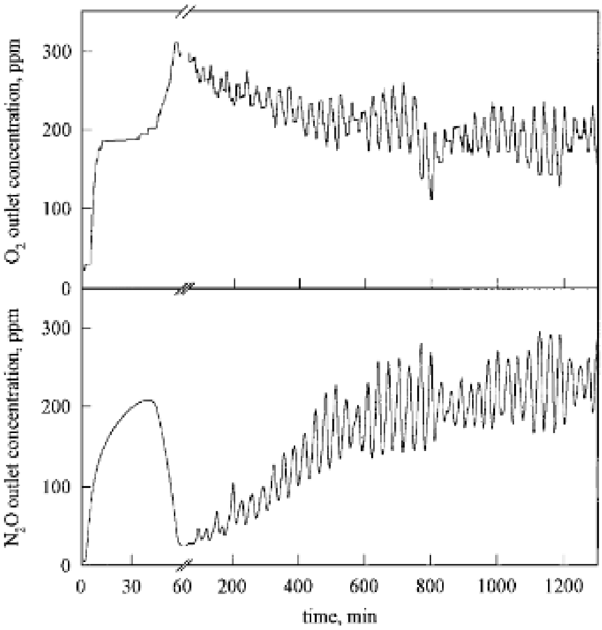

Figure 2.7 N_2O and O_2 outlet concentrations as functions of time in N_2O decomposition at 344°C on pre-reduced Cu–ZSM5. Feed: N_2O (600 ppm) in He. [28]

During the first 30 minutes of the run, the constant values of O_2 concentration agreed stoichiometrically only with the maximum N_2O concentrations at the peak. During the remaining time of the run, Ciambelli et al. measured that N_2O and O_2 outlet average concentrations were in a strict stoichiometric ratio ($O_2/N_2O=1:2$) meaning that the initial consumption of N_2O was higher than that expected from O_2 production. This phenomenon was associated to the catalyst's original reduced copper state, which was generated by the high-temperature helium pre-treatment. It is proposed that a fraction of Cu^+ ions is reoxidized to Cu^{2+} according to the following reaction ***(2.6)***, which explains the apparent higher decomposition rate in the initial minutes:

$$N_2O + 2Cu^+ \rightarrow N_2 + Cu^{+2}–O^{-2}–Cu^{+2} \qquad (2.6)$$

Experiments on the influence of the catalyst's initial state of oxidation on the dynamic behaviour of the N_2O decomposition rate were conducted to support the previously made assumption. ***Figure 2.8*** shows the N_2O outflow concentration as a function of time for three separate runs that were performed under the same experimental conditions but with various catalyst pre-treatments (pure He, 4% vol O_2 in He, and pure O_2).

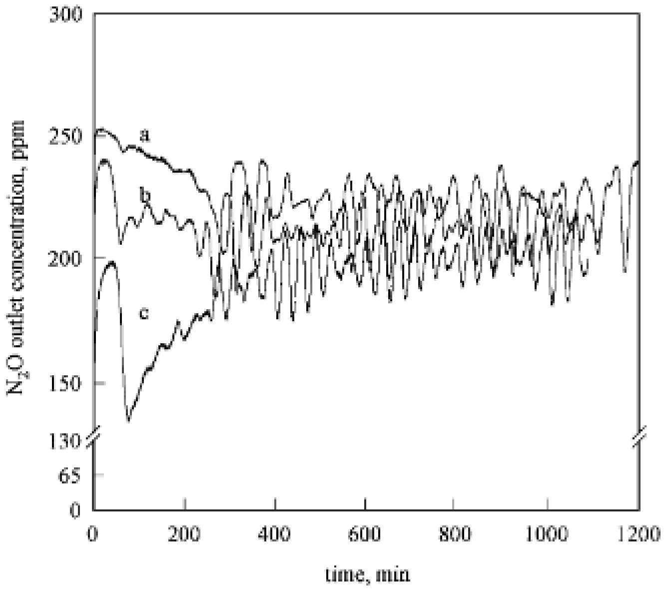

Figure 2.8 N_2O outlet concentration as a function of time in N_2O decomposition at 344°C after different Cu-ZSM-5 pre-treatments: (a) O_2; (b)4% vol O_2/He mixture; and (c) He. Feed: N_2O (300 ppm) in He. [28]

The pre-oxidized catalyst (curve a) induced the presence of the delay before the beginning of the oscillations, whereas the pre-reduced catalyst (curve c) clearly showed the presence of a peak of N_2O concentration in the first 60 minutes, which was considerably less evident for the sample pre-treated in O_2/He mixture. Additionally, the pre-treatment had a significant impact on the catalytic activity in the transient phase, with the reduced form of Cu-ZSM-5 consuming significantly more N_2O at first than the oxidized form. These results provide significant evidence in favour of the hypothesis that the initial reduced state of copper sites should be related to the average value of the outlet N_2O concentrations, which were lower in the transient phase compared to the dynamic regime. In all the cases, the average N_2O conversion value was reached after around 600 minutes of reaction, arriving at a relatively similar value. Furthermore, it seems that the catalyst's initial activity after being pre-treated with the gas mixture of O_2 and He (curve b) is in between the other two values (curves a and c).

In addition to this, Ciambelli et al. investigated the effect of O_2 in the feed on the catalytic activity. They discovered that at 344°C, 5000 ppm of O_2 in the feed is sufficient to extinguish oscillations on the prereduced catalyst, whereas the average conversion of N_2O to N_2 and O_2 declines when the inlet O_2 concentration is raised. On the other hand, Lintz and Turek detected only a minor effect of O_2 on the catalytic activity. [30] The disparities between these two findings are probably the result of the various experimental setups examined, for instance different Si/Al ratio, diluent gas and their concentration, variance in temperature etc. For example, Lintz and Turek employed a Cu-ZSM-5 catalyst with a different Si/Al ratio with respect to Ciambelli et al., they also used a different diluent gas, and a greater N_2O inlet concentration in their test. Moreover, the various temperature ranges investigated are likely to account for a further significant variance.

On the other hand, Ciambelli et al. carried out their experiments with an oxygen concentration ranging from 150 to 20 000 ppm in the feed, and an N_2O inlet concentration of 300 ppm. [28] According to the results reported in ***Figure 2.9***, N_2O outlet concentration oscillates even in the presence of O_2 up to a value of 3000 ppm inlet concentration (curve d). The oscillations only stopped when the level of 5000 ppm of oxygen was reached (curve e). However, even at 150 ppm, the average N_2O conversion declines with increasing O_2 inflow concentration, and it drops by nearly 50% at 20 000 ppm.

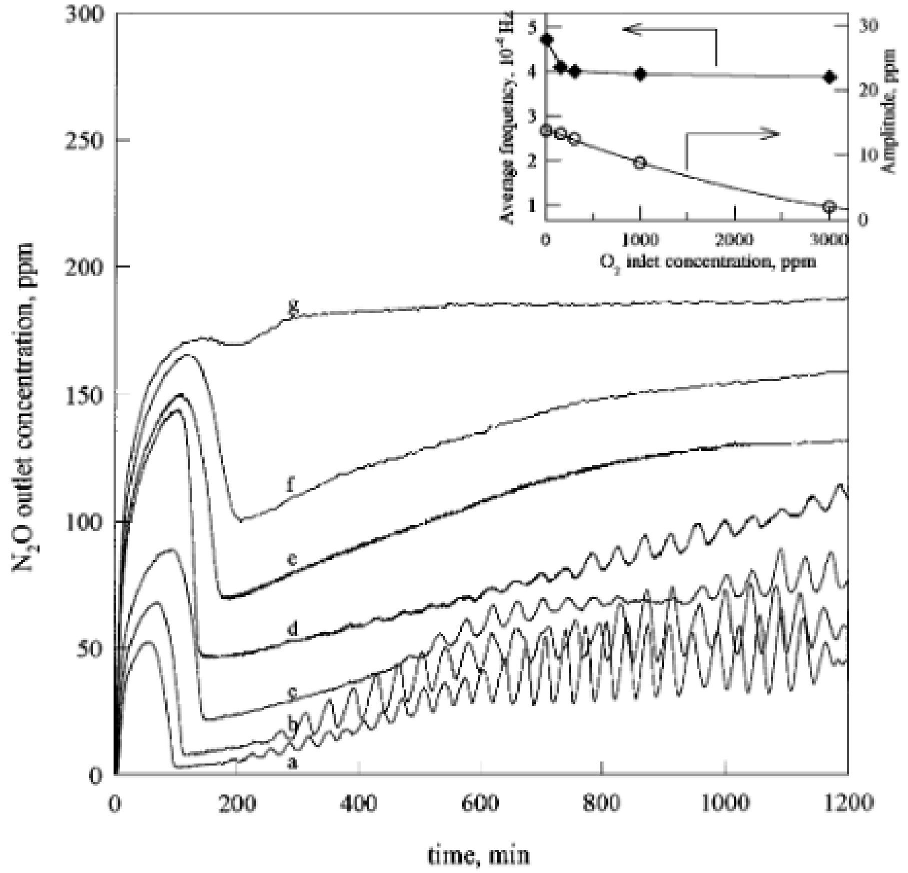

Figure 2.9 N_2O outlet concentration as a function of time in N_2O decomposition on Cu-ZSM-5 at 344°C and different O_2 inlet concentrations: (a) 0;(b) 150; (c) 1000; (d) 3 000; (e) 5000; (f) 10 000; and (g) 20 000 ppm. Feed: N_2O (300 ppm) in He. [28]

In another study, Ciambelli et al. discovered that when nitric oxide was added to the feed, the resulting effects were comparable to those of oxygen addition. [31] It took just 500 ppm of NO to have the quenching effects comparable to those at the feed's highest O_2 concentrations. Additionally, as it can be seen from ***Figure 2.10***, the presence of nitric oxide in the feed affected the transient behaviour of the N_2O outlet concentration at the beginning of the run, with the initial peak in N_2O concentration being absent. This phenomenon can be explained by the fact that NO has a higher oxidation power than O_2 in modifying the copper's oxidation state within the catalyst and, as a result, the N_2O outlet concentration's transient behaviour.

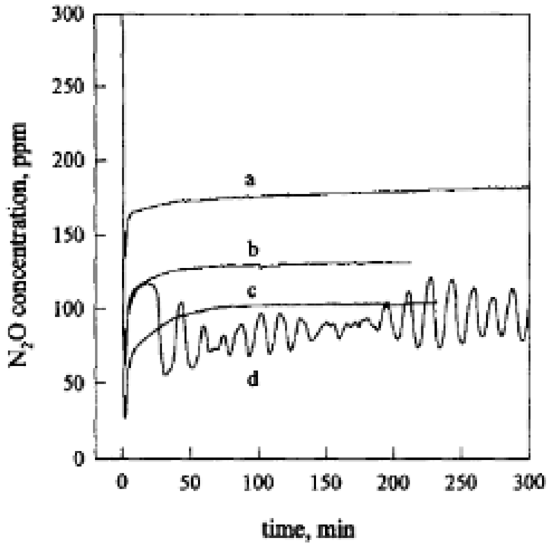

Figure 2.10 Effect of NO addition to the feed on N_2O decomposition. Feed: N_2O (300 ppm); NO (a) 5000 ppm, (b) 2000 ppm, (c) 500 ppm, (d) 0; T = 370°C. Catalyst pre-treated in He at 550°C for 2 h. [31]

In order to support their results, Ciambelli et al also proposed the first mechanistic model describing the emergence of kinetic oscillations in nitrous oxide decomposition. According to Turek et al, these authors did not observe any NO as a direct reaction product because of the low N_2O concentrations and reaction temperatures used. [32] Therefore the only components of the reaction mechanism proposed by Ciambelli et al. are adsorbed oxygen species and the gaseous reactants. They hypothesized that the oscillations of the gas phase concentration were due to periodic changes in the state of copper oxidation in the catalyst. The reaction mechanism consists of the following steps [28]:

$$N_2O + Cu^{+} \rightarrow [N_2O^{-}–Cu^{+2}] \qquad (2.7)$$

$$[N_2O^{-}–Cu^{+2}] + Cu+ \rightarrow [Cu^{+2}–O^{-2}–Cu^{+2}] + N_2 \qquad (2.8)$$

$$N_2O + [Cu^{+2}–O^{-2}–Cu^{+2}] \rightarrow N_2 + O_2 + 2Cu^{+} \qquad (2.9)$$

$$[Cu^{+2}–O^{-2}–Cu^{+2}] \rightleftarrows O_{ads} + 2Cu^{+} \qquad (2.10)$$

$$2O_{ads} \rightleftarrows O_2 \qquad (2.11)$$

The mechanism in ***Eqs. (2.7) -(2.11)***is based on the well acknowledged fact that, depending on the experimental circumstances, the Cu sites of Cu-ZSM-5 can exist as Cu^{2+} or Cu^{+} while N_2O can act as either oxidant or a reductant of the catalytic sites. In fact, step ***(2.9)*** expresses an alternative option for N_2O's reaction with the oxidized site to produce reduction to Cu^{+} and decomposition into N_2 and O_2, whereas step ***(2.7)*** represents the adsorption of N_2O on Cu^{+} sites, explaining the oxidation to Cu^{+2}. It is important to keep in mind that the reaction scheme described by ***Eqs. (2.7) -(2.11)*** involves two nearby copper sites. This assumption comes from the usually accepted conclusion concerning over-exchanged Cu–ZSM–5: at high copper loading level the catalyst is known to contain copper pairs, such as Cu^{+2}-O^{-2}-Cu^{+2}, where the extralattice oxygen (ELO) is kept bridged between Cu^{2+} ions. Additionally, it is well known that ELO readily desorbs with a simple temperature increase, resulting in the reduction of copper sites. Finally, steps ***(2.10)*** and ***(2.11)*** represent the possibility of spontaneous desorption of extra-lattice oxygen (ELO) as a dioxygen molecule from Cu^{+2}-O^{-2}-Cu^{+2} species. [28] The different N_2O reaction rates with the oxidized and reduced copper sites are thought to be the cause of the oscillations in N_2O decomposition. The transitory phase of the reduced catalyst is explained by steps ***(2.7)*** and ***(2.8),*** which are equivalent to Eq. ***(2.6).***

As mentioned earlier, although this model can predict changes in the nitrous oxide conversion, it neglects the importance of nitric oxide. Ochs and Turek's research have demonstrated that this component definitely plays a role in the emergence of oscillations. Specifically, whenever the catalyst is in the more active state, NO is always produced in proportions that may be easily detected. [29] Therefore, another important and more complex mechanism was developed accounting for the fact of the formation of NO and its role in the emerging oscillating behaviour.

2.2.2 Ochs and Turek's mechanism

For the following research, the Cu-ZSM-5 catalysts were prepared by threefold aqueous ion-exchange of Na-ZSM-5 with copper acetate solution at room temperature. The catalyst was then pretreated in flowing helium for 1 h at 500°C. Results of the catalytic tests were performed in the integral reactor at 425°C, shown on the ***Figure 2.11***, demonstrating the exit concentrations as a function of time. It is possible to distinguish between two distinct phases of catalytic activity with regard to nitrogen production, which correspond to nitrous oxide conversions of roughly 55 and 75%. During the transition from lower to higher activity, it is possible to observe a characteristic desorption of nitric oxide and higher oxygen concentrations than expected from the stoichiometry of the decomposition reaction. At the end of each high-activity period, the catalyst takes up oxygen. The right-hand part of ***Figure 2.11*** depicts the response to a step change from 1000 ppm nitrous oxide at reactor inlet to pure He in the period of lower decomposition activity. It is noticeable that the concentrations of nitrous oxide and nitrogen rapidly decreased reaching zero value, indicating that under reaction conditions, these species are not or are only weakly adsorbed. On the other hand, it can be noted that the catalyst releases oxygen and nitric oxide over a period of around 100 seconds. It's interesting to note that NO desorption is delayed, and NO and O_2 exist in equimolar amounts throughout the final desorption stage. According to previous research (Turek, 1998), this desorption pattern is most likely caused by the presence of two adspecies (atomic oxygen and NO_3) on the catalyst surface.

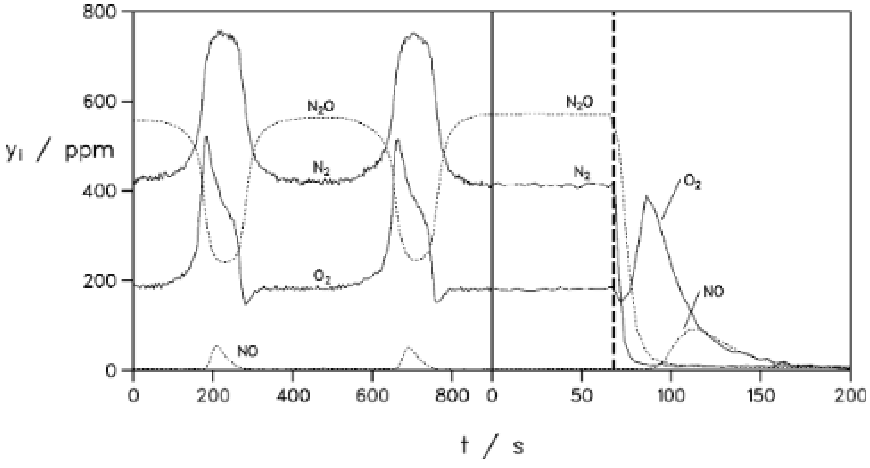

Figure 2.11 Exit concentrations in the integral reactor versus time at 425°C. Feed:1000 ppm N_2O in He. Left-hand side: Sustained oscillations. Right- hand side: Transient response at switching to pure He at reactor inlet. [29]

In order to explains the development of the sustained oscillations, Ochs and Turek proposed a reaction scheme consisting of five reactions. They also pointed out that this mechanism is as simplification of the more complex overall chemistry:

$$N_2O + 2\square \rightarrow O_{ads} + N_2 \quad (2.12)$$

$$2O_{ads} \rightarrow O_2 + 4\square \quad (2.13)$$

$$N_2O + O_{ads} \rightarrow 2NO + 2\square \quad (2.14)$$

$$NO + 2O_{ads} \rightarrow NO_{3,ads} + 3\square \quad (2.15)$$

$$NO_{3,ads} \rightarrow NO + O_2 + \square \quad (2.16)$$

This mechanism suggests that the catalyst is deactivated by the deposition of atomic oxygen on the active, monovalent copper sites. In agreement with Ciambelli et al., it is hypothesized that adsorbed oxygen takes up two active copper sites (□), resulting in the formation of a bridged copper species. The rapid development of a high oxygen coverage and subsequent decrease in the decomposition activity are caused by the relatively low rate of the recombination of atomic oxygen ***(2.13).*** Nitric oxide is created in a slow side reaction ***(2.14)*** at the expense of oxygen that has been absorbed. During the times of low catalytic decomposition activity, NO is not seen in the gas phase because it quickly reacts with adsorbed nitrate in accordance with reaction ***(2.15).*** Moreover, it is expected that the nitrate species are only stable for as long as the catalyst surface has enough adsorbed oxygen. If the coverage of atomic oxygen reaches a crucial value, nitrate immediately decomposes into NO and O_2. Nitric oxide facilitates oxygen desorption and keeps the catalyst in a high-decomposition activity state as long as it is present in the gas phase. After the reactor is cleared of NO, the oscillatory cycle starts with the intake of oxygen.

The oscillating decomposition of nitrous oxide over Cu-ZSM-5 catalysts is a very complex chemical reaction, and this research have provided some fundamental understanding of it. But there are still unanswered questions. It is undeniably true that nitrate species are produced and accumulated on the catalyst surface, but it is still unclear how these species can be stabilized at high reaction temperatures and why, on the other hand, they can spontaneously dissolve under some conditions.

2.3 Copper species on the Cu-ZSM-5 zeolite

Despite the extensive scientific research, some issues that are crucial to comprehending the Cu-ZSM-5 catalytic system are still discussed in the literature. The oxidation state of copper under various conditions, or the entire redox chemistry of copper in the zeolitic framework, is one of the most unresolved problems. The understanding of this system is crucial for defining the type of copper centres that are present in the active catalyst under varied conditions, and it serves as a starting point to the other, fiercely disputed issue of the catalytic reaction mechanism. [33] Cu-ZSM-5's excellent activity and selectivity result from the zeolite matrix's distinctive structure, which allows for the stability of polyvalent species inside the zeolite's pores. ***Figure 2.12*** is a schematic representation of how the counterion (G) could be positioned on the framework of the zeolite, in order to balance the negative charge. G could be any copper species, ranging from monomeric and dimeric oxo species to oligomers and metal-oxide clusters of various sizes, depending on the zeolite structure, the Si/Al ratio, and the copper loading. [34]

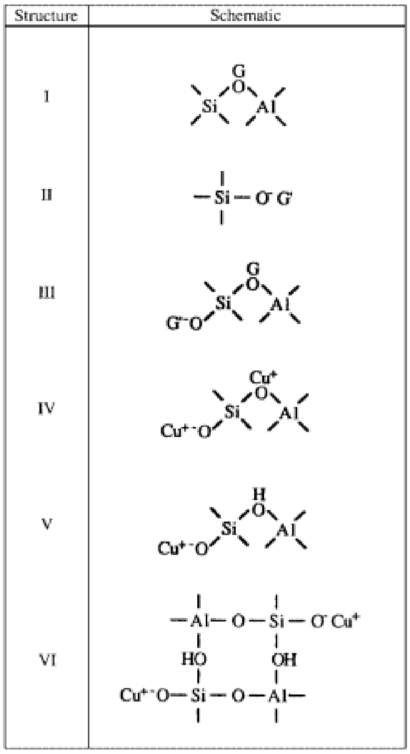

where G,G' = Na^+, H^+, Cu^+, $[Cu^{2+}(O^-)]^+$, $[Cu^{2+}(OH^-)]^+$, and $[Cu^{2+}(H_2O)_{n-1}(OH^-)]^+$

Figure 2.12 Schematic representations of sites for stabilized cations in Cu–ZSM-5. [35]

The synthesis process is important as well, because it can affect the structural composition of the zeolite and change the redox characteristics of Cu. The 2 principal methods of Cu-ZSM-5 preparation are ion-exchange and impregnation, principals of which will be describer in more details in the ***Chapter 3.1***. For instance, it is generally accepted that Cu-ZSM-5 produced via the excess ion-exchange method would encourage the development of copper dimers with extra-lattice oxygen (ELO) bridges $[Cu\text{-}O\text{-}Cu]^{2+}$, where the oxygen comes from either the zeolite framework or from structural OH groups [36]. In addition to this, the ion-exchange approach enables also the formation of distributed oligonuclear CuO species as well as single Cu^{2+} ions in structural cationic locations. These are some of the copper species that can be found in the Cu-ZSM-5 zeolite:

- Three types of double-O-bridged Cu pairs are frequently found and classified by the structural arrangement of the Cu_2O_2core atoms: bis(μ-oxo)dicopper, (μη2: η2-peroxo)dicopper, and trans(μ-1,2-peroxo)dicopper, as depicted in ***Figure 2.13*** [37].

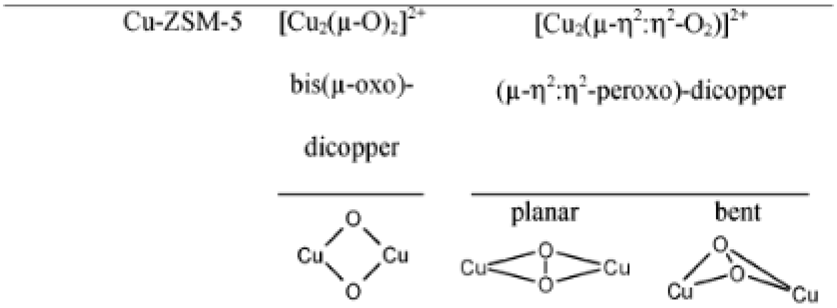

Figure 2.13 Graphic representation of O-bridged copper species in the Cu-ZSM-5 zeolite. [37]

Thanks to spectroscopic and structural characterizations, Groothaert et al. found that over-exchanged Cu-ZSM-5 zeolite contain mainly bis(μ-oxo)dicopper species. These are important because they play the crucial role of continuous O_2 production and release during steady-state reaction, in order to ensure the sustained high activity of Cu-ZSM-5. Cu-ZSM-5's low temperature peaks during thermal reduction by H_2 or CO have also been explained by the existence of these oxocation. [37]

- Yashnik et al. have demonstrated that calcined Cu-ZSM-5 catalysts contain chain-like $\bullet\bullet\bullet O^{2-\bullet\bullet\bullet}Cu^{2+}\bullet\bullet\bullet O^{2-}\bullet\bullet\bullet Cu^{2+}\bullet\bullet\bullet O^{2-}\bullet\bullet\bullet$ structures inside the zeolite channels, which are stabilized by water molecules. Due to the ease of copper reduction and reoxidation as well as their capacity to sustain bonded states of copper ions with mixed valence, these chain structures are one of the most fascinating species present on the zeolite. Most likely, samples with a Cu/Al ratio between 75 and 100% show the highest concentration of chain-like copper-oxide structures in the ZSM-5 channels. [36]

- Cu^{2+} ions are believed to be present in two forms of distorted octahedral coordination: square-pyramidal and square-plane. In Cu-ZSM-5 zeolites with low exchange levels, isolated Cu^{2+} ions with square pyramidal coordination predominate, whereas those with square-plane coordination predominate in catalysts with high Si/Al ratios and/or high copper contents. Moreover, an increase of the zeolite Si/Al ratio leads to a decrease of the number of ion exchange sites and, consequently, the concentration of isolated Cu^{2+} ions. Yashnik et al. have discovered that in samples characterized by the ratio Cu/Al<50%, the majority of copper ions are found in the form of isolated Cu^{2+} ions.[36] These ions can undergo the so-called "autoreduction" or "self-reduction," one of the most prevalent yet poorly understood processes. It implies that certain Cu^{2+} species can spontaneously convert to Cu^+ at high temperatures, usually above 673 K, in an inert environment, without the presence of a reducing agent. [34] The most reasonable explanation offered by Hall and co-workers for this simple copper reduction is that Cu^{2+} cations are connected to extra-lattice oxygen (ELO), as it can be seen from ***Eq. (2.17)***. [38] They also claimed that the release of molecular oxygen is accompanied by a reduction in the weight of the copper-exchanged zeolite. [34]

$$2[CuOH]^+ \leftrightarrow Cu^{2+}O^{2-}Cu^{2+} \leftrightarrow Cu^+\square Cu^+ + \tfrac{1}{2}\,O_2 \qquad (2.17)$$

The $Cu^{2+}O^{2-}Cu^{2+}$ species are first produced by removing water from two nearby hydroxyl-bridged species. Copper-oxo sites decompose into Cu^+ and molecular oxygen at high temperature, which desorbs from the material. The symbol □ denotes a vacancy of the extra-lattice oxygen. In general, the Si/Al ratio and the zeolite structure both influence the temperature at which autoreduction begins and the rate at which it proceeds. Thanks to some findings of infrared spectroscopy in their research, Yashnik et al. proposed that the autoreduction is favoured in materials having copper-oxo oligomers, such as the Cu-ZSM-5. This may be related to the structure of such sites having a second oxygen atom, which facilitates the release of oxygen upon heating. [34] This is an expected result since an increase of the zeolite Si/Al ratio leads to a decrease of the number of ion-exchange sites and, consequently, the concentration of the isolated Cu^{2+} ions.

- The CuO (copper oxide) species are characterized by an ionic character of the Cu-O bond, which makes it difficult of the Cu^{2+} ions to be reduced in mild conditions (particularly at low temperature). The impregnated Cu-ZSM-5 catalysts were found to have noticeable differences in their chemistry and structure with respect to the ion-exchanged samples. In particular, in the impregnated samples there is usually present a substantial amount of aggregation in the copper-containing clusters, which are preferentially located at the external surface of the material. [38] In the ion-exchange samples they can contain hydroxyl groups, that are then transformed into Cu-O-Cu species after calcination. Yashnik et al. found that the copper oxide clusters localized on the zeolite surface have been found to predominate in the samples with Cu/Al>140%.

3 Materials and Methods

3.1 Catalyst preparation methods

The preparation of catalytic materials is a complex process, the ultimate goal of which is to obtain the catalyst with high stability, activity and selectivity. In order to achieve this objective, the active phase (in this case, the metal) must be highly dispersed, resulting in an extensive specific surface area and, as a result, a maximum specific activity. For this reason, the active metal component is often deposited on the surface of a highly porous and thermostable support, that is able to not only disperse the metal but also prolong its thermal stability and, as a result, the catalyst life. [39]

Every stage of preparation, along with the quality of the raw materials, has a significant impact on the characteristics of heterogeneous catalysts. Depending on the physical and chemical properties desired in the finished composition, a particular catalyst preparation technique is chosen.[40]

There can be defined the following principal methods of synthesis:

- In an ion-exchange: in this method different ions of the same charge that were initially present in the solid are replaced by ions of positive charge in some cases (cations) and negative charge in other cases (anions) from the solution that comes in contact with the zeolite. Ion-exchange technique is widely used as a tool in order to introduce an additional "phase" that could alter the material's properties. Zeolites' ion-exchange ability is a result of the availability of additional cations that situated in the channels and cages of the zeolite, where each one of the cations has a different framework location and, consequently, bond energy.

Additionally, it should be remembered that the polarization of the support's surface varies depending on the pH level of the solution and the solid's isoelectric point.

As shown in ***Figure 3.1***, when the pH is below the isoelectric point (acidic medium), the surface will be positively charged, which will cause the surface to attract and absorb anions. When the pH is above the isoelectric point (basic medium), the surface will become negatively charged and surrounded by cations, which will cause them to be absorbed from the solution. [40]

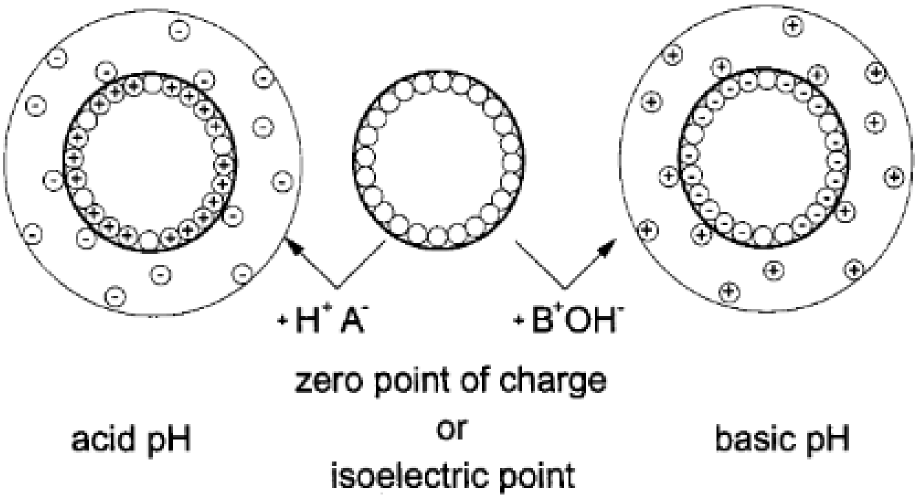

Figure 3.1 Schematic representation of a surface polarisation of a particle as a function of the solution pH. [40]

- Impregnation: there are two types of impregnation methods, based on the volume of solution used. The first one is referred to as "incipient wetness" or "dry" impregnation since the volume of the solution containing the precursor does not exceed the pore volume of the support. It can be obtained simply by nebulizing the support with the impregnating solution, while it’s kept under stirring. The second kind of impregnation, referred known as "wet" or "soaking," uses more solution than is necessary for the support's pore volume. The system is aged for a predetermined amount of time while being stirred, filtered, and dried. As a result, in addition to the solution's concentration and the support's pore volume, the concentration of metal precursors on the support will also depend on the kind and/or quantity of adsorbing sites that are present at the surface.

The temperature, which influences both the precursor solubility and the solution viscosity, are the major operating variable for both procedures. The impregnation profile of the final catalyst is determined by an appropriate control of the operating parameters during impregnation and drying.

Both of the overmentioned preparation techniques are extensively used for the synthesis of Cu-ZSM-5 catalyst, used in the decomposition reaction of N_2O. It is important to mention that the change of synthesis parameters has a major influence on the induction and modification of the oscillatory behaviour in this specific reaction. In particular, Armandi et al. demonstrated that the catalysts needed to exhibit a series of peculiar characteristics (dependant on the type of preparation) in order for the oscillations to take place. For example, a minimum amount of copper must first be present in order to obtain a periodic oscillating pattern of the N_2O concentration at the reactor outlet as well as to acquire a particular activity in the reaction. [8]

Many studies have used the ion-exchange method to synthesize Cu-ZSM-5 since it is thought to encourage the formation of $[Cu\text{-}O\text{-}Cu]^{2+}$ species, which are believed to actively participate in the reaction. This method requires copper cations to be present in excess with respect to available zeolite sites (i.e., an "over-exchanged" metal-zeolite). In contrast to the impregnation method of Cu-ZSM-5 preparation, where resulting copper is usually present in large aggregates at the zeolite external surface, an over-exchanged Cu-ZSM-5 has copper present in small clusters or as isolated Cu^+/Cu^{2+} ions (depending on the reaction atmosphere). [8]

For the scope of my Master thesis activities, both of overmentioned techniques were used to synthesise Cu-ZSM-5 zeolites, which were subsequently employed in the catalytic decomposition reaction of N_2O. The aim of the current work is to investigate the dependence of change in certain synthesis parameters (Cu content, Si/Al ratio, type of synthesis etc.) of the catalyst on the oscillatory behaviour that it induces in the nitrous oxide decomposition.

Three types of NH_4-ZSM-5 with different Si/Al ratios (***Figure 3.2***) were used as parent zeolites while copper (II) acetate monohydrate, whose properties are listed in ***Table 3.1***, was used as copper precursor.

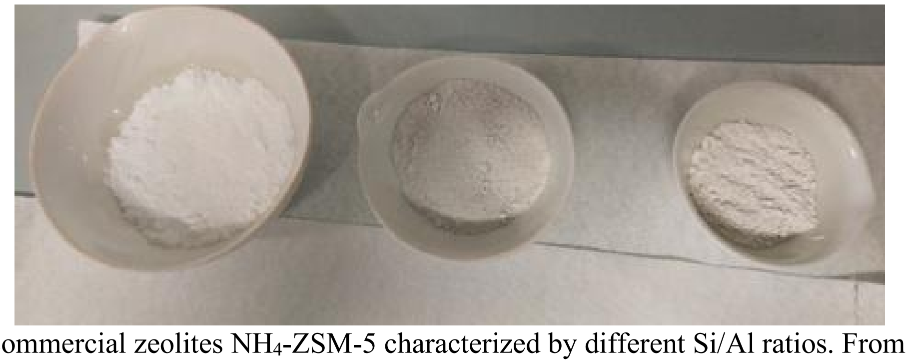

Figure 3.2 Commercial zeolites NH_4-ZSM-5 characterized by different Si/Al ratios. From left to right: Si/Al = 12, Si/Al = 25 and Si/Al = 40.

Before being employed in the synthesis, the parent zeolites were calcinated at 550°C for 5 hours in order to obtain the protonic form of the zeolite (H-ZSM-5).

Table 3.1 Properties of Copper (II) acetate monohydrate

Chemical Formula	$Cu(CH_3COO)_2•H_2O$
Molecular weight	199.65 g/mol
Appearance	Blue crystals
Melting point	116 °C
Boiling point	240 °C
Density	1.88 g/cm^3

To prepare the ion-exchanged samples, $Cu(CH_3COO)_2•H_2O$ was mixed with 100 mL of bidistilled water and 1 g of H-ZSM-5. Subsequently, the mixture was kept under vigorous stirring at room temperature (RT) for 2h. Finally, the ion-exchanged zeolite was recovered by centrifugation and washed three times with bidistilled water to eliminate the precursor that hasn't been exchanged, followed by drying overnight at 60 °C in the oven.

Similarly to the ion-exchanged samples, the impregnated zeolites were obtained by mixing $Cu(C_2H_3O_2)_2•H_2O$ with 100 mL of bidistilled water and 1 g of H-ZSM-5. The solution was kept under vigorous stirring at 80 °C, until complete water evaporation (***Figure 3.3***). Subsequently, the zeolites were dried overnight at 60 °C.

Figure 3.3 Synthesis of impregnated samples. A hot plate stirrer enables both the mixing and the heating of the solution, until complete evaporation of the water.

Unlike the previous method, the impregnated samples did not undergo any washing and centrifugation. This means that all the introduced copper precursor is expected to be fully present in the sample, resulting in the higher contents in the catalysts obtained by this method. The nomenclature of the samples was decided according to the following scheme:

ZXX_IMS/SIS_YY_W

Where:

- XX - Si/Al ratio of the parent zeolite, with the possible values of 12, 25 or 40.
- IMS/SIS - synthesis method (impregnation or ion-exchange respectively).
- YY - type of copper precursor used in the synthesis.
- W - quantity of precursor in grams.

For example, Z12_IMS_Ac_0,2 is an impregnated zeolite (IMS) which was synthetized by using a parent zeolite having a Si/Al ratio equal to 12. Moreover, 0,2 g of copper (II) acetate monohydrate (Ac) were used as precursor.

It's possible to calculate the theoretical amount of copper (in percentage) introduced into the samples, by utilising this simple equation:

$$w_{Cu}(\%) = \frac{m_{precursor}}{PM_{precursor}} * PM_{Cu} * 100 \tag{3.1}$$

Therefore, it's possible to classify the samples according to the theoretical percentage of copper introduced during the synthesis. ***Table 3.2*** reports the synthetized samples as well as the molarity on the initial solution (denoted as M), based on a volume of 100 mL.

Table 3.2 List of the synthetized samples, characterized by the theoretical quantity of copper precursor

SAMPLE	Theoretical w_{Cu} (%)	M (mmol/L)
Z12_IMS_Ac_0,2	6,4	10
Z12_SIS_Ac_0,2	6,4	10
Z25_IMS_Ac_0,2	6,4	10
Z25_SIS_Ac_0,2	6,4	10
Z40_IMS_Ac_0,2	6,4	10
Z40_SIS_Ac_0,2	6,4	10
Z12_IMS_Ac_0,1	3,2	5
Z12_SIS_Ac_0,1	3,2	5
Z25_IMS_Ac_0,1	3,2	5
Z25_SIS_Ac_0,1	3,2	5
Z40_IMS_Ac_0,1	3,2	5
Z40_SIS_Ac_0,1	3,2	5
Z25_IMS_Ac_0,05	1,6	2,5
Z40_SIS_Ac_0,05	1,6	2,5

As it can be seen, three different quantities of copper acetate (II) monohydrate have been used, to better investigate the effect of the precursor loading on the oscillatory behaviour. For the samples with 0,2 and 0,1 g of precursor, all the three parent zeolites have been employed, and each of them had been synthetized both with the impregnation and the ion-exchange techniques. When it comes to the lower quantity of precursor (0,05 g) only the zeolites with Si/Al ratios of 40 and 25 have been used, since among all the samples, they're the one who convert N_2O the most (as it will be seen in ***Chapter 4***).

In addition to this, the following samples have been synthetized in an effort to investigate the effect of every possible parameter:

- **Z25_SIS_Ac_0,5**: This sample had been synthetized by ion-exchange with the excess quantity of precursor (w_{Cu} = 15,9 %), in order to investigate better the effect of the precursor.
- **Z25_SI50°C_Ac_0,2**: during the ion-exchange procedure of this sample, the temperature was kept at 50°C to investigate the influence of temperature on the level of Cu loading during the ion-exchange. In all the other cases of ion-exchanged zeolites, the mixture was kept at ambient temperature.
- **Z25_IMS_Nt_0,2**: in this case copper nitrate was used as a precursor instead of copper acetate. This sample was prepared by impregnating the zeolite with 0,2 g of copper nitrate trihydrate (Nt).
- **NS1_IMS_Ac_0,2**: in this case the parent zeolite is a porous silicate with the MFI type of framework, which has been synthetised by following the work of Kremer et al [41]. No aluminium is present in this zeolite; therefore the Si/Al ratio tends to infinity. The synthesis procedure was performed as the following: first, the silicon precursor (tetraethyl orthosilicate or TEOS) is hydrolysed in the presence of tetra propylammonium hydroxide (TPAOH). The solution was mixed at ambient temperature for 24h, in order to favour the creation of zeolite nuclei. Subsequently, Triton X-100 was added to the mixture and stirred for other 24h. Finally, crystallization has been performed at 110°C in an autoclave for 72 h. After this, the product was separate from the solution by centrifugation, while washing it a few times with deionized water to remove any precursor residual and subsequently calcinated in the oven at 550°C. The obtained zeolite is impregnated with 0,2 g of copper (II) acetate monohydrate according to the method described earlier.

3.2 Experimental Setup

In ***Figure 3.4*** it's possible to observe the experimental setup that has been employed both for the calcination and the catalytic tests of the samples.

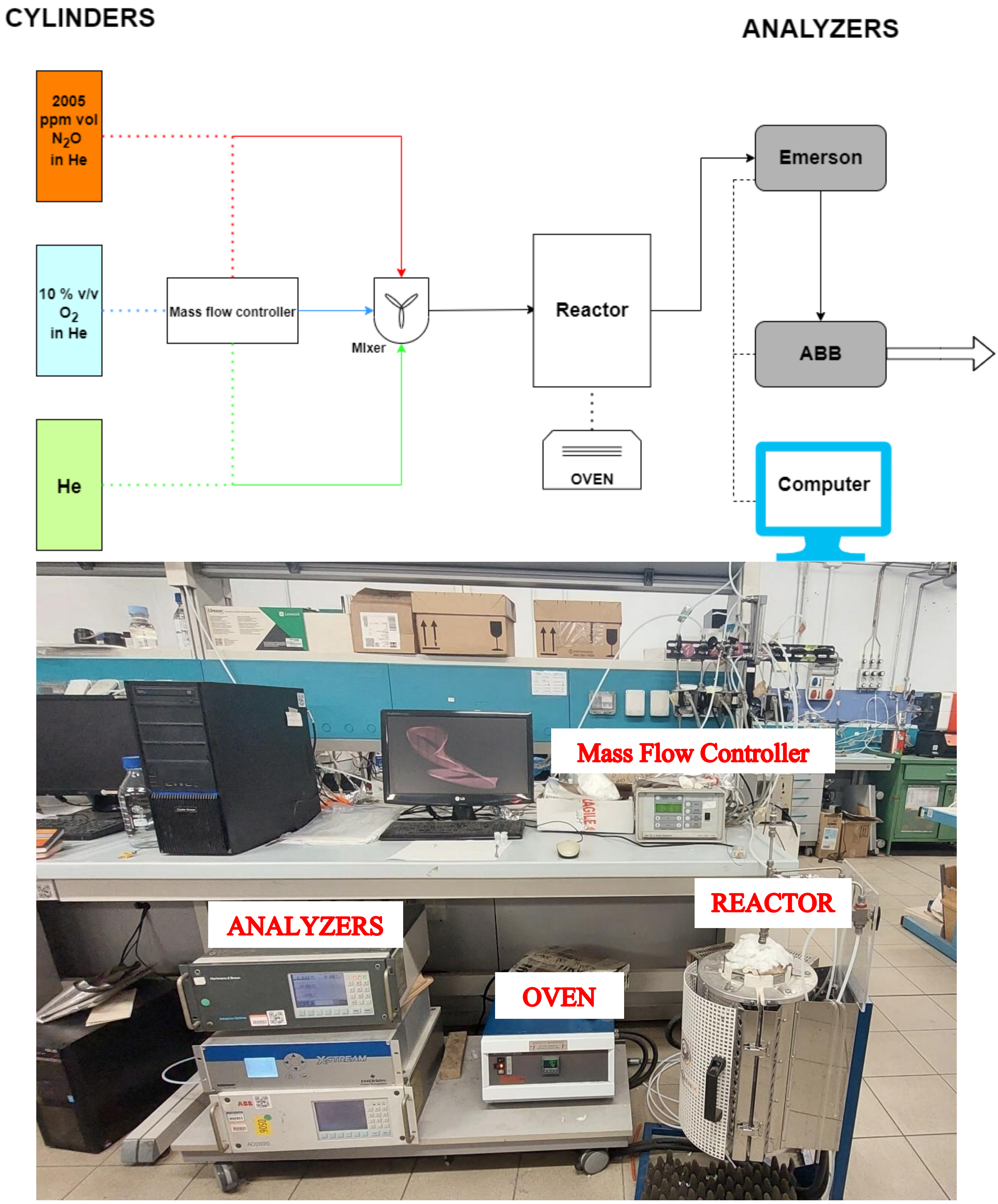

Figure 3.4 Experimental setup. Above: schematic representation. Below: photograph of the system

Three cylinders provide the system with O_2, N_2O and He gases. They are linked to the respective mass flow Brooks, which are controlled by manual valves and a Brooks mass controller. The gases are sent to the reactor, which is heated thank to a Lenthon Thermal Design oven.

The concentrations of the gases utilized at the reactor inlet at the following:

- 1000 ppm of N_2O for the catalytic tests
- 20 mL/min of O_2 for the calcination procedure

The desired concentration of the O_2 and N_2O were obtained by diluting the concentration of the gases coming from the cylinders (***Figure 3.4***) with pure He stream. The flow exiting from the reactor passes through three different analysers in series with the following characteristics:

- EMERSON XSTREAM monitors the concentrations of O_2, N_2O, NO and NO_2
- ABB monitors the concentrations of N_2O

The analysers are connected to the computer which records the data while the exiting stream is sent to the exhaust.

3.2.1 Calcination of the samples

Calcination was performed for all the synthetized samples after the ion-exchange or impregnation procedure, in order to eliminate the organic species deriving from the precursor. The powder is placed upon the catalytic bed of a tubular quartz reactor, having a diameter of 4 mm (***Figure 3.5***).

Figure 3.5 Tubular quartz reactor for calcination

The calcination process consists of the following step:

1. Reducing atmosphere: the reactor is heated up until 550°C with a ramp of 5°/C while the catalyst is treated by a He flux of 200 mL/min. Once the temperature was reached, these conditions are maintained for 2h.

2. Oxidizing atmosphere: 200 mL/min of a mixture containing 1% v/v of O_2 is sent to the reactor for 2h at 550°C, in order to eliminate completely the organic residue.

3. Cooling of the reactor until ambient temperature.

After calcination, the zeolites were compressed and sieved to an average size of 250 µm prior to the catalytic experiments.

3.2.2 Catalytic tests

A tubular quartz reactor with a diameter of 4 mm has been used for the catalytic tests. The catalytic bed is constituted by glass wool, which was inserted manually to form the support for the catalyst pellets that were subsequently introduced (***Figure 3.6***).

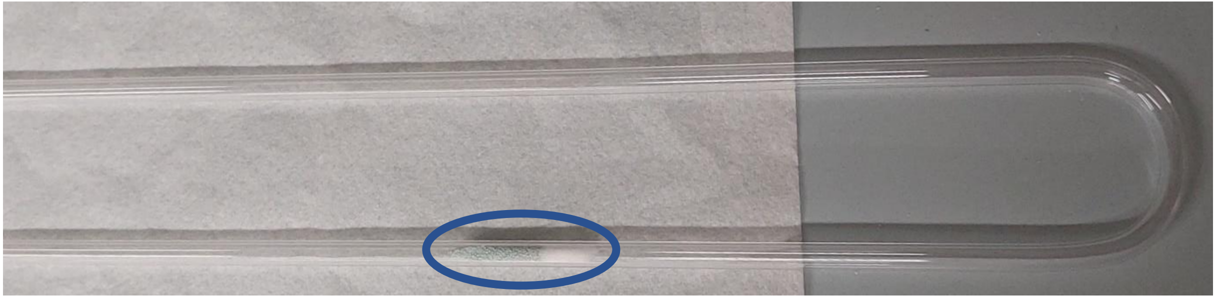

Figure 3.6 Tubular quartz reactor for the catalytic tests

All the tests have been conducted by using 100 mg of calcinated zeolites, respecting the following steps:

1. Pre-treatment, where the reactor was heated up until 550°C with a ramp of 5°/C while the catalyst was treated by flowing in He flux of 200 mL/min. Once the temperature is reached, these conditions are maintained for 2h.
2. Cooling of the reactor until the desired temperature for the test.
3. Catalytic test, flowing of 200 mL/min of N_2O with a concentration of 1000 ppm in He, while the reactor temperature was kept isothermal during the whole duration of the test. The mixture is characterized by a W/F ratio = 0,5 g*min/L, where W is the catalyst weight and F is the volumetric flow rate of the feed.
4. Cooling of the reactor until ambient temperature.

3.3 Physicochemical characterizations

All the synthesized samples have been analysed using a multi-technique approach, in order to have a comprehensive understanding of the properties of the obtained material.

3.3.1 H_2-TPR (Temperature Programmed Reduction)

The catalysts reducibility was tested by H_2-TPR (Temperature Programmed Reduction) on a TPD/R/O instrument represented in ***Figure 3.7***.

Figure 3.7 Thermoquest CE instruments TPDRO 1100 employed for the H_2-TPR analysis

The TPR analysis was carried out by feeding 20 cm^3/min of 5% v/v H_2 in Ar to the sample holder and under a gradual heating until 800 °C, at a rate of 10 °C/min. Prior to the analysis, two types of pre-treatments have been applied to the catalysts:

- **Reductive pre-treatment** - a flux of 20 cm^3/min of He gas was sent to the equipment, while it was heated with a ramp of 10°C/min until reaching the temperature of 550°C. These conditions were held for 1 h.
- **Oxidative pre-treatment** - a flux of 20 cm^3/min of O_2 gas was sent to the equipment, while it was heated with a ramp of 10°C/min until reaching the temperature of 550°C. These conditions were held for 30 min, after which the sample was cooled with O_2 until reaching 40°C and cleaned with a flux of He.

The 2 types of pre-treatments were used in order to investigate the possible changes in the reducibility of Cu present in the catalyst prepared by changing the Si/Al ratio and the preparation method.

3.3.2 FT-IR spectroscopy using CO as probe molecule.

The Fourier transform infrared spectroscopy (FT-IR) has been used for the evaluation of surface properties of the obtained materials. The FT-IR spectra were recorded at 2 cm^{-1} resolution on a BRUKEREQUINOX-66 spectrometer, equipped with a mercury cadmium telluride (MCT) cryodetector (***Figure 3.8***).

Figure 3.8 FT-IR setup for analysis. On the right: BRUKEREQUINOX-66 spectrometer. On the left: vacuum line

When exposed to air or, in the case of supported catalysts, during the deposition of the active phase, the solid surfaces are typically covered with adspecies, most frequently water and carbonates. As a consequence, the samples under investigation are often activated at high temperatures in order to provide a clean surface, prior to IR analysis. [42] First, the calcinated zeolites were pressed as self-supported thin wafers. The preparation procedure consisted of first depositing the small amount of finely grinded powder in uniform way forming a very thin layer on the top of stainless-steel disc. Afterwards, another disc was carefully placed on top of it, and then transferred to the hydraulic press where pressure of max 2000 kg/cm^3 was applied for 10 seconds. The preparation of the pellets was done in a way to keep a specific surface density under 10 mg/cm^2. Subsequently, the resulting pellets were inserted in a gold envelope in order to be mechanically protected and outgassed at 500 °C for 2 h in a homemade quartz cell equipped with KBr windows (***Figure 3.9***).

The IR study of carbon monoxide adsorption was performed at RT allowing the interaction of CO with all the available Cu surface sites. After the pre-treatment procedure, the IR cell was moved to the spectrometer and connected to the vacuum line, where the spectra were recorded by dosing at room temperature increasing amounts of CO (1–3000 Pa equilibrium pressure range) on the previously outgassed samples.

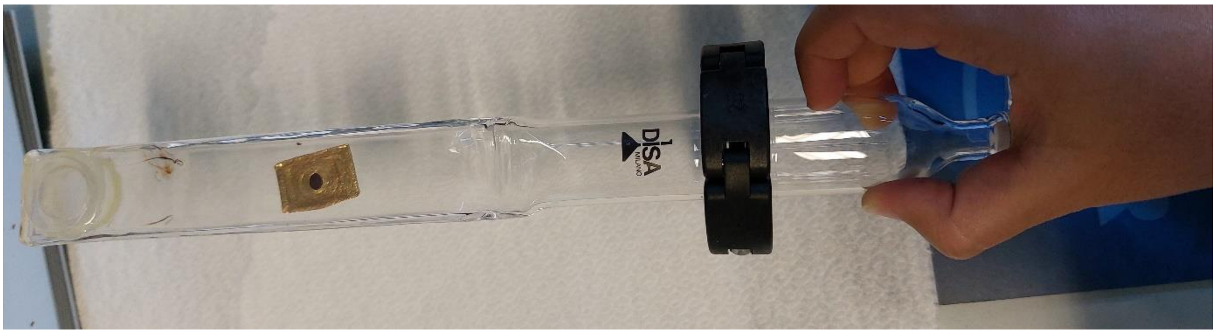

Figure 3.9 Handmade quartz cell with KBr window used for FT-IR measurements, containing the self-supporting pellet.

3.3.3 N_2 physisorption at 77 K

The catalysts specific surface area (SSA) was measured by N_2 physisorption at 77 K by employing the equipment represented in ***Figure 3.10***. Before this, the calcinated catalyst have all been pre-treated by N_2 at 200°C for 2 h. This step is important because it ensures that all of the physiosorbed species are removed from the surface of the adsorbent, while avoiding irreversible changes of the surface or the solid structure. [43]

Figure 3.10 Picture of Tristar II 3020 Micromeritics, the equipment employed for the physisorption.

Physisorption occurs whenever an adsorbable gas (the adsorptive) is brought into contact with the surface of a solid (the adsorbent). It is common practice to study physical adsorption at temperatures that are close to or equivalent to the boiling point of the related liquid (77 K in case of N_2). [44] Adsorption isotherms display in graphical form the amount adsorbed plotted against the equilibrium relative pressure (p/p_0), where p_0 is the saturation pressure of the pure adsorptive at the operational temperature. Their characteristic shapes provide an important preliminary information about the pore structure of the analysed material. ***Figure 3.11*** depicts 6 types of physisorption isotherms defined by IUPAC. [43]

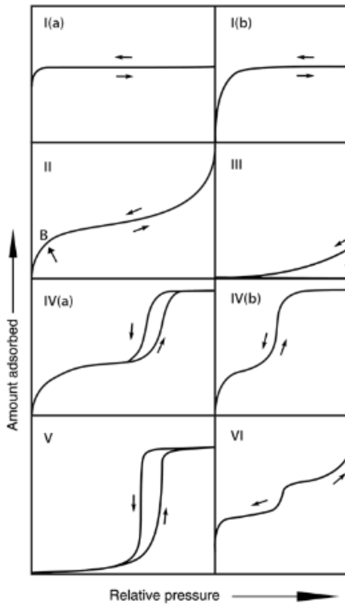

Figure 3.11 Types of physisorption isotherms. [43]

- **Reversible Type I** – they can be found for microporous solids having relatively small external surfaces, such as molecular sieve zeolites and some types of porous oxides. In particular, type I(a) isotherms are given by microporous materials with mostly narrow micropores (of width <~ 1 nm), while type I(b) isotherms are found with materials having pore size distributions characterized by a broader range, including wider micropores and possibly narrow mesopores (<~ 2.5 nm).
- **Reversible Type II** – they are given by the physisorption of the majority of gases on nonporous or macroporous adsorbents. If the knee (point B) is sharp, it usually means that the monolayer coverage has been completed. On the other hand, a more gradual curve (less pronounced point B) is a sign of the beginning of multilayer adsorption.
- **Type III** - there is no discernible monolayer formation. The adsorbent-adsorbate interactions are rather weak, and the adsorbed molecules are grouped around the most favourable sites on the surface.
- **Type IV** – they are usually generated by mesoporous adsorbents such as many oxide gels and mesoporous molecular sieves. In this case, the initial adsorption on the mesopore walls is followed by pore condensation, in which a gas condenses to a liquid-like phase in a pore at a pressure p that is lower than the saturation pressure p0 of the bulk liquid. A final saturation plateau, which can vary in length, is a typical characteristic of Type IV isotherms. Type IV(a) isotherms are characterized by hysteresis, which occurs when the pore width is greater than a critical value. In the case

of nitrogen adsorption in cylindrical pores at 77 K, hysteresis happens if the pores are wider than 4 nm. Type IV(b) isotherms are completely reversible and are observed for adsorbents with mesopores of smaller width.

- **Type V** - it can be attributed to relatively weak adsorbent–adsorbate interactions.
- **Reversible Type VI** – it represents a layer-by-layer adsorption on a highly uniform nonporous surface. The sharpness of the step in this type of isotherm depends on the system and the temperature.

The catalysts specific surface area (SSA) was calculated according to the BET (Brunauer-Emmett-Teller) method. In the BET theory, it is assumed that there is a multilayer adsorption in which all layers are in equilibrium and do not interact with each other. In particular, the molecules in the initial layers act as sites for adsorption for molecules in the upper layers. The BET equation is defined as follows: [45]

$$\frac{P/P_0}{n(1-P/P_0)} = \frac{1}{n_m C} + \frac{C-1}{n_m C}\left(\frac{P}{P_0}\right) \tag{3.1}$$

where P/P_0 is the relative pressure, n is the specific amount of the adsorbed gas, n_m is the monolayer capacity of the adsorbed gas, and C is the BET constant, which is exponentially related to the energy of monolayer adsorption. From the parameter C, the shape of an isotherm in the BET range can be obtained. The BET method application process consists of two steps. First of all, the physisorption isotherm (***Figure 3.11***) is converted into a "BET plot," from which the BET monolayer capacity, n_m, can be calculated. The BET-area is estimated from n_m by using ***Eq. (3.2),*** after choosing a suitable value for average area, σ_m (molecular cross-sectional area), occupied by the adsorbate molecule in the complete monolayer:

$$a_s = n_m L \sigma_m / m \tag{3.2}$$

where L is the Avogadro constant and m is the mass of adsorbent.[45]

3.3.4 XRD (X-Ray Powder Diffraction)

The XRD (X-Ray Powder Diffraction) technique is used to elucidate the crystalline nature of materials. The XRD instrument (***Figure 3.12***) emits X-Rays using the radiation source given by Cu anode ($K\alpha = 1.5418$ Å), which fall over the sample and diffract in a pattern characteristic to its structure. The result obtained is called diffractogram, which plots the intensity of the diffraction pattern against the angle of the detector, 2θ. The instrument is working at 40 kV and 40 mA. Bragg-Brentano geometry was used acquiring the XRD pattern in the range of 5–70° 2θ angles using the 1/4-1/4 pair of optical slits.

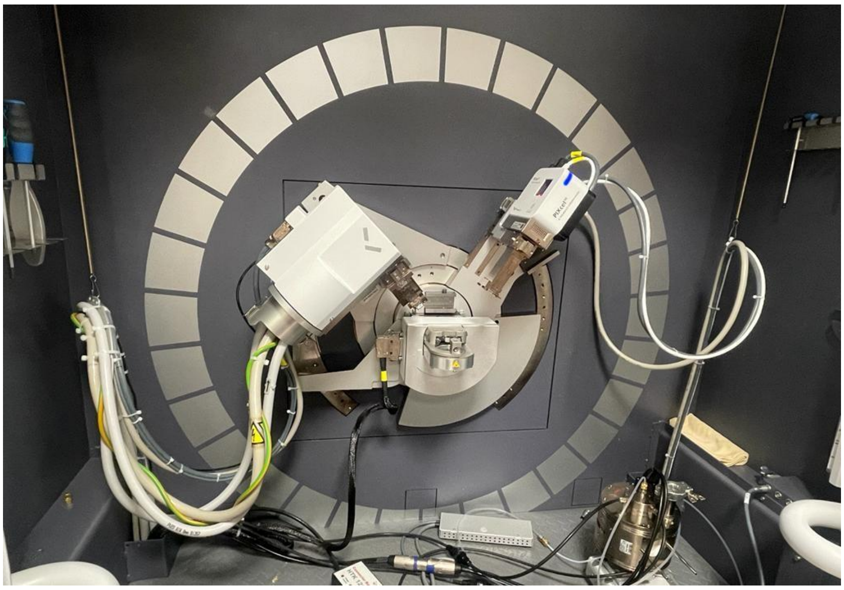

Figure 3.12 XRD instrument

Comparing the position of the reflections in the obtained patterns with the XRD patterns of parent (non-exchanged) samples of the XRD patterns of MFI present in the literature provided us with the information of the possible presence of CuO deposited on the surface of the zeolites, if the corresponding to it additional peaks were detected.

3.3.5 EDX and XRF

The copper loading of each sample was measured by means of two types of analysis: EDX (energy dispersive X-ray) and XRF (X-Ray fluorescence) spectroscopies, and the results of those analysis were compared with each other. In the case of EDX the JEOL JSM-IT200 instrument is used, which is a rugged scanning electron microscope with a tungsten source capable of resolution below 10 nm. For this analysis the small amount of each sample was pelletized and then deposited on the metal stabs, covered with carbon tape. Three different areas of about 0,1 mm^2 were analysed for each of the samples and the resulting Cu % loading value is a media value of these measurements.

XRF is a non-destructive analytical technique used to identify the elemental composition of materials. The fluorescence (or secondary) X-ray that a sample emits when it is energized by a primary X-ray source is measured by the analysers, in order to determine the chemistry of the sample. This method is ideal for the quantitative and qualitative examination of materials' composition since each element in a sample produces a distinct set of characteristic fluorescence X-rays ("a fingerprint"). The samples for XRF analysis were prepared by first mixing in the mortar 100 mg of the analysed catalyst together with the wax powder in the proportion of 1:1,1. Then the obtained mixture was transferred to the sample holder, filled up with the boric acid, and then put under the hydraulic press for 2-3 minutes.

4 Experimental Results

4.1 Results of the physiochemical characterizations

This section provides the results obtained by the physiochemical characterizations, which were previously described in ***Chapter 3.3***.

4.1.1 XRD results

The XRD analysis was carried out in order to check the crystallinity of the different Cu-ZSM-5 catalysts (Si/Al = 25) and the possible formation of metal oxides.

Figure 4.1 shows the XRD patterns of the commercial zeolites used for the synthesis, which are characterized by three different Si/Al ratios.

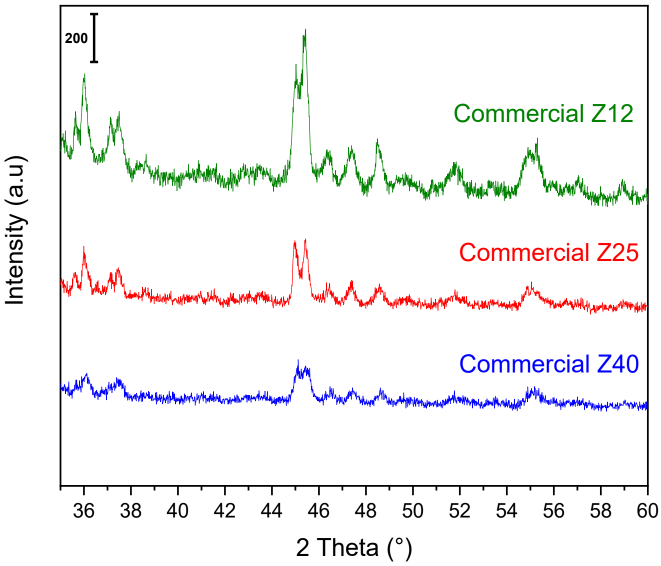

Figure 4.1 XRD patterns of the commercial zeolites.

As it can be clearly seen from ***Figure 4.1***, all three commercial zeolites samples exhibit the XRD patterns of the MFI zeolitic topology with an orthorhombic symmetry (signals at 2θ Ranged 7–9°, 23–25° and 45°), showing a high crystallinity degree. [46]

Figure 4.2-Figure 4.5 show the XRD spectra of all the samples which have been synthetized starting from the three parent zeolites. The samples in each figure have all been synthetized with the same quantity of copper precursor, varying the Si/Al ratio and the type of synthesis (impregnation or ion-exchange).

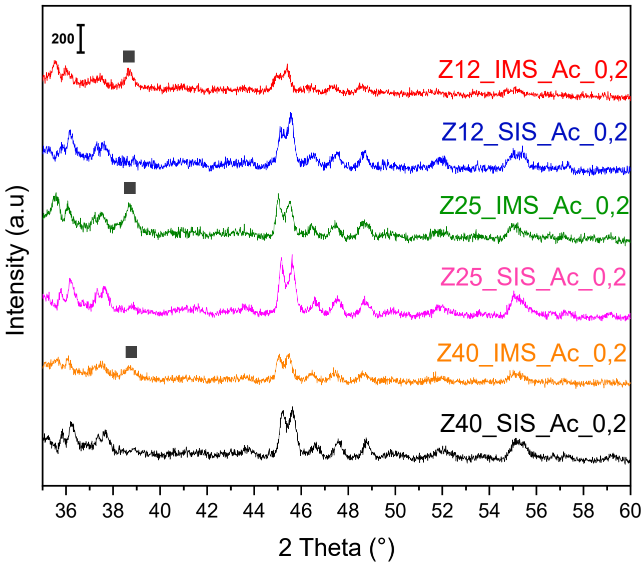

Figure 4.2 XRD patterns of the zeolites synthetized with 0,2 g of precursor.

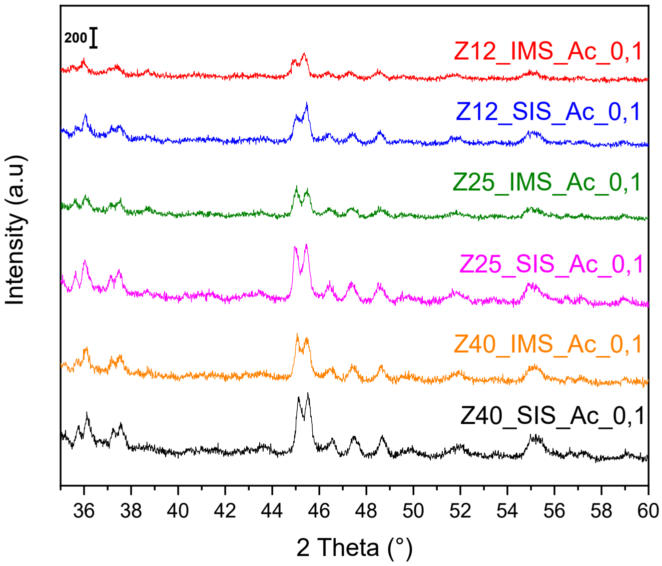

Figure 4.3 XRD patterns of the zeolites synthetized with 0,1 g of precursor.

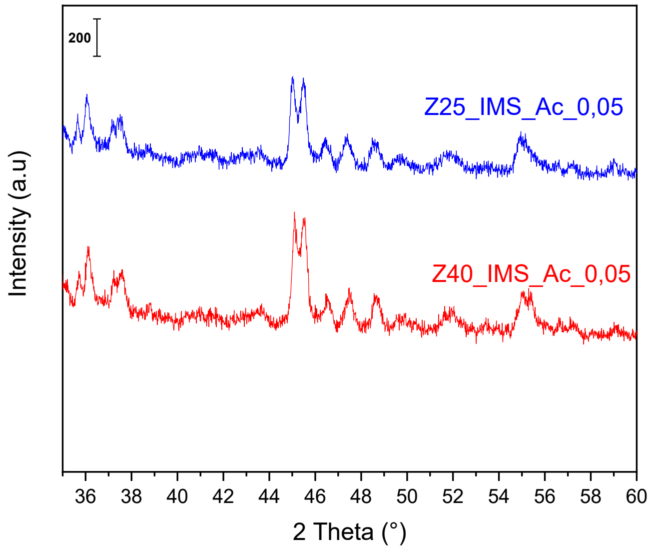

Figure 4.4 XRD patterns of the zeolites synthetized with 0,05 g of precursor.

All the diffractograms of these samples exhibit the XRD patterns of the MFI zeolitic topology, which can be seen in ***Figure 4.1***. This confirms that the utilized synthesis procedures did not affect the original structure of the zeolite.
Out of all the samples synthetized with 0,2 g of precursor (**Figure *4.2***), it's possible to notice that only the ones prepared with impregnation exhibit a peak at 2θ=38,8°, which corresponds to the plane (111) of CuO. The presence of CuO clusters in this impregnated samples is also supported by the H_2-TPR results, due to the peaks at 250-270 °C. This feature is absent in the impregnated samples prepared with 0,1 and 0,05 g of precursor. This could be due to the fact that CuO is present in these samples as small and dispersed particles which can't be detected by the instrument. In fact, XRD is a bulk sensitive technique which requires crystallites of minimum dimensions near 5 nm. [47]
The diffractograms of the remaining samples are depicted in **Figure *4.5***.

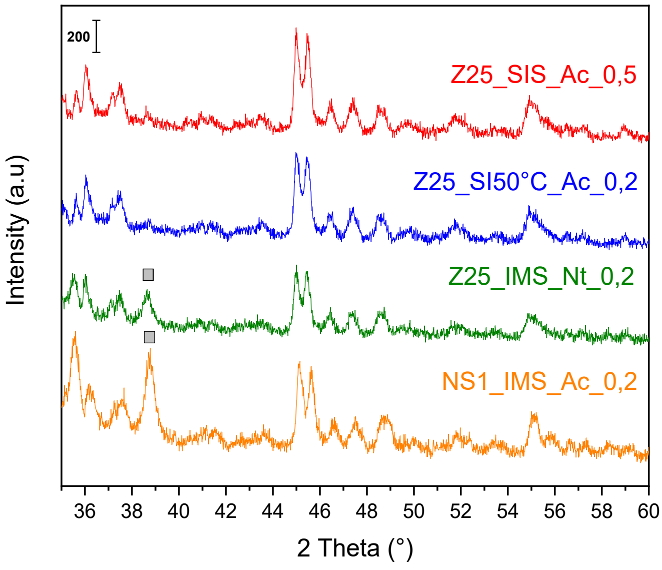

Figure 4.5 XRD patterns of the remaining samples.

Even in this case the MFI structure has been preserved in all the analysed samples. In addition to this, Z25_IMS_Nt_0,2 and NS1_IMS_Ac_0,2 exhibit a noticeable peak at 2θ=38,8°, similarly to the impregnated samples synthetized with 0,2 g of precursor, evidencing the presence of CuO clusters.

4.1.2 H_2-TPR results

The results of the H_2-TPR analysis are divided according to the type of pre-treatment used (in He or O_2 atmosphere), which is used to eliminate any humidity or impurities in the zeolite before the actual reductive analysis phase. Each curve obtained by the instrument can be seen as the sum of different curves (represented by the dotted lines), which are representative of the most significant peaks. This is done through a peak deconvolution process, which allows to identify the different contributions which make up the TPR spectra. Finally, for each sample the H_2 consumption has been calculated by integrating the area below the TPR spectra. The obtained results are later used to calculate the Cu/H_2 ratio and the %Cu(II) in ***Chapter 4.1.3***.

4.1.2.1 *Reducing (He) pre-treatment*

Figure 4.6-Figure 4.20 report the H_2-TPR spectra of the impregnated samples, starting from the ones synthetized with the higher nominal quantity copper precursor.

In zeolites, the reduction of copper species typically takes place in two temperature ranges: below 300 °C, where Cu^{2+} is reduced to Cu^{+} and/or to Cu^{0}, and above 300 °C, where Cu^{+} is reduced to Cu^{0}. In the majority of cases, the reduction ends between 400 and 450 °C, which is to be expected for samples with an excess amount of copper. [8]

As it was explained in ***Chapter 2.3***, at least four different copper species may be present in the samples:

- exchanged copper (II) ions (Cu^{2+})
- exchanged copper (I) ions (Cu^{+})
- segregated CuO particles, which may be different in size and location (inside or outside the pores)
- Double-O-bridged Cu pairs with ELO

Figure 4.6-Figure 4.8 depict the TPR spectra of the impregnated samples, synthetized with 0,2 g of precursor. The graphs of each group share the same scale with the equivalent samples pre-treated in O_2, in order to allow a better comparison between them.

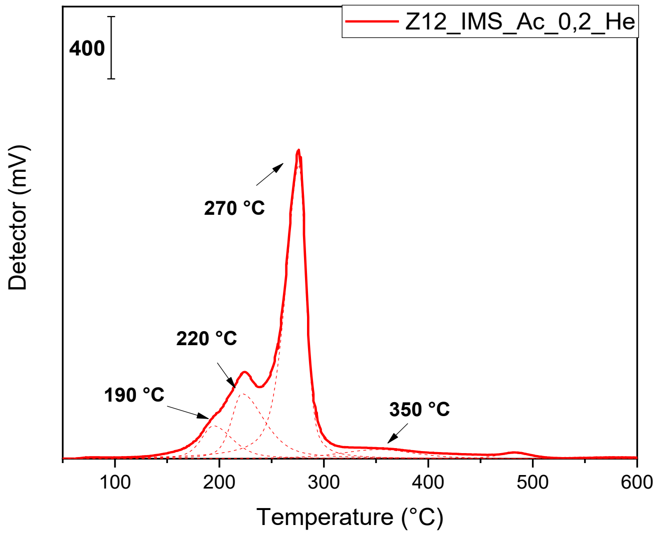

Figure 4.6 H_2-TPR spectrum of Z12_IMS_Ac_0,2 sample pre-treated in He at 550 °C.

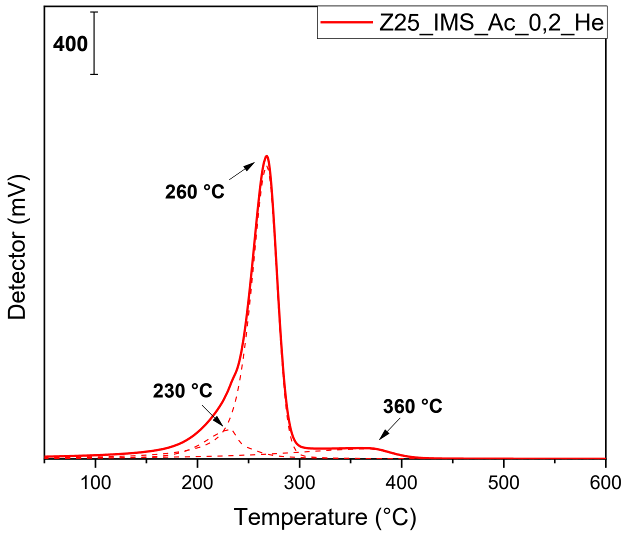

Figure 4.7 H_2-TPR spectrum of Z25_IMS_Ac_0,2 sample pre-treated in He at 550 °C.

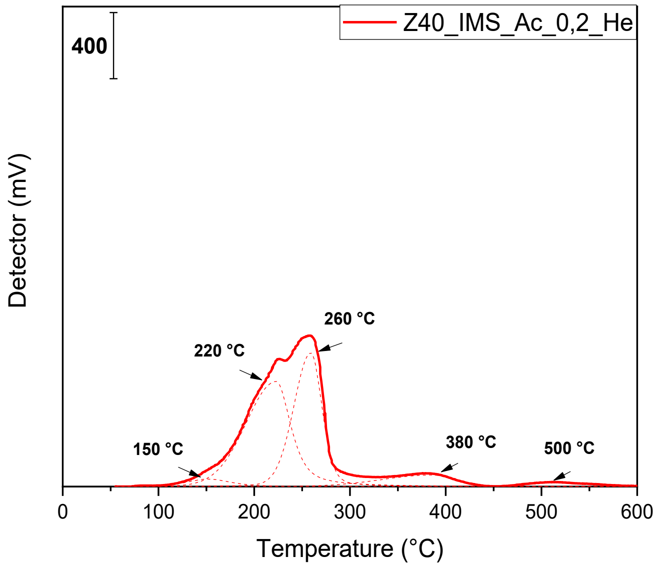

Figure 4.8 H_2-TPR spectrum of Z40_IMS_Ac_0,2 sample pre-treated in He at 550 °C.

As it can be seen from the figures above, all the impregnated samples with 0,2 g of precursor exhibits a central and sharp peak at 260 and 270°C. According to the literature, this peak corresponds to the autocatalytic reduction process ***(4.1)*** involving the CuO clusters present within the zeolite channels [48].

$$CuO + H_2 \rightarrow Cu^0 + H_2O \qquad (4.1)$$

It is observed that the samples containing copper oxide can exhibit the TPR peak characteristic of CuO species at slightly different temperature. This may be due to the different bonding strengths of copper oxide inside the zeolite, which mostly depend on the dispersion of CuO species. Usually, low copper concentrations in Cu-ZSM-5 do not include such CuO cluster species. [49] The asymmetry of the main peak in the sample Z40_IMS_Ac_0,2 may be due to the presence of CuO particles characterized by different sizes.

The peaks at lower temperature (T < 250 °C) are due to the reduction of Cu^{2+} to Cu^{+}, while at higher temperature (T > 300 °C) the reduction of Cu^{+} to Cu^{0} occurs. The following are the reactions responsible for the reduction process of copper ions in zeolites, according to previous studies by Tounsi et al. and Delahay et al.[50] :

$$Cu^{2+} + \frac{1}{2} H_2 \rightarrow Cu^{+} + H^{+} \qquad (4.2)$$

$$Cu^{+} + \frac{1}{2} H_2 \rightarrow Cu^{0} + H^{+} \qquad (4.3)$$

Moreover, as it can be seen from ***Figure 4.6***, the Z12_IMS_Ac_0,2 sample exhibits the most noticeable and sharpest peak at 270°C, which is attributed to the reduction of CuO cluster. This is due to the fact that Z12_IMS_Ac_0,2 is characterized by the biggest amount of Al sites, which allow the deposition of CuO, as it was also demonstrated by the XRD analysis (***Figure 4.2***). The peak correspondent to this species declines in intensity with the increase of the Si/Al ratio.

Figure 4.9-Figure 4.11 represent the H_2-TPR spectra of the impregnated samples synthetized with 0,1 g of copper precursor:

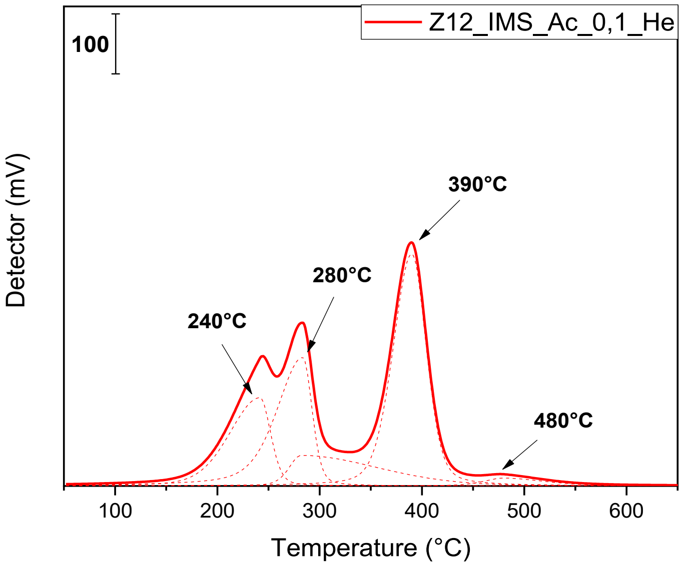

Figure 4.9 H_2-TPR spectrum of Z12_IMS_Ac_0,1 sample pre-treated in He at 550 °C.

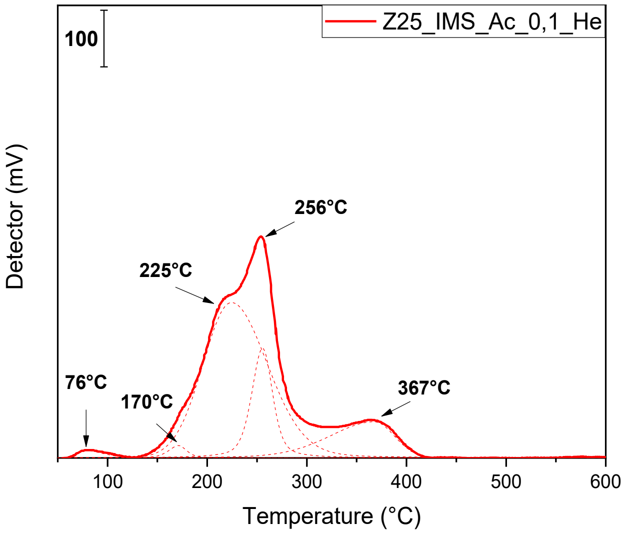

Figure 4.10 H_2-TPR spectrum of Z25_IMS_Ac_0,1 sample pre-treated in He at 550 °C.

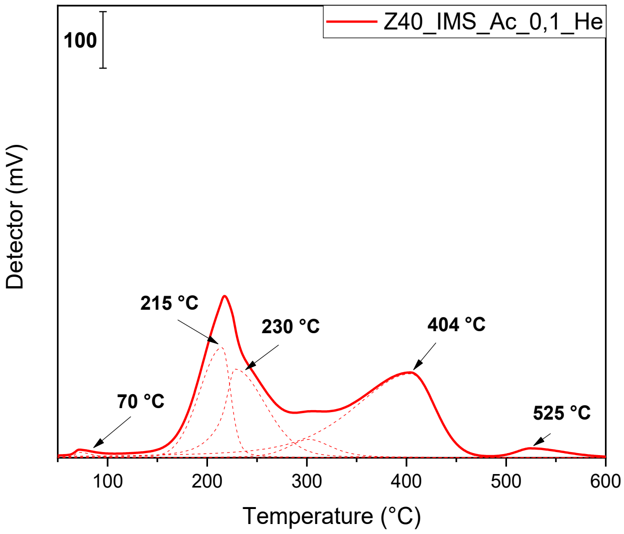

Figure 4.11 H_2-TPR spectrum of Z40_IMS_Ac_0,1 sample pre-treated in He at 550 °C.

It appears that only the sample Z25_IMS_Ac_0,1 (***Figure 4.10***) exhibit the sharp peak correspondent to the CuO clusters reduction, which is located at slightly lower temperatures than the previous samples. Z40_IMS_Ac_0,1 is characterized with two noticeable peaks, at low and high temperature (***Figure 4.11***). As it was observed earlier, the former could be attributed to the reduction of Cu^{2+} to Cu^{+}, while the broad peak at 440°C could correspond to the reduction of Cu^{+} to Cu^{0}. These copper species are more difficult to reduce because they're located in a less accessible site in the structure of the zeolite.

As it can be seen from ***Figure 4.9***, Z12_IMS_Ac_0,1 is the only impregnated sample in which the sharpest peak is located at high temperature (390°C), as opposed to the previous samples in which it was situated in the temperature range between 250-270°C. The peak at 390°C in this case might be attributed to the reduction of finely dispersed CuO particles to elemental Cu^{0}. [51]

Figure 4.12-Figure 4.14 represent the H_2-TPR spectra of the ion-exchanged samples synthetized with 0,2 g of precursor:

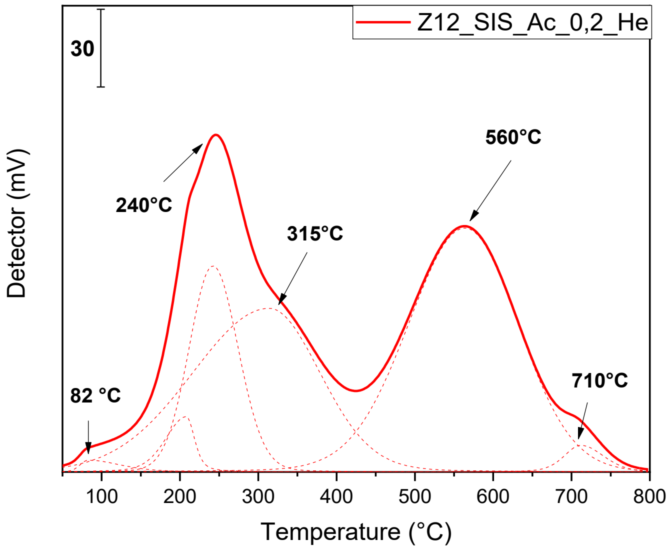

Figure 4.12 H_2-TPR spectrum of Z12_SIS_Ac_0,2 sample pre-treated in He at 550 °C.

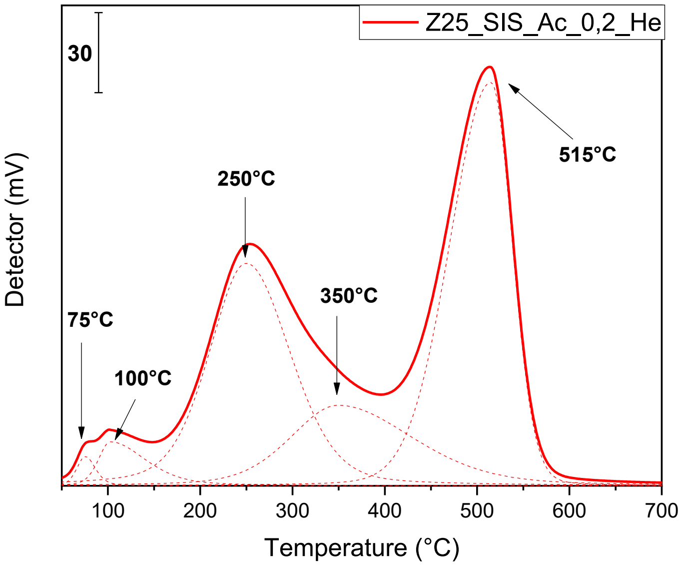

Figure 4.13 H_2-TPR spectrum of Z25_SIS_Ac_0,2 sample pre-treated in He at 550 °C.

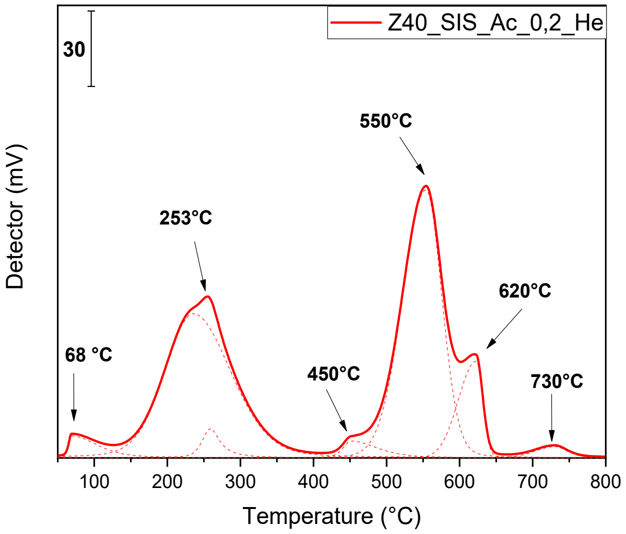

Figure 4.14 H_2-TPR spectrum of Z40_SIS_Ac_0,2 sample pre-treated in He at 550 °C.

As it can be seen from the previous figures, there are some differences between the spectra of the ion-exchange samples compared to the impregnated ones:

- In the ion-exchange samples reduction starts at lower temperature (from 68 °C) and ends at higher temperature (up to 730°C for the sample Z40_SIS_Ac_0,2).
- The peak correspondent to the reduction of CuO clusters is absent.
- The number of peaks is higher than the impregnated samples.

The high peak temperature is representative of a strong metal-support interaction, which makes the species less reducible. For example, the peaks between 300 and 350 °C could be attributed to the reduction of the distributed Cu^{2+} species, as it was shown by Bond et al.[52] The existence of such Cu^{2+} species (chemically interacting with a silica substrate) and their reducibility in a similar temperature range have also been confirmed by Chang et al. [8] In addition to this, Bulánek et al. demonstrated that at decreasing copper levels, the last peak position in the H_2-TPR spectra is pushed to higher temperatures. It was discovered that the conversion of exchanged Cu^{2+} ions to metallic copper in zeolites takes place over the course of two steps, with Cu^{+} acting as a stable intermediate. In particular, the reducibility of the Cu ions increased with the increasing content of copper and decreasing concentration of Al in the framework. [49]

The peaks at lower temperature (< 100 °C) might be due to the reduction of oxygen bridged oxocations $[Cu\text{-}O\text{-}Cu]^{2+}$, which are one of the many species existing on the Cu-ZSM-5 zeolites. The oxocations are easily reducible thanks to the removal of the bridging oxygen, therefore all the peaks happening at temperatures lower than 100°C can be attributed to this reaction [53]:

$$[Cu\text{-}O\text{-}Cu]^{2+} + H_2 \rightarrow 2Cu + H_2O \qquad (4.4)$$

Finally, the absence of the peak corresponding to CuO clusters in the ion-exchanged samples may be due to a low copper concentration. In fact, since the exchange solution was rinsed with water three times during the synthesis, resulting in the removal of most of the non-exchanged precursor, that could have led to the formation of CuO clusters in the corresponding impregnated samples. (***Chapter 3.1***).

4.1.2.2 Oxidizing (O_2) pre-treatment

Figure 4.15-Figure 4.23 represent the H_2-TPR spectra of the samples which were pre-treated with O_2, as it was previously described in ***Chapter 3.3.1***. During the pre-treatment, the oxygen which flows through the sample reacts with the copper species present in it, raising their oxidation state.

The impregnated samples are reported first, starting from the highest nominal copper content (0,2 g of copper acetate).

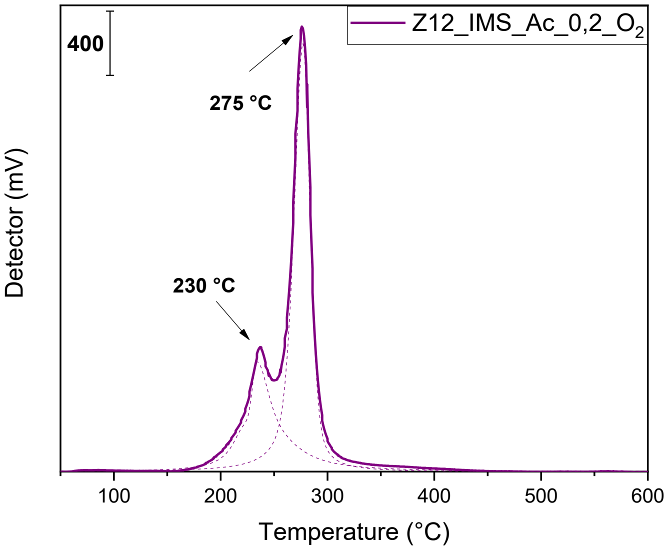

Figure 4.15 H_2-TPR spectrum of Z12_IMS_Ac_0,2 sample pre-treated in O_2 at 550 °C.

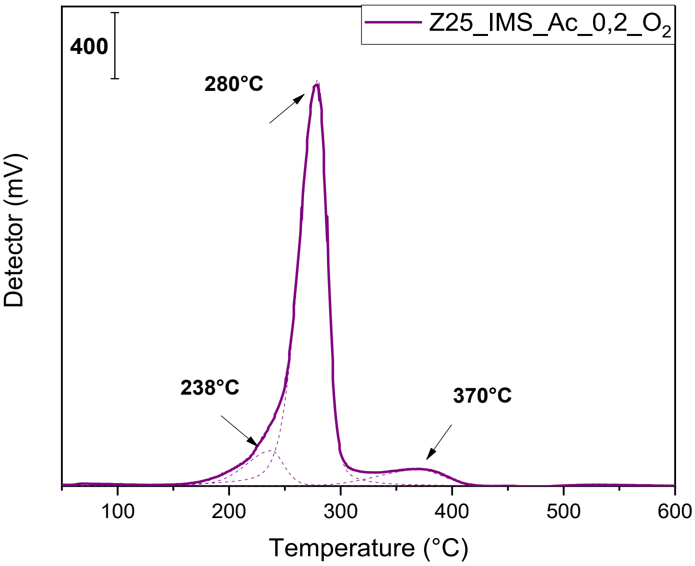

Figure 4.16 H_2-TPR spectrum of Z25_IMS_Ac_0,2 sample pre-treated in O_2 at 550 °C.

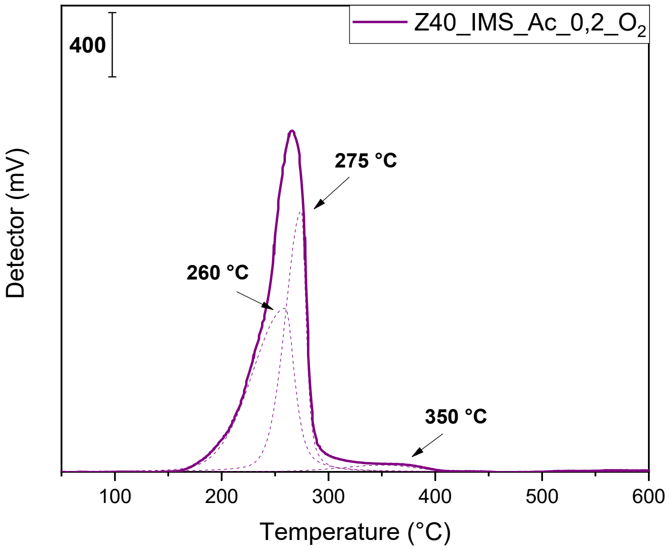

Figure 4.17 H_2-TPR spectrum of Z40_IMS_Ac_0,2 sample pre-treated in O_2 at 550 °C.

As it can be seen from the previous figures, the impregnated samples with 0,2 g of precursor all exhibit the sharp peak correspondent to the reduction of CuO clusters. These samples present two main differences when compared with the corresponding samples pre-treated in He:

- The oxidizing pre-treatment generates spectra with a smaller number of peaks. For instance, the sample Z12_IMS_Ac_0,2 in ***Figure 4.15*** exhibits only two peaks, while the spectrum of its counterpart pre-treated in He is characterized by 5 peaks (***Figure 4.8***).
- The oxidizing pre-treatment generates spectra characterized by a higher signal. For example, the signal of the sample Z25_IMS_Ac_0,2 (***Figure 4.15***) is significantly higher than his counterpart which has been pre-treated in He (***Figure 4.6***). The same can be observed for the other samples.
- Both of these features are attributed to the higher presence of CuO clusters, that are formed as a consequence of the oxidizing pre-treatment.

Figure 4.18-***Figure 4.20*** represent the H_2-TPR spectra of the impregnated samples synthetized with 0,1 g of copper precursor:

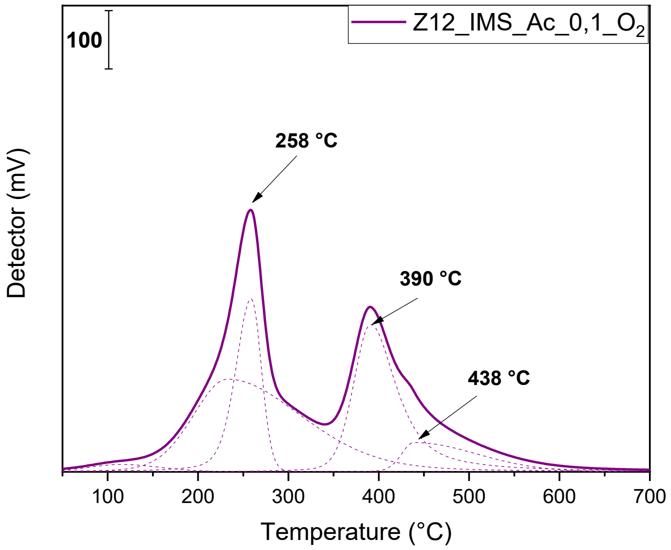

Figure 4.18 H_2-TPR spectrum of Z12_IMS_Ac_0,1 sample pre-treated in O_2 at 550 °C.

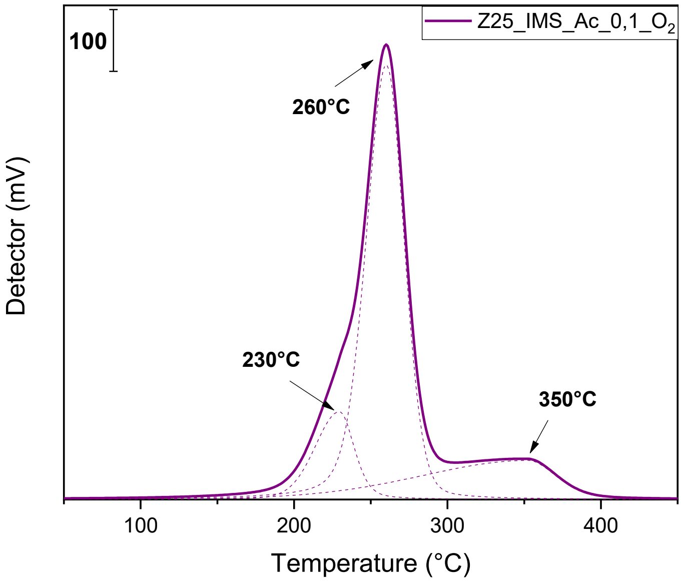

Figure 4.19 H_2-TPR spectrum of Z25_IMS_Ac_0, 1 sample pre-treated in O_2 at 550 °C.

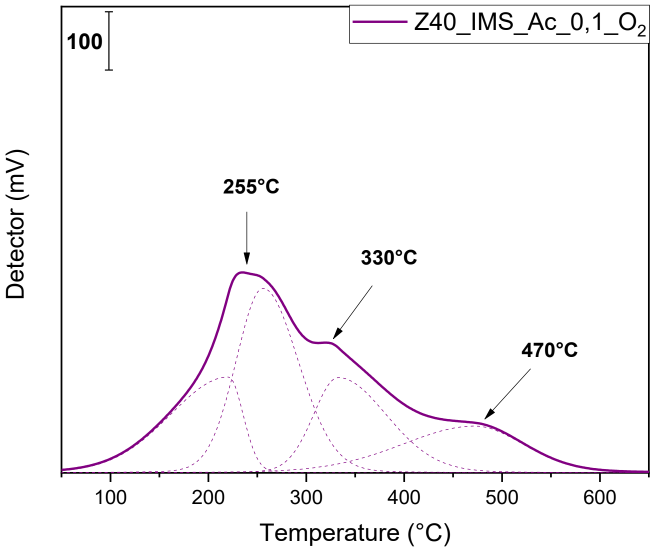

Figure 4.20 H_2-TPR spectrum of Z40_IMS_Ac_0, 1 sample pre-treated in O_2 at 550 °C.

All the samples exhibit the peak correspondent to the reduction of CuO clusters, in the range of temperature between 250 and 260°C. In addition to this, Z40_IMS_Ac_0,1 ***(Figure 4.20***) and Z12_IMS_Ac_0,1 (***Figure 4.18***) are characterized by multiple peaks at lower and higher temperatures (up to 470°C). The peaks at lower temperature could be due to the reduction of Cu^{2+} ions, while at higher temperatures the reduction of Cu^{+} ions or of finely dispersed CuO particles could occur. Even in this case the detector's signals are higher than the ones of the samples pre-treated in He.

Figure 4.21-Figure 4.23 represent the H_2-TPR spectra of the ion-exchanged samples synthetized with 0,2 g of copper precursor:

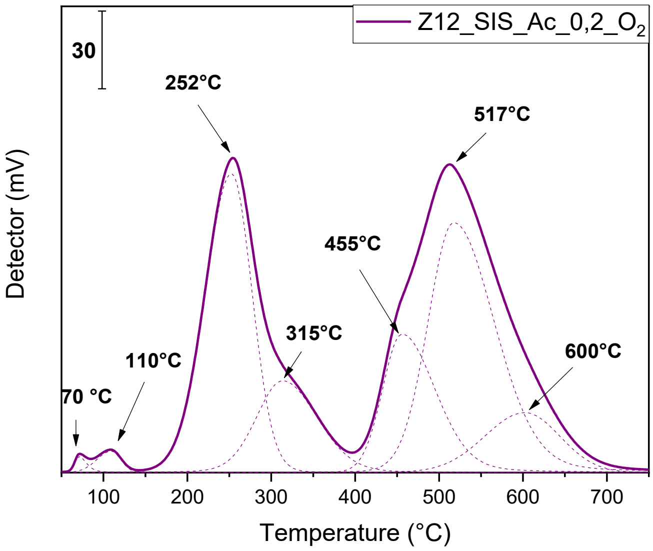

Figure 4.21 H_2-TPR spectrum of Z12_SIS_Ac_0, 2 sample pre-treated in O_2 at 550 °C.

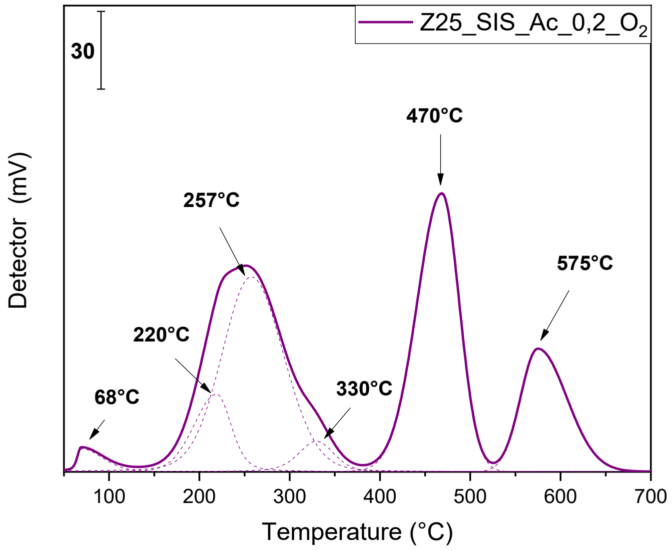

Figure 4.22 H_2-TPR spectrum of Z25_SIS_Ac_0, 2 sample pre-treated in O_2 at 550 °C.

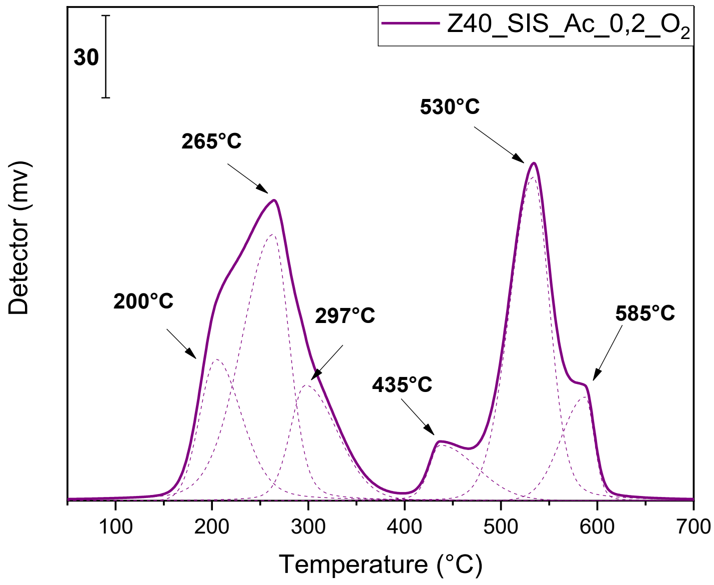

Figure 4.23 H_2-TPR spectrum of Z40_SIS_Ac_0, 2 sample pre-treated in O_2 at 550 °C.

As opposed to the ion-exchanged samples pre-treated in He, the ones pre-treated in O_2 exhibits a sharp and noticeable peak at 250-260 °C. These could be related to the presence of CuO clusters, which were probably formed on the surface of the catalyst thought the oxidation reactions deriving from the pre-treatment atmosphere. However, similarly to their counterparts, these samples exhibit a greater number of peaks when compared to the impregnated ones. As it was explained in the previous section, these peaks could be related to many species, including the oxocations which are reduced at lower temperatures (<100°C).

4.1.3 EDX and XRF results

These techniques have been used to determine the real quantity of copper in the samples, in order to calculate the H_2 consumption during the TPR analysis. ***Table 4.1*** reports the average values of the copper quantity (wt%), and of the Cu/Al and Si/Al ratios.

Table 4.1 EDX values for the samples synthetized with 0,2 and 0,1 g of precursor.

SAMPLE	Cu (wt%)	Cu/Al (at%)	Si/Al (at%)
Z12_IMS_Ac_0,2	6,38	0,79	11,64
Z25_IMS_Ac_0,2	6,29	1,83	29,11
Z40_IMS_Ac_0,2	6,86	3,09	41,52
Z12_SIS_Ac_0,2	2,71	0,32	11,99
Z25_SIS_Ac_0,2	1,31	0,2	27,87
Z40_SIS_Ac_0,2	1,49	0,41	42,19
Z12_IMS_Ac_0,1	4,08	0,5	11,34
Z25_IMS_Ac_0,1	4,14	1,23	30,2
Z40_IMS_Ac_0,1	3,63	1,46	41,16
Z12_SIS_Ac_0,1	1,55	0,19	11,91
Z25_SIS_Ac_0,1	1,46	0,42	30,86
Z40_SIS_Ac_0,1	1,4	0,69	45,94

As it can be seen from ***Table 4.1,*** the Si/Al values calculated with EDX are relatively close of the theoretical ones of the commercial zeolites used in the synthesis.

The Cu quantity is influenced mainly by these parameters:

- Procedure of synthesis: the quantity is significantly higher for the impregnated samples, as opposed to the ion-exchanged ones. This is because during the synthesis of the impregnated samples, most of the precursor is introduced in the zeolite, thanks to the evaporation of the solution, as opposed to the ion-exchanged ones where the excess of the precursor is eliminated through centrifugation.
- Si/Al ratio: in most of the cases, the zeolite with the lower Si/Al ratio contains more precursor than the other two samples. This is because the zeolite with Si/Al ratio equal to 12 contain more Al sites, which can bond with the various copper species.

The quantity of Cu detected by EDX decreases with the quantity of precursor used in the synthesis. As a result, all the samples synthetized with 0,1 g of precursor exhibit a lower Cu quantity than the others.

The evaluation of copper content given by EDX gives the additional information to the results of TPR. ***Table 4.2*** originates from the combination of the EDX and TPR results, and it reports the hydrogen consumption of the samples.

Table 4.2 Values of H_2 consumption based on the EDX analysis, according to the type of pre-treatment (He or O_2) prior to the TPR.

SAMPLE	Cu (wt%)	Cu (mol)	H_2 consumption (mol)		H_2/Cu ratio		% Cu (II)	
			He	O_2	He	O_2	He	O_2
Z12_IMS_Ac_0,2	6,38	5,0807E-05	4,50219E-05	4,23833E-05	0,8861	0,8342	77,23	66,84
Z25_IMS_Ac_0,2	6,29	4,9694E-05	4,3095E-05	4,67543E-05	0,8672	0,9408	73,44	88,17
Z40_IMS_Ac_0,2	6,86	5,4953E-05	4,01841E-05	4,95195E-05	0,7312	0,9011	46,25	80,22
Z12_SIS_Ac_0,2	2,71	2,1325E-05	2,41481E-05	2,43129E-05	1,1324	1,1401	126,47	128,02
Z25_SIS_Ac_0,2	1,31	1,0329E-05	1,96737E-05	1,46753E-05	1,9047	1,4208	280,94	184,16
Z40_SIS_Ac_0,2	1,49	1,1771E-05	1,38353E-05	1,3416E-05	1,1753	1,1397	135,06	127,94
Z12_IMS_Ac_0,1	4,08	3,2362E-05	2,38572E-05	3,29934E-05	0,7372	1,0195	47,44	103,90
Z25_IMS_Ac_0,1	4,14	3,2968E-05	2,21435E-05	2,50375E-05	0,6717	0,7594	34,33	51,89
Z40_IMS_Ac_0,1	3,63	2,8736E-05	2,12965E-05	3,03084E-05	0,7411	1,0547	48,22	110,94

The H_2 consumption has been calculating by integrating the area below the H_2-TPR spectra's peaks. The percentage of copper (II) species is obtained from the H_2/Cu ratio, assuming that the moles of consumed H_2 equal the sum of the Cu^{2+} moles of and half of the Cu^{+} moles. [8]
Theoretically, for each divalent metal cation (Cu^{2+}) reduced to Cu^0, the H_2/Cu ratio in the ideal case should be equal to 1. H_2/Cu values less than 1 may indicate incomplete metal reduction, whereas values greater than 1 may be attributed to the concurrent reduction of species other than the Cu^{2+} cations. [51]
As it can be seen from ***Table 4.2***, the H_2/Cu ratio for most of the impregnated samples is close to 1, meaning that there has been complete reduction of the copper species. Moreover, the values corresponding to the O_2 pre-treatment are higher, since it raises the oxidation state of the copper species, thus resulting in a greater reduction. The same pattern can be observed for the %Cu (II) values as well.

On the other hand, the values of H_2/Cu ratio for the ion-exchanged samples are greater than 1. These samples are the ones in which the quantities of Cu are the lowest, which could result in the deposition of carbonate species (CO_x), as opposed to the impregnated samples where the quantity of Cu is significantly higher, thus occupying more sites in the zeolite. These carbonate species could derive from the copper acetate, which was used as precursor in the synthesis procedure. They can be eliminated at high temperature (~800°C), whereas for these samples the temperature of the pre-treatment doesn't exceed 550°C. As a result, these species can be reduced by H_2 along with the copper species, leading to a H_2/Cu ratio higher than 1. Moreover, this could also be due to the fact that the TPR instrument used in this work is unable to estimate correctly the copper species when they are present in low quantities, which is the case of the ion-exchanged samples.
Table 4.3 reports the calculations of H_2 consumption based on the copper content found by the XRF analysis, which was performed to confront the Cu content estimated by the EDX analysis.

Table 4.3 Values of H_2 consumption based on the XRF analysis, according to the type of pre-treatment (He or O_2) prior to the TPR.

SAMPLE	Cu (wt%)	Cu (mol)	H_2 consumption (mol)		H_2/Cu ratio		% Cu (II)	
			He	O_2	He	O_2	He	O_2
Z12_IMS_Ac_0,2	**7,54**	6,0044E-05	4,50219E-05	4,23833E-05	0,7498	0,7059	49,96	41,17
Z25_IMS_Ac_0,2	**6,95**	5,4908E-05	4,3095E-05	4,67543E-05	0,7848	0,8515	56,97	70,30
Z40_IMS_Ac_0,2	**6,49**	5,1989E-05	4,01841E-05	4,95195E-05	0,7729	0,9525	54,59	90,50
Z12_SIS_Ac_0,2	**2,65**	2,0853E-05	2,41481E-05	2,43129E-05	1,1580	1,1659	131,60	133,18
Z25_SIS_Ac_0,2	**1,34**	1,0565E-05	1,96737E-05	1,46753E-05	1,8620	1,3890	272,41	177,79
Z40_SIS_Ac_0,2	**1,21**	9,5596E-06	1,38353E-05	1,3416E-05	1,4473	1,4034	189,45	180,68

The values of Cu (wt%) found for the ion-exchanged samples are similar to the EDX ones, whereas the values of the impregnated samples differ slightly between the two types of analysis, reaching a maximum deviation of 18 % (for Z12_IMS_Ac_0,2). Even in this case, most of the values corresponding to the oxidizing pre-treatment are the highest, except for the zeolite having the Si/Al ratio equal to 25.

4.1.4 FT-IR results

For the IR spectroscopic studies of the synthetised samples CO has been used as probe molecule. This molecule typically gives information on the oxidation and coordination state of the extra-framework cations as well as their surface concentration. CO probe has been used to confirm the high coordinative unsaturation of Cu+ cations hosted in zeolites.

The C-end lone pair of CO is transferred to the metal cation in the presence of an acceptor of electron pairs, such as a transition metal cation with empty orbitals of the suitable energy (and so acting as a Lewis acidic centre), giving rise to a σ-coordination (Mn^{+}-CO). The interaction between CO and the metal cation in this case also results in a shift in CO's stretching frequency toward a value greater than that of the gas. In fact, depending on the temperature and the equilibrium pressure of CO, carbonyl compounds with high structural and spectroscopic qualities can be formed at Cu^{+} sites. Adducts such monocarbonyl $[Cu(CO)]^{+}$ and dicarbonyl $[Cu(CO)_2]^{+}$ complexes are relatively stable and can be observed at room temperature. [54]

The simultaneous formation of σ and π bonds between the CO and the metal ion and the synergism of both bonds account for the great stability of the Cu^{+}-CO carbonyls. In contrast, Cu^{2+}-CO species are unstable because its bond is characterized by only a σ character. [55] For these reasons, CO adsorption at RT followed by IR spectroscopy is widely used in the characterization of Cu-ZSM-5.

Figure 4.24-Figure 4.26 show the IR spectra of the impregnated samples synthetized with 0,2 g of copper precursor. All the spectra in this section were collected outgassing CO starting from the highest equilibrium pressure introduced (30 mbar) and arriving to the complete degas. All the IR spectra are normalized with respect to the specific surface density of the pellet, to allow a better comparison.

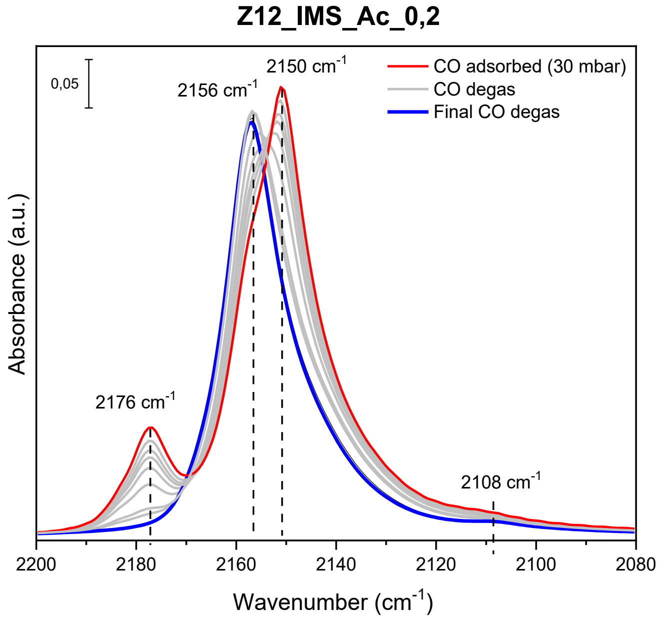

Figure 4.24 IR spectra of CO adsorbed at decreasing equilibrium pressure on Z12_IMS_Ac_0,2.

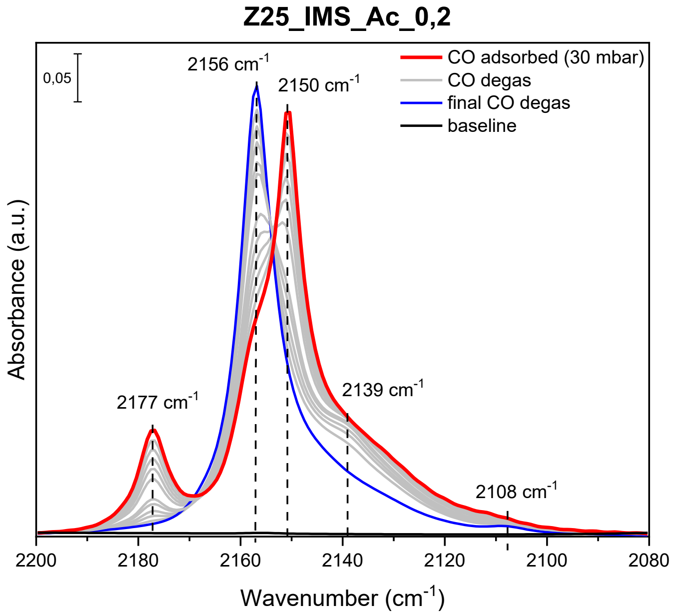

Figure 4.25 IR spectra of CO adsorbed at decreasing equilibrium pressure on Z25_IMS_Ac_0,2.

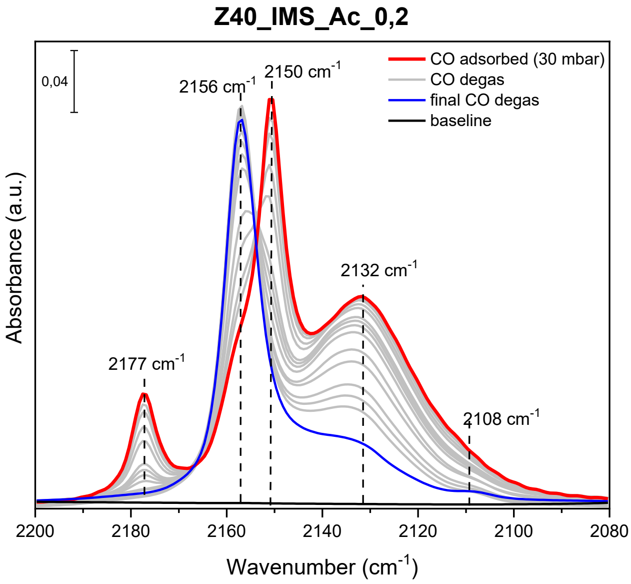

Figure 4.26 IR spectra of CO adsorbed at decreasing equilibrium pressure on Z40_IMS_Ac_0,2.

Many studies have found that, at room temperature and in the presence of CO, the monocarbonyls (Cu^+-CO) tend to be converted to dicarbonyl species (Cu^+-$(CO)_2$), according to the following reaction [56]:

$$Cu^+\text{-}CO + CO \leftrightarrow Cu^+\text{-}(CO)_2 \qquad (4.5)$$

The absorption ascribed to monocarbonyl (Cu^+(CO)) species is observed in all the samples at low coverage, at **2156** cm^{-1}. By increasing the CO equilibrium pressure such species are gradually consumed, and simultaneously two bands due to dicarbonyl complexes start to grow in intensity.

In all the samples, the dicarbonyl complexes can be identified by their IR features at **2177** cm^{-1} and **2150** cm^{-1}, which corresponds to the symmetric and antisymmetric intramolecular C-O stretches respectively. [8]

Besides IR bands due to the carbonyl species, Z40_IMS_Ac_0,2 (***Figure 4.26***) exhibits a noticeable shoulder at **2132** cm^{-1}, which is formed gradually through the adsorption of CO. These complexes absorbing at 2132-2137 cm^{-1} have also been observed to form on both supported Cu_2O and CuO.[8] As it was seen in the previous section, the H_2-TPR analysis supports the presence of copper oxide species on the impregnated catalysts. As a result, the shoulder at 2132 cm^{-1} in the IR spectra of Z40_IMS_Ac_0,2 may be attributed to the formation of Cu^+-CO complexes on the partially reduced surface of some CuO particles. In the sample Z25_IMS_Ac_0,2 (***Figure 4.25***) a less pronounced peak at **2139** cm^{-1} can be attributed to CuO particles, while Z12_IMS_Ac_0,2 (***Figure 4.24***) doesn't exhibit this feature at all. This seems to go in contrast with the H_2-TPR results, where Z12_IMS_Ac_0,2 presents the CuO peak similarly to the other two samples (***Figure 4.6***).

Finally, all the samples exhibit a sightly noticeable peak at **2108** cm^{-1}, which is observed after the evacuation of CO at RT. According to Armandi et al., this peak could be due to either to CO molecules adsorbed through the O end or to the adsorption of CO molecules on reduced copper species (i.e.Cu^0-CO). [8]

Figure 4.27-Figure 4.29 present the IR spectra of the impregnated samples synthetized with 0,1 g of copper precursor.

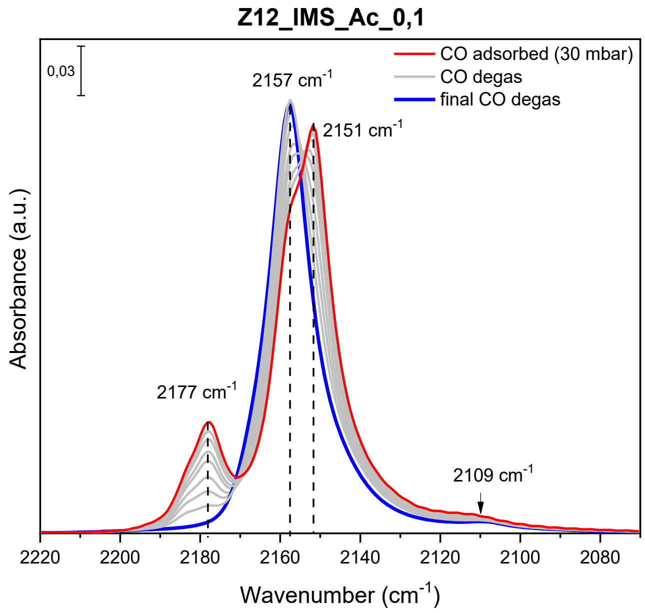

Figure 4.27 IR spectra of CO adsorbed at decreasing equilibrium pressure on Z12_IMS_Ac_0,1.

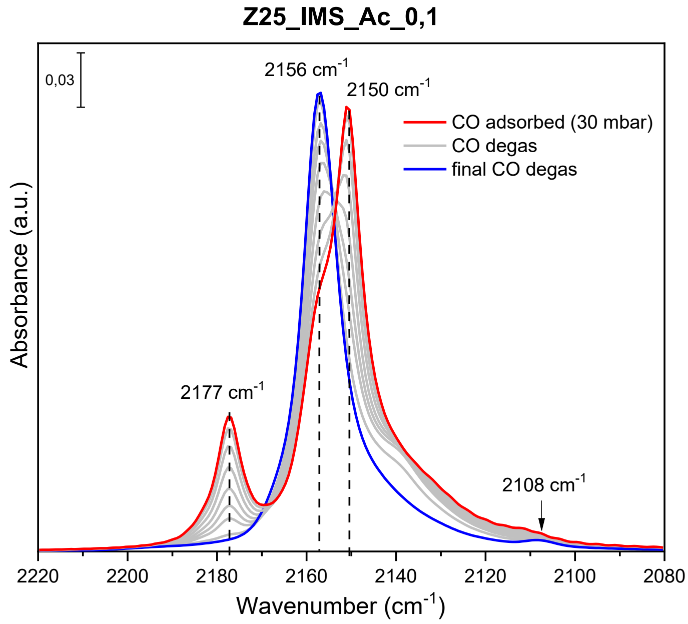

Figure 4.28 IR spectra of CO adsorbed at decreasing equilibrium pressure on Z25_IMS_Ac_0,1.

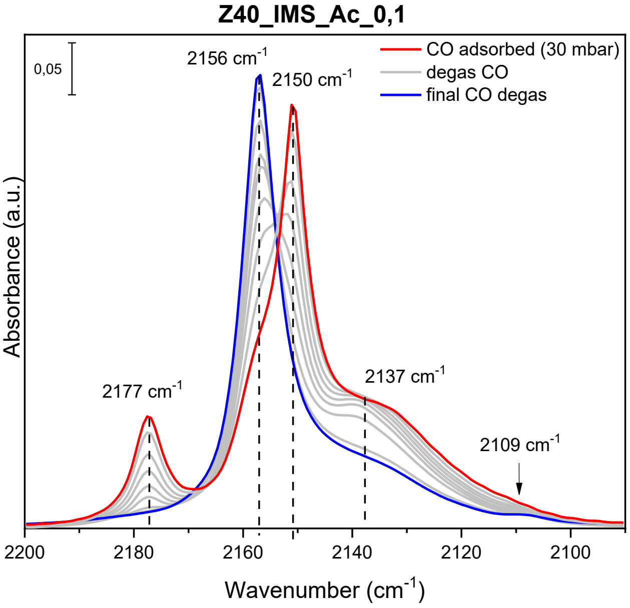

Figure 4.29 IR spectra of CO adsorbed at decreasing equilibrium pressure on Z40_IMS_Ac_0,1.

Similarly to the previous samples, all these spectra are characterized by the presence of peaks associated to monocarbonyl and dicarbonyl. As it can be seen from ***Figure 4.29***, only the sample Z40_IMS_Ac_0,1 exhibits a slightly pronounce shoulder at **2137** cm^{-1}, which could be ascribed to the presence of CuO particles.

Figure 4.30-Figure 4.32 show the IR spectra of the ion-exchanged sample synthetized with 0,2 g of precursor.

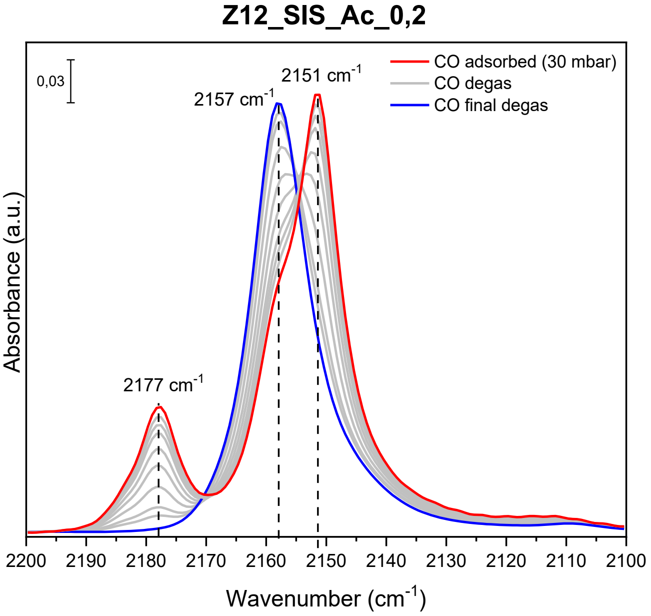

Figure 4.30 IR spectra of CO adsorbed at decreasing equilibrium pressure on Z12_SIS_Ac_0,2.

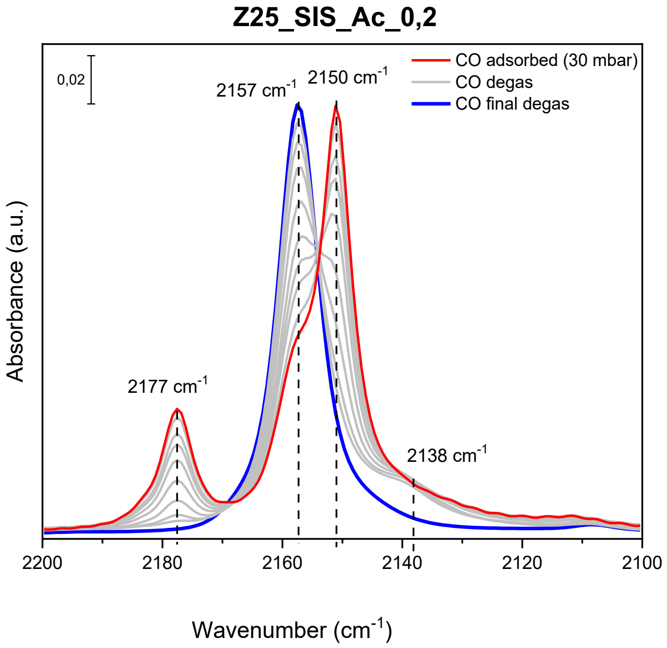

Figure 4.31 IR spectra of CO adsorbed at decreasing equilibrium pressure on Z25_SIS_Ac_0,2.

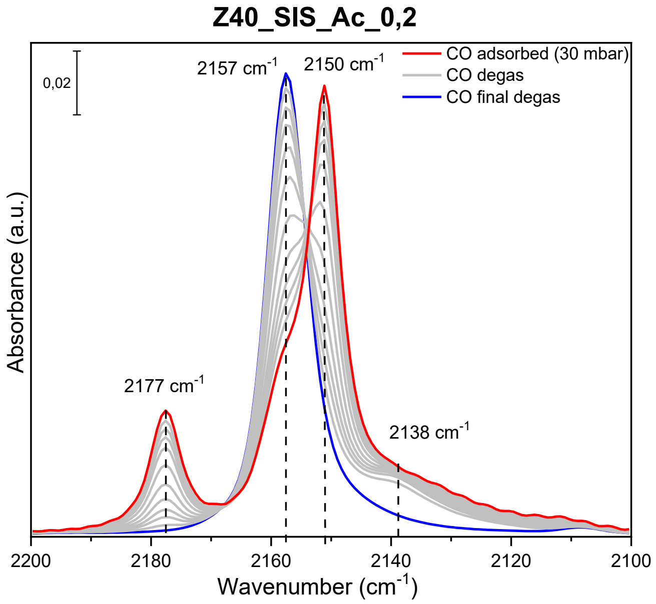

Figure 4.32 IR spectra of CO adsorbed at decreasing equilibrium pressure on Z40_SIS_Ac_0,2.

Contrary to all the previous cases, none of the ion-exchanged samples shows the peak attributed to the CuO particles. In addition to this, even the peak at 2108 cm^{-1} is absent after the CO degas. As mentioned earlier, this peak could be due to either CO molecules adsorbed through the O end or to the adsorption of CO molecules on reduced copper species.

Finally, in some samples such as Z25_SIS_Ac_0,2 in ***Figure 4.31***, it can be seen how the isosbestic point at 2153 cm^{-1} is well defined. This behaviour suggests that the copper species are homogeneous within the sample, therefore it’s possible to observe clearly the formation of the dicarbonyl species at the expense of the monocarbonyl ones. If, on the other hand, the isosbestic point is not well-defined, it means that there is a possible heterogeneity of the copper species in the sample. This latter phenomenon can be clearly observed in ***Figure 4.24*** for the sample Z12_IMS_Ac_0,2.

Another interesting part could be extracted from the IR analysis, such as for example the exchange level. Percentage of exchange could be obtained from the intensity ratio between the integrated IR absorbance of the 3610 cm^{-1} band in the parent H-ZSM-5 and of the same band in exchanged samples. ***Figure 4.33-Figure 4.35*** report the IR spectra in the O-H stretching region of the parent zeolite, compared to the sample obtained from it after the synthesis.

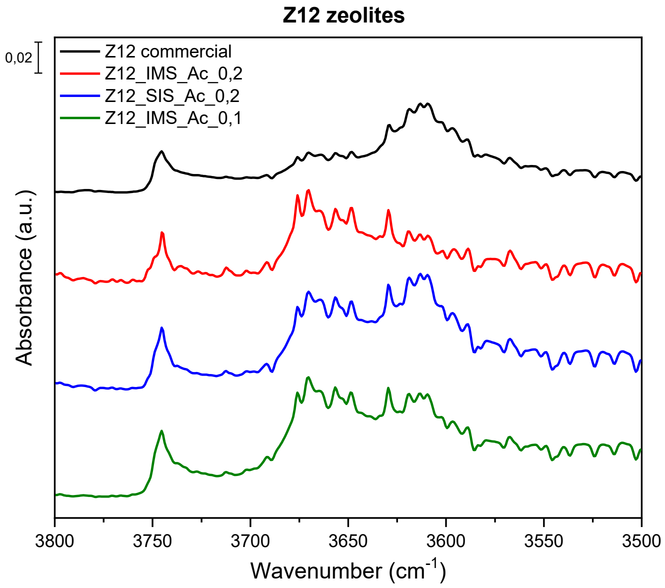

Figure 4.33 IR spectra of the commercial zeolite having Si/Al ratio equal to 12 compared with the sample obtained after synthesis.

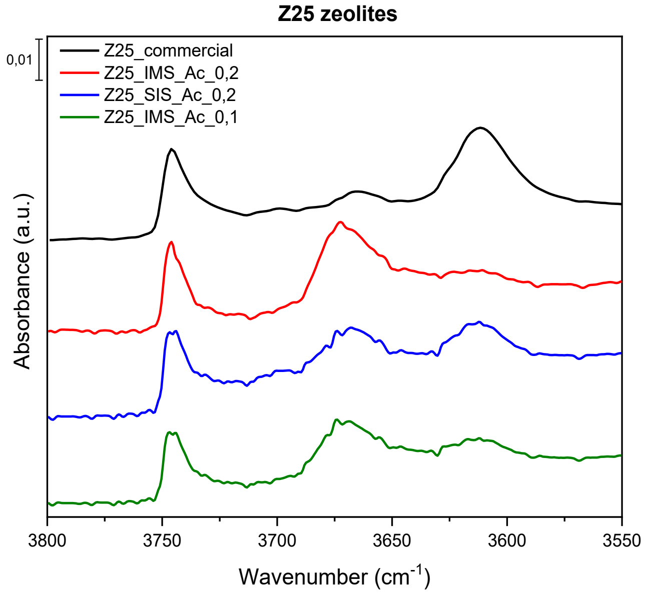

Figure 4.34 IR spectra of the commercial zeolite having Si/Al ratio equal to 25 compared with the sample obtained after synthesis.

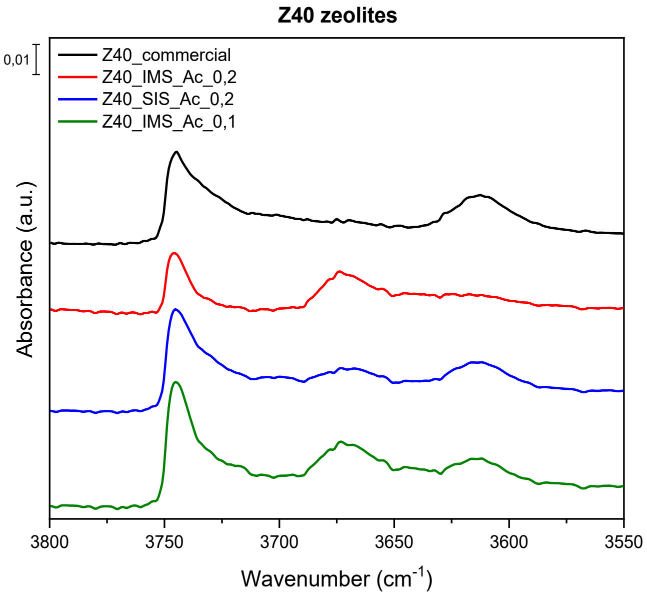

Figure 4.35 IR spectra of the commercial zeolite having Si/Al ratio equal to 40 compared with the sample obtained after synthesis.

The parent zeolites (black curve) all exhibit a sharp peak at **3745** cm^{-1}, a broad and weak absorption centred at **3672** cm^{-1} and a noticeable band at **3610** cm^{-1}. According to the literature, these three bands are respectively assigned to the O-H stretching vibrations of [8]:

- defective Si-OH groups (silanols), which are mostly located at the zeolite external surface.
- extra-framework Al-OH groups, originating from dealumination.
- Si-(OH)-Al groups (Brønsted acidic sites).

After the introduction of Cu ions, it can be observed that the intermediate band grows in intensity for all the samples, which is probably due to the addition of imperfections in the zeolites' structure during the synthesis. Moreover, in all the samples the band attributed to the Brønsted sites is partially consumed, independently of the synthesis procedure. The exchange percentages (%EX) are calculated as the ratio between the integrated absorbance of the 3610 cm^{-1} band of the parent H-ZSM-5 and of the same band in the synthetized samples.[8] ***Table 4.4*** reports the values of the exchange percentage for each sample.

Table 4.4 Values of the exchange percentages relative to the Brønsted sites.

SAMPLE	EX (%)
Z12_IMS_Ac_0,2	75
Z25_IMS_Ac_0,2	89
Z40_IMS_Ac_0,2	75
Z12_SIS_Ac_0,2	44
Z25_SIS_Ac_0,2	69
Z40_SIS_Ac_0,2	37
Z12_IMS_Ac_0,1	30
Z25_IMS_Ac_0,1	81
Z40_IMS_Ac_0,1	76

In all the cases, it can be observed from ***Table 4.4*** that the zeolites which exhibit the highest exchange percentage are the ones characterized by the Si/A ratio equal to 25. Theoretically, this feature should be attributed to the zeolites with the lower Si/Al ratio, since they contain more Al sites that can undergo the exchange. The results obtained for the Z12 zeolites are lower than expected, and this could be due to the noisy IR spectra of these samples (***Figure 4.33***), which results in a less accurate integration of the areas below.

Finally, the ion-exchanged samples show the lowest value of exchange percentage compared to the other samples.

4.1.5 N_2 physisorption results

Figure 4.36-Figure 4.38 reports the adsorption and desorption isotherms of all the synthetized samples.

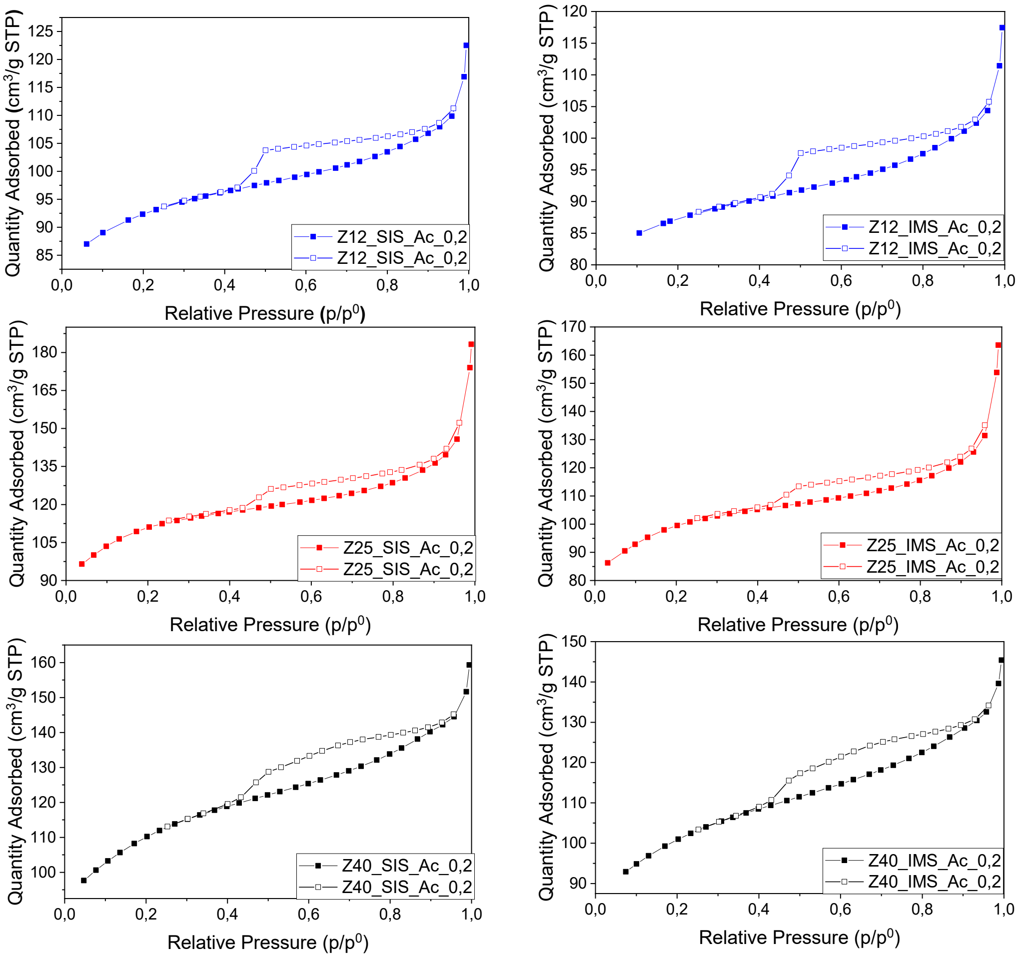

Figure 4.36 N_2 adsorption-desorption isotherms at 77 K of the samples synthetized with 0,2 g of precursor (full dots: adsorption, empty dots: desorption). On the left: ion-exchanged samples. On the right: impregnated samples.

All the samples exhibit a type I isotherm, which was previously described in ***Chapter 3.3.3***. The fact that there is no plateau at the end of the curve means that there could be a possible formation of multilayers, which is mostly limited by the small dimensions of the pore in the microporous zeolite. Moreover, the synthesized samples exhibit a hysteresis loop at P/P_0 in the range of 0.4–0.8, which is due to the interparticle voids filling.[57]

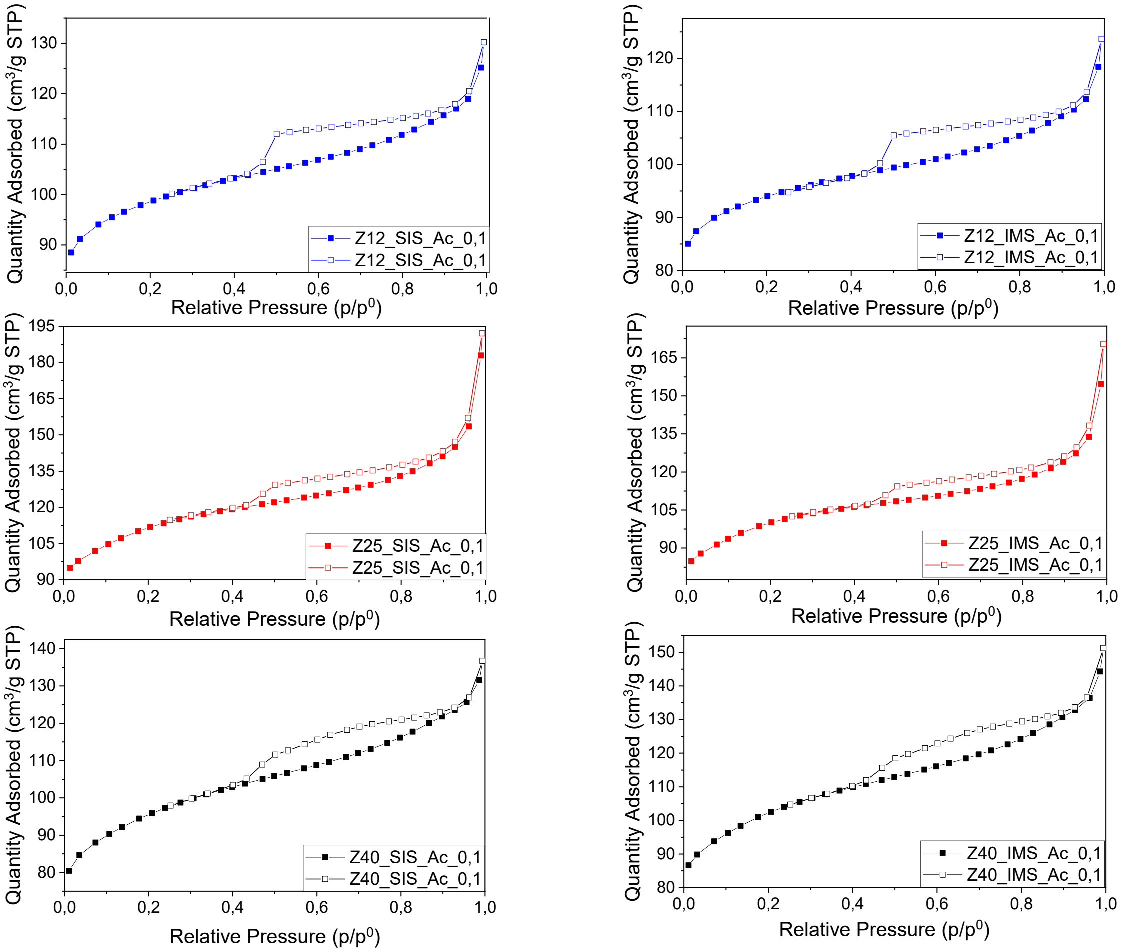

Figure 4.37 N_2 adsorption-desorption isotherms at 77 K of the samples synthetized with 0,1 g of precursor (full dots: adsorption, empty dots: desorption). On the left: ion-exchanged samples. On the right: impregnated samples.

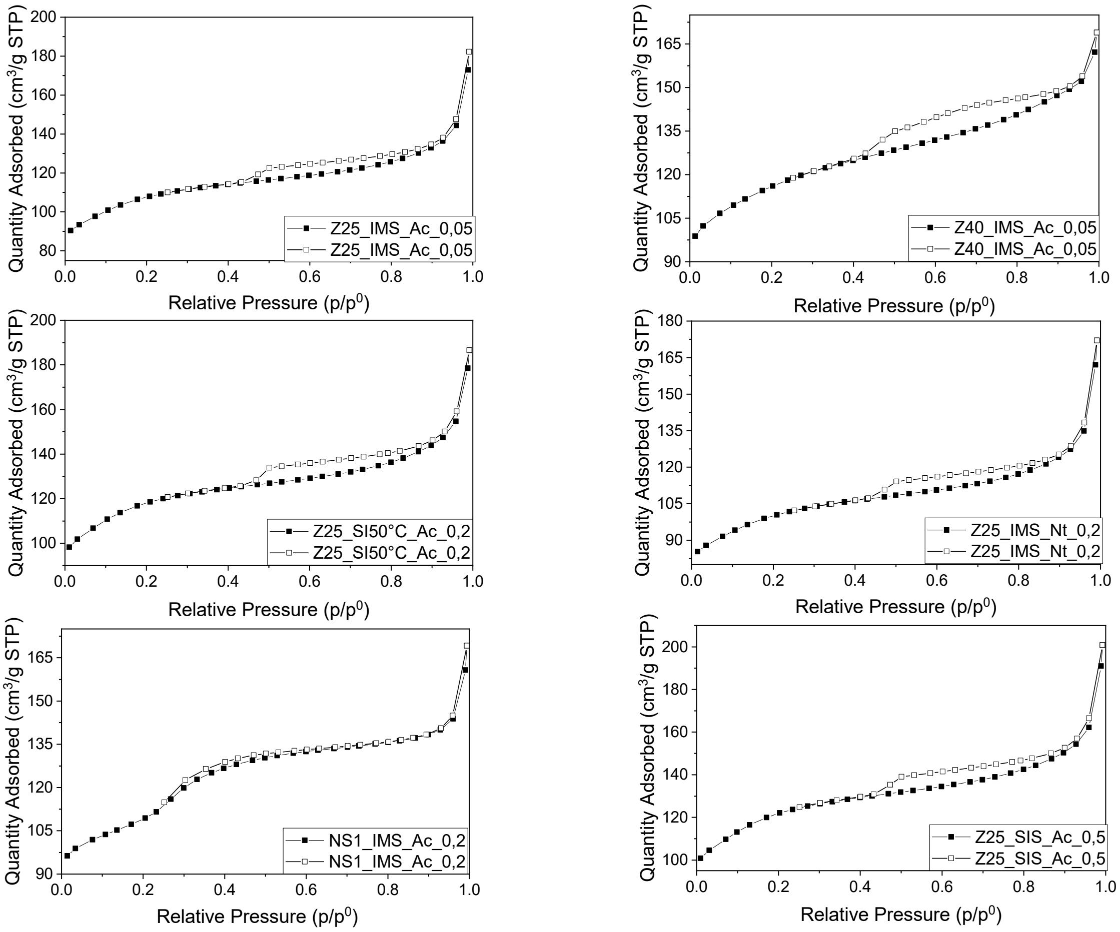

Figure 4.38 N_2 adsorption-desorption isotherms at 77 K of the remaining samples (full dots: adsorption, empty dots: desorption).

The sample NS1_IMS_Ac_0,2 represented in ***Figure 4.38*** exhibits a noticeable horizontal plateau, which is due to the micropore filling, suggesting the presence of sole micropores in the synthetized zeolite structure. [57] ***Table 4.5*** reports the values of the superficial area calculated through the BET method:

Table 4.5 Values of superficial area calculated through the BET method.

SAMPLE	**S_{BET} (m^2/g)**	**SAMPLE**	**S_{BET} (m^2/g)**
Z12_IMS_Ac_0,2	261	**Z12_IMS_Ac_0,1**	297
Z25_IMS_Ac_0,2	324	**Z25_IMS_Ac_0,1**	325
Z40_IMS_Ac_0,2	328	**Z40_IMS_Ac_0,1**	331
Z12_SIS_Ac_0,2	279	**Z12_SIS_Ac_0,1**	311
Z25_SIS_Ac_0,2	361	**Z25_SIS_Ac_0,1**	362
Z40_SIS_Ac_0,2	359	**Z40_SIS_Ac_0,1**	308
Z25_IMS_Ac_0,05	349	**Z25_SI50°C_Ac_0,2**	381
Z40_IMS_Ac_0,05	374	**NS1_IMS_Ac_0,2**	355
Z25_SIS_Ac_0,5	398	**Z25_IMS_Nt_0,2**	322

Most of the values in ***Table 4.5*** are close to 363 m^2/g, which is the average superficial area of the commercial zeolite.[57] The superficial area decreases with the increase of the quantity of copper in the sample. In particular, this phenomenon is more noticeable for the impregnated zeolites, in which most of the precursor was introduced in the structure, thanks to the synthesis procedure. Moreover, the values of superficial area are their minimum for the samples with the lowest Si/Al ratio, and this could be due to the presence of more Al sites in the structure. As a matter of fact, the lowest area belongs to Z12_IMS_Ac_0,2, which is an impregnated sample synthetized with the highest amount of precursor and characterized by the lowest Si/Al ratio.

4.2 Catalytic tests

All the catalytic tests in this section have been carried out at 400°C, flowing 1000 ppm of N_2O. In order to observe the effect of temperature, tests at 350°C and 375°C were executed for the samples which exhibited an oscillating behaviour and/or a good catalytic activity. All the samples have undergone a reductive pre-treatment with He (***Chapter 3.2.2***). For the sake of simplicity, the results of the catalytic tests will be split in two sections, according to the method of synthesis (i.e., ion-exchange and impregnation).

4.2.1 Ion-exchanged Cu-ZSM-5 samples

The following figures show the evolution of N_2O outlet concentration as a function of time over the catalysts prepared from different ZSM-5 parent zeolites, through the ion-exchange method. ***Figure 4.39*** and ***Figure 4.40*** report the catalytical activity of the ion-exchanged samples synthetized with 0,2 and 0,1 g of precursor respectively. The initial peak, which can be seen in each curve, is due to the switching of the gas flows from the bypass to the reactor system.

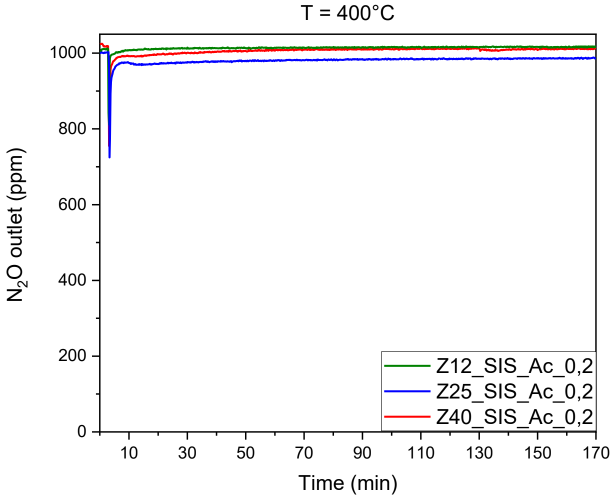

Figure 4.39 Outlet concentration of N_2O during the catalytic activity testing of the ion-exchanged samples synthetized with 0,2 g of precursor.

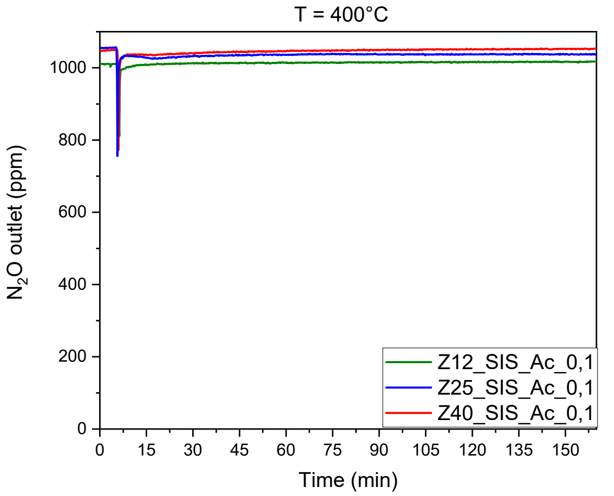

Figure 4.40 Outlet concentration of N_2O during the catalytic activity testing of the ion-exchanged samples synthetized with 0,1 g of precursor.

As it can be seen from the previous figures, no sample between the ion-exchange ones exhibits an oscillatory behaviour. Moreover, the catalytic activity is significantly low even at 400°C, which is the highest temperature used for catalytic tests in this thesis. Therefore, for these samples, temperatures lower than 400°C haven't been considered as an additional parameter for the tests. The sample with the highest content of copper acetate has also been tested in order to investigate better the effect of the precursor (***Figure 4.41***).

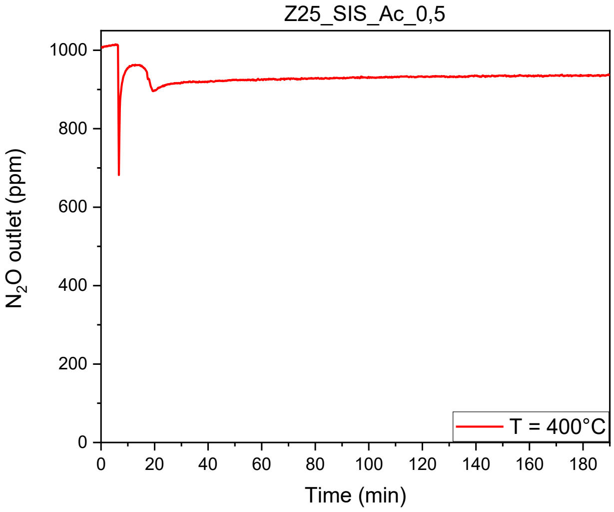

Figure 4.41 Outlet concentration of N_2O during the catalytic activity testing of Z25_SIS_Ac_0,5 (the ion-exchanged sample with the highest copper precursor content).

In this case the conversion results to be slightly higher than the other cases (5%), however no oscillations have been recorded. It's also possible to observe an overshoot behaviour in the transitory phase, which is absent in the previous samples. In an effort to investigate better the ion-exchanged samples, the sample Z25_SI50°C_Ac_0,2 has been tested as well (***Figure 4.42***), which was prepared using the work of Armandi et al. as starting point. [8] As explained in ***Chapter 3.1***, this sample is different from the others because the ion-exchange solution was kept at 50°C for 2h, instead of ambient temperature.

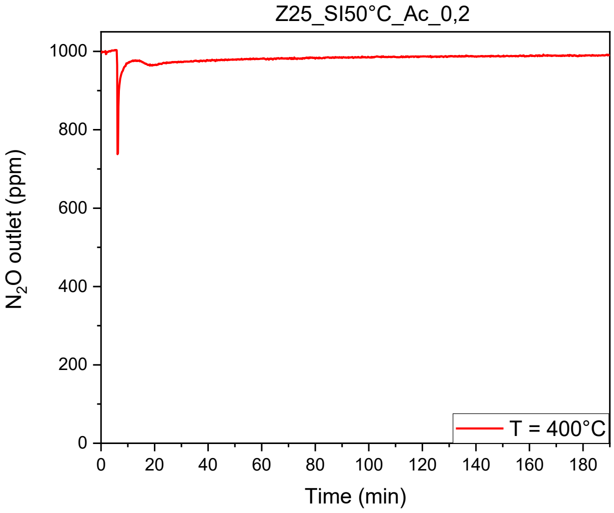

Figure 4.42 Outlet concentration of N_2O during the catalytic activity testing of Z25_SI50°C_Ac_0,2.

Even in this case no oscillation or relevant catalytic activity can be observed. Based on the results seen so far, it can be said that for the ion-exchanged samples neither the Si/Al ratio nor the theoretical copper content have any significant effect on the behaviour of the catalyst. This could be due to the fact that, as it was previously demonstrated by the EDX and XRF results, the ion-exchanged samples are the ones characterized with the lower copper content in their structure (***Chapter 4.1.3***).

Table 4.6 reports the conversion values (%), which has been calculated for each sample on the basis of the initial concentration of N_2O (~1000 ppm) and the one recorded right after the bypass has been removed:

Table 4.6 Conversion values of the ion-exchanged samples

SAMPLE	Conversion (%)
Z40_SIS_Ac_0,2	2
Z25_SIS_Ac_0,2	2,5
Z12_SIS_Ac_0,2	0
Z40_SIS_Ac_0,1	1,3
Z25_SIS_Ac_0,1	2,3
Z12_SIS_Ac_0,1	0
Z25_SIS_Ac_0,5	5
Z25_SI50°C_Ac_0,2	3

The lowest performance is given by the samples deriving from the parent zeolite with the Si/Al ratio equal to 12, since they don't convert at all the inlet N_2O gas. As mentioned earlier, the highest conversion is achieved by the sample Z25_SIS_Ac_0,5, which has been synthesized with the maximum amount of copper possible.

4.2.2 Impregnated Cu-ZSM-5 samples

Figure 4.43-Figure 4.61 show the evolution of N_2O outlet concentration as a function of time over the catalysts prepared through the impregnation method. As it was done for the previous section, the first graphs in this chapter refer to the catalysts prepared with 0,2 g of copper precursor.

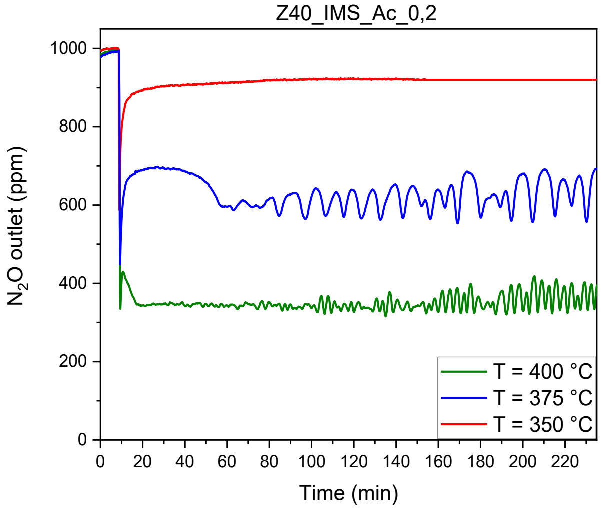

Figure 4.43 Outlet concentration of N_2O during the catalytic activity testing of Z40_IMS_Ac_0,2.

Since the Z40_IMS_Ac_0,2 sample exhibits oscillations at 400°C, its behaviour has been studied at 375°C and 350°C as well, to investigate the effect of the temperature. ***Figure 4.43*** reveals that at 375°C and 400°C oscillations of N_2O at the reactor outlet occur. In both cases, it can be observed that the frequency of the oscillations decreases with the temperature, while their period increases. Moreover, the oscillations at 375°C appears to be more regular than the ones at higher temperature. At 350 °C no oscillation is observed, and this could be probably due to a too short isotherm duration, as it was suggested by [8] .

In correspondence of the temperature at which the oscillations occur, it’s possible to observe a peak of N_2O concentration in the transient phase, which is more pronounced at 375°C. This phenomenon can be related this to the initial reduced state of copper in the catalyst, induced by the helium pre-treatment, as it was suggested by Ciambelli et al. [28]

Figure 4.44 shows how the N_2O oscillations are also accompanied by the oscillations of the produced O_2, and of the by-products NO and NO_2 as well. The magnification of the oscillatory behaviour has been carried out for the final part of the tests, where the oscillations appear to be more regular and stable.

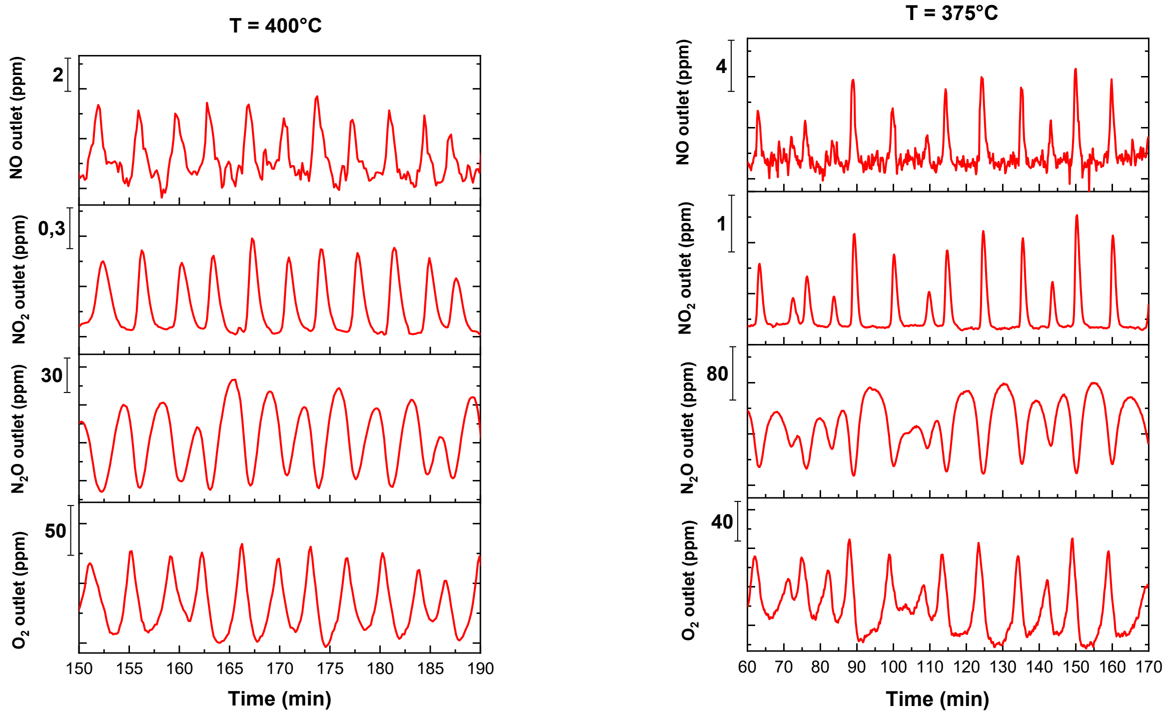

Figure 4.44 Composition of NO, NO_2, N_2O and O_2 at the reactor outlet during the catalytic testing of the sample Z40_IMS_Ac_0,2.

O_2 is expected as a product since it originates from the decomposition reaction of N_2O into molecular N_2 and O_2. On the other hand, NO and NO_2 are not expected from the stoichiometry of pure N_2O decomposition. As it was explained in ***Chapter 2.2.2***, Turek at al. already observed the production of NO in the oscillating decomposition of N_2O. Moreover, Fanson et al. [58] presented spectroscopic evidence claiming that surface nitrate species are present under oscillatory conditions. In particular, they suggested that during oscillating cycles, there was a slow build-up of surface nitrates, followed by a quick nitrate decomposition that increased the rate of N_2O decomposition.

As it can be seen from ***Figure 4.44***, the O_2 production and the NO_x by-production appear in the form of spikes, rather than proper oscillations. The peak production of O_2, NO, and NO_2 always happens at the start of the period of the catalyst's maximum activity in the decomposition of N_2O. As a matter of fact, the concentration of the unconverted nitrous oxide is at its minimum in the cycle while the O_2, N_2O and NO production is reaching the maximum.

Moreover, the average production of molecular oxygen is basically in agreement with the average conversion of nitrous oxide, although the shape of the two signals seems varied. [8]

Regarding the catalytic activity, this sample presents a high activity in the decomposition of N_2O, especially if it's compared to its equivalent prepared with the ion-exchange technique (Z40_SIS_Ac_0,2). At 400°C the latter presents an N_2O conversion of 2%, while the impregnated sample converts 65% of the inlet gas. Finally, the conversion decreases with the temperature, reaching 8% at 350°C.

The same graphs have been produced for Z25_IMS_Ac_0,2, which is characterized by a lower Si/Al ratio that the previous sample.

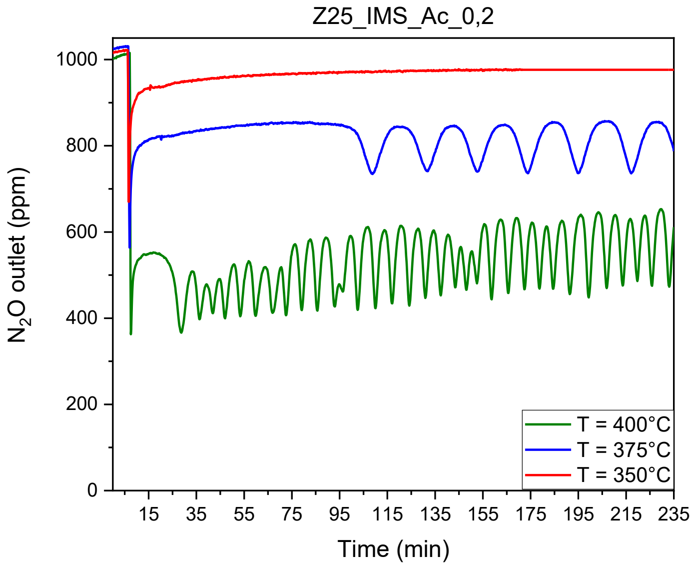

Figure 4.45 Outlet concentration of N_2O during the catalytic activity testing of Z25_IMS_Ac_0,2.

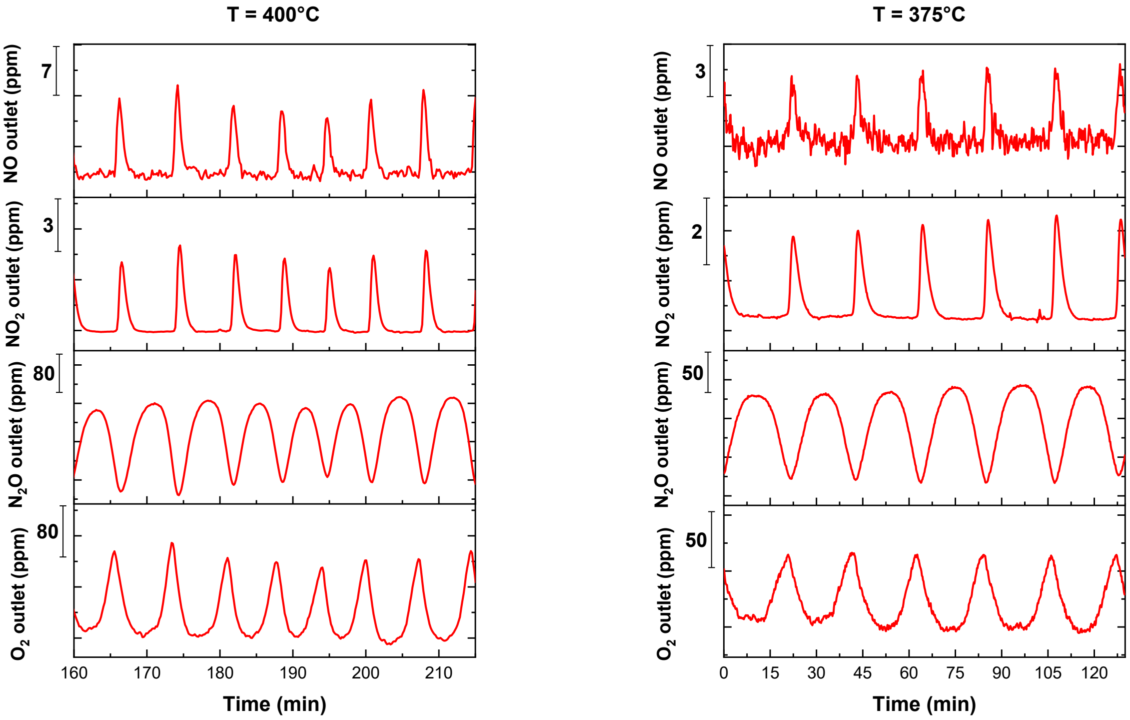

Figure 4.46 Composition of NO, NO_2, N_2O and O_2 at the reactor outlet during the catalytic testing of the sample Z25_IMS_Ac_0,2.

As it can be seen from ***Figure 4.45***, Z25_IMS_Ac_0,2 induces the oscillating behaviour of the N_2O decomposition at the two higher temperatures as well. Similarly to the previous sample (Z40_IMS_Ac_0,2), their frequency decreases with the temperatures, while their period increases. However, contrary to Z40_IMS_Ac_0,2, the oscillations appear to be more regular, and they are characterized by longer periods (***Figure 4.46***). For instance, at 400°C, the period relative to Z40_IMS_Ac_0,2's oscillations is 3,5 minutes long, while the one relative to Z25_IMS_Ac_0,2 has doubled, reaching 7 minutes. Moreover, the conversion of Z25_IMS_Ac_0,2 is lower than the previous sample, reaching 47% at 400°C.

Subsequently, the catalyst with the lower Si/Al and with the higher amount of Al in its structure (Z12_IMS_Ac_0,2) has been tested as well.

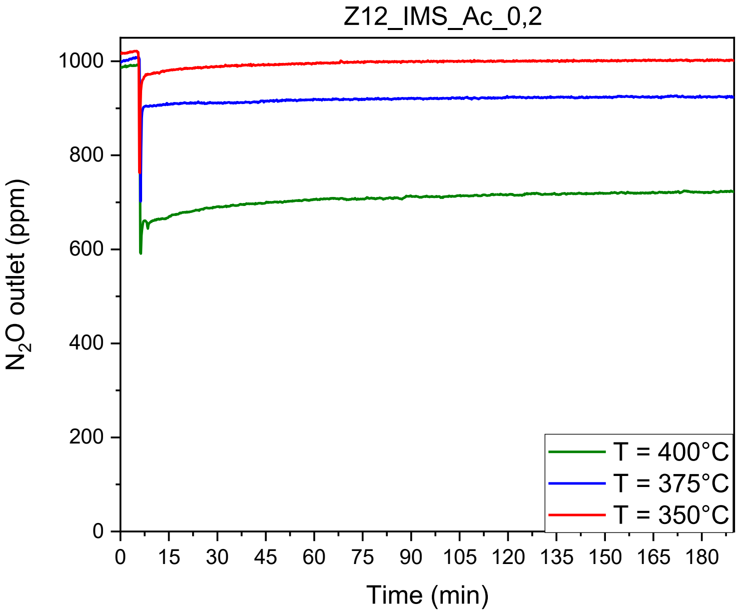

Figure 4.47 Outlet concentration of N_2O during the catalytic activity testing of Z12_IMS_Ac_0,2.

As it can be seen from ***Figure 4.47***, this sample doesn't exhibit any oscillation, not even at the higher temperature. In this case the conversion spans from 4% to 28%, the highest conversion being achieved at 400°C.

Table 4.7 reports the catalytic properties of the samples analysed so far, which have been all synthetized with 0,2 g of copper acetate, the highest quantity of precursor used in this thesis for the impregnated samples.

Table 4.7 Catalytic properties of the impregnated samples synthetized with 0,2 g of precursor.

SAMPLE	Temperature (°C)	Conversion (%)	Period (min)	Residence time (min)	Amplitude (ppm)
Z40_IMS_Ac_0,2	400	65	3,5	37	70
	375	40	11	57	125
	350	8	-	∞	-
Z25_IMS_Ac_0,2	400	47	7	28	174
	375	23	21	108	131
	350	5	-	∞	-
Z12_IMS_Ac_0,2	400	28	-	∞	-
	375	9	-	∞	-
	350	4	-	∞	-

As it was mentioned earlier, for all the catalysts the conversion decreased with the temperature and with the Si/Al ratio. In fact, the highest value is achieved for the Z40_IMS_Ac_0,2 sample at 400°C, while the lowest one is reached by the Z12_IMS_Ac_0,2 sample at 350°C. Both of these samples contain the highest amount of copper recorded by EDX in their group (***Chapter 3.3.5***). Moreover, both exhibit features attributed to the presence of CuO clusters in their H_2-TPR and FT-IR spectra. Regarding the oscillations, the period and the amplitude have been calculated in the latest section of the test, as a mean value of the most regular oscillations. The period of the oscillations increases when the temperature and the Si/Al ratio decrease. As a matter of fact, the longest period is achieved at 350°C for the Z25_IMS_Ac_0,2 sample, which also presents the most regular oscillations in this group of samples. This sample is also characterized by the highest amplitudes. Finally, the residence time has been calculated as the timespan since the beginning of the test until the start of the oscillations, and it is representative of the transient phase of the system. The value ∞ is relative to those sample which do not exhibit any oscillations. As it can be seen from ***Table 4.7***, the residence time increase significantly as the temperature decreases. In particular, for the sample Z25_IMS_Ac_0,2 there is an increase of 286 % (going from 28 to 108 min), even though the temperature has been lowered by only 25°C. By observing this trend, it's possible to assume that perhaps no oscillation is seen at 350°C because of the extreme long residence time that could originate from the decrease of the temperature, thus exceeding the period of testing.

In conclusion, ***Figure 4.48*** reports the behaviour of the three catalysts with different Si/Al ratio at a fixed temperature.

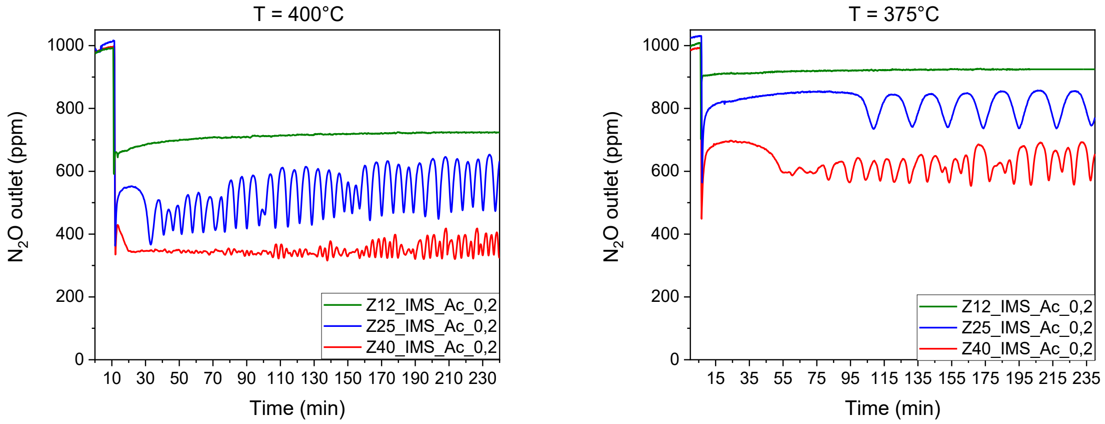

Figure 4.48 Comparison between the samples the impregnated samples synthetized with 0,2 g of precursor at 400°C (on the left) and at 375°C (on the right).

It can be clearly seen that the conversion decreases with the temperature and that between all sample, Z40_IMS_Ac_0,2 presents the best catalytic activity while Z25_IMS_Ac_0,2 is characterized by the most regular oscillations. The oscillations of the sample Z25_IMS_Ac_0,2 appear later than the ones relative to Z40_IMS_Ac_0,2, for both the temperatures. As a result, the residence time of the latter is significantly lower than the former's (***Table 4.7***).

The following figures show the evolution of N_2O outlet concentration as a function of time for the impregnated catalysts, synthetized with 0,1 g of copper precursor.

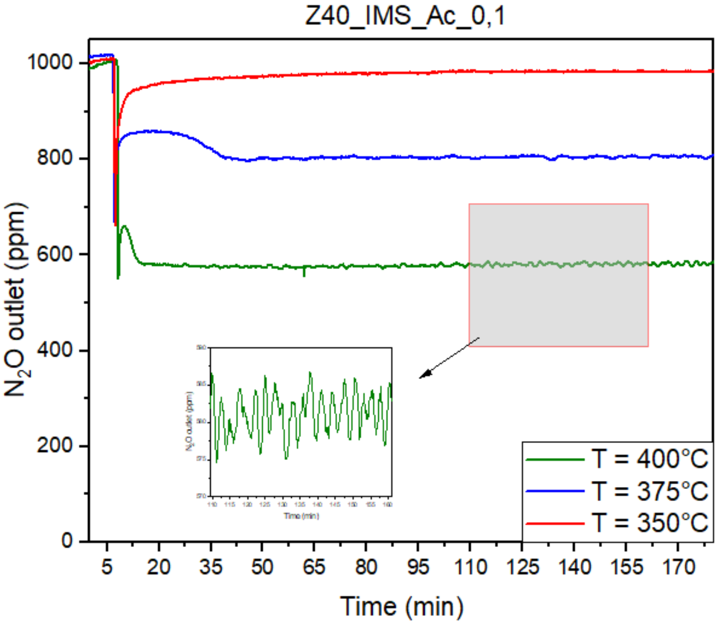

Figure 4.49 Outlet concentration of N_2O during the catalytic activity testing of Z40_IMS_Ac_0,1. The decomposition curve at 400°C has been magnified to better observe the oscillations.

As it can be seen from ***Figure 4.49***, the sample Z40_IMS_Ac_0,1 doesn't present any regular oscillations. At the highest temperature, some irregular oscillations can be observed, while at 375°C it exhibits a noisy signal, which could be a sign of an incipient oscillatory phenomena. In both cases it's possible to observe the overshoot due to the reducing He pre-treatment. When it comes to the catalytic activity, even in this case the conversion decreases with the temperature and it's slightly lower than the sample Z40_IMS_Ac_0,2.
The same graph has been produced for Z25_IMS_Ac_0,1, along with the magnification of the oscillating phenomena.

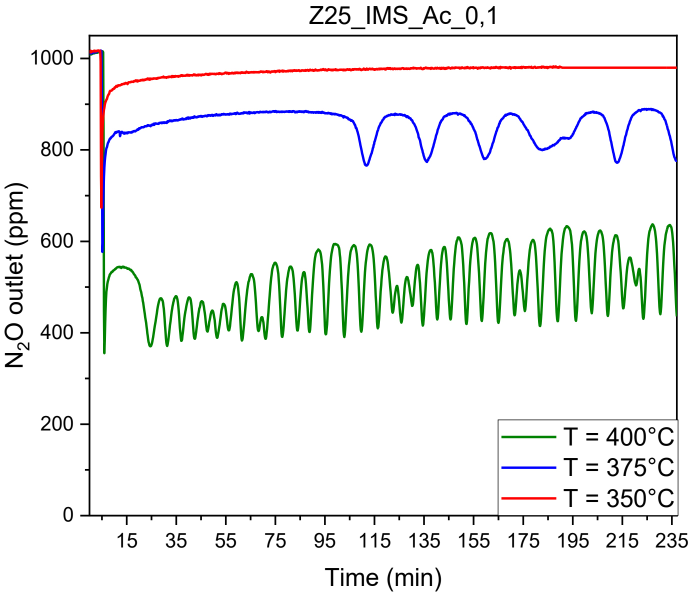

Figure 4.50 Outlet concentration of N_2O during the catalytic activity testing of Z25_IMS_Ac_0,1.

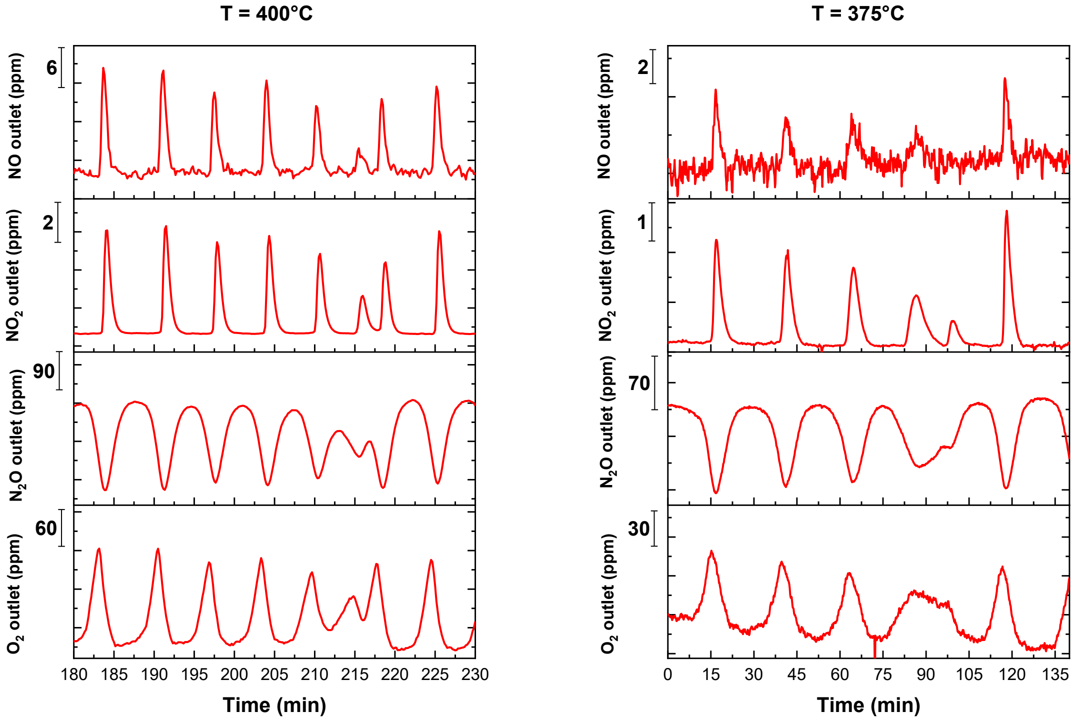

Figure 4.51 Composition of NO, NO_2, N_2O and O_2 at the reactor outlet during the catalytic testing of the sample Z25_IMS_Ac_0,1.

Z25_IMS_Ac_0,1 is the only impregnated sample prepared with 0,1 g of precursor that exhibits regular oscillations, specifically at 375°C and 400°C. In ***Figure 4.51*** it's possible to observe the oscillations of all the components. Even in this case the oscillations of O_2, NO and N_2O appears in form of spikes, and are in opposite phase with respect to the oscillations of the reactant.

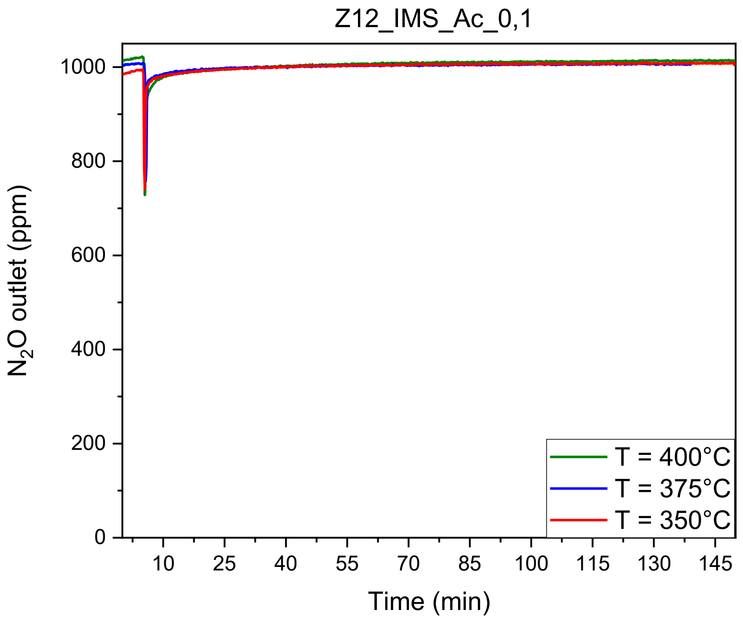

Figure 4.52 Outlet concentration of N_2O during the catalytic activity testing of Z12_IMS_Ac_0,1.

As it can be seen from ***Figure 4.52***, the catalyst with the lowest Si/Al ratio (Z12_IMS_Ac_0,1) doesn't exhibit any oscillations.
Table 4.8 reports the catalytic properties of the impregnated samples, synthetized with 0,1 g of copper acetate.

Table 4.8 Catalytic properties of the impregnated samples synthetized with 0,1 g of precursor.

SAMPLE	Temperature (°C)	Conversion (%)	Period (min)	Residence time (min)	Amplitude (ppm)
Z40_IMS_Ac_0,1	400	42	-	12	-
	375	21	-	∞	-
	350	3	-	∞	-
Z25_IMS_Ac_0,1	400	48	7,5	23	197
	375	18	23	111	111
	350	5	-	∞	-
Z12_IMS_Ac_0,1	400	2,6	-	∞	-
	375	1,3	-	∞	-
	350	1	-	∞	-

The amplitude and the period of the oscillations have been calculated for the sample Z25_IMS_Ac_0,1, since it's the only one which presents a regular pattern. These parameters, along with the conversion values, are very similar to those found with the sample Z25_IMS_Ac_0,2, even though the latter had been synthetized with twice the amount of copper precursor (***Table 4.7***). On the other hand, at 400°C, Z40_IMS_Ac_0,2 exhibits a conversion of 65%, while Z40_IMS_Ac_0,1 converts approximately 42% of the inlet N_2O gas. The same can be observed for Z12_IMS_Ac_0,1, which presents a significant low conversion of 2,5 % at 400°C, as opposed to Z12_IMS_Ac_0,2, which converts 28% of the inlet gas at the same temperature. Therefore, only for these two samples, the decrease of the nominal amount of copper during the synthesis has significantly impacted the catalytic activity.

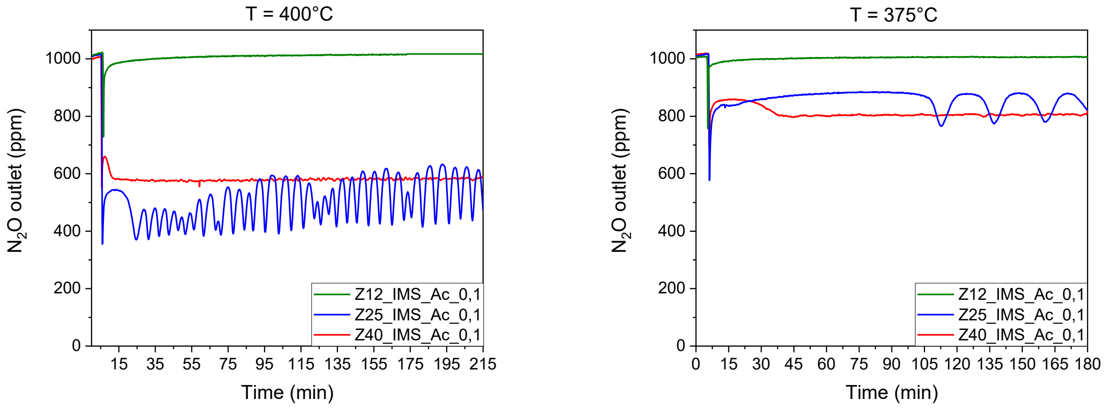

Figure 4.53 Comparison between the impregnated samples synthetized with 0,1 g of precursor at 400°C (on the left) and at 375°C (on the right).

In ***Figure 4.53*** it's possible to see more clearly that the only sample which exhibits regular oscillations for this group is Z25_IMS_Ac_0,1. Moreover, at 400°C, this sample presents the higher conversion, as opposed to the ones impregnated with 0,2 g of precursor, in which the most performant has always been the sample with the highest Si/Al ratio (Z40_IMS_Ac_0,2). However, at 375°C the situation changes and the sample with the highest Si/Al ratio (Z40_IMS_Ac_0,1) exhibits the highest conversion again. In all cases, the less performant sample remains Z12_IMS_Ac_0,1.

Figure 4.54-Figure 4.56 represent the catalytic activities of the impregnated samples synthetized with 0,05 g of copper precursor, which is the lowest quantity used for the impregnated catalysts. Only two samples have been prepared, by excluding the parent zeolite having the Si/Al ratio of 12. This choice has been made on the basis of the previous results, since the samples with the lowest Si/Al ratio didn't exhibit any oscillatory behaviour, in addition to a low catalytic activity.

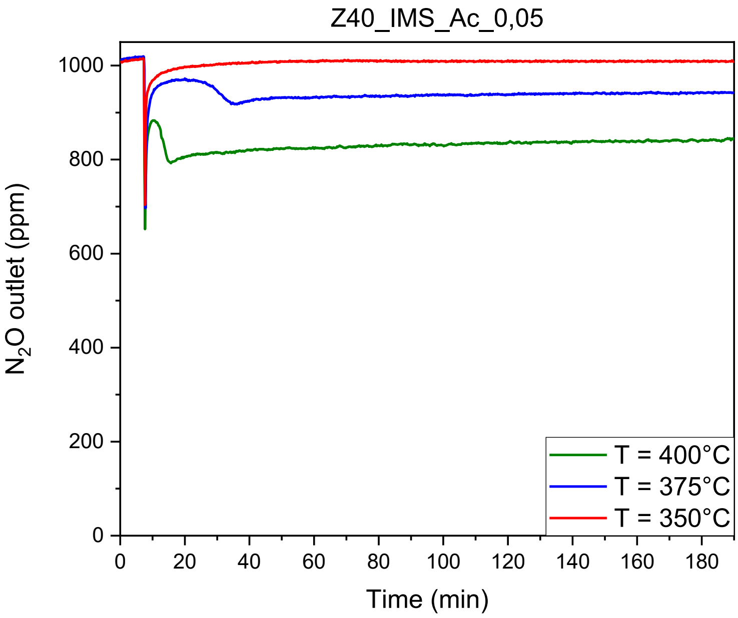

Figure 4.54 Outlet concentration of N_2O during the catalytic activity testing of Z40_IMS_Ac_0,05.

As it can be seen from ***Figure 4.54***, Z40_IMS_Ac_0,05 doesn't exhibit any oscillations.

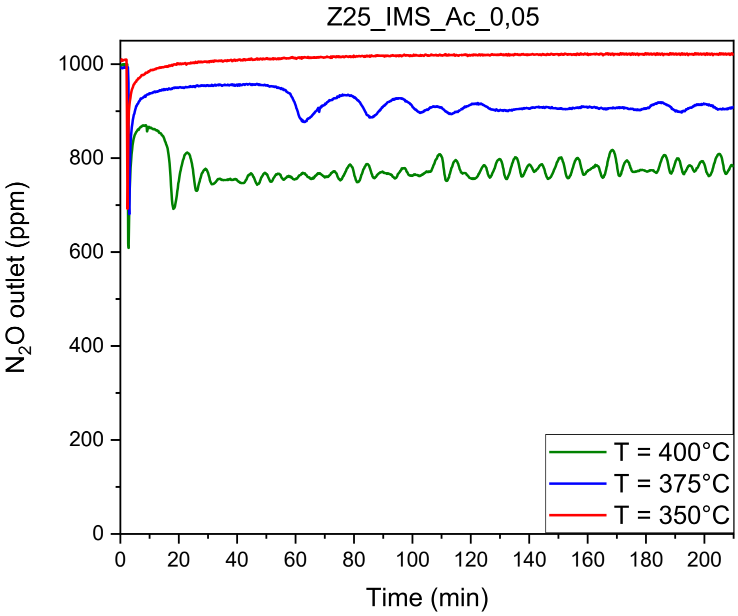

Figure 4.55 Outlet concentration of N_2O during the catalytic activity testing of Z25_IMS_Ac_0,05.

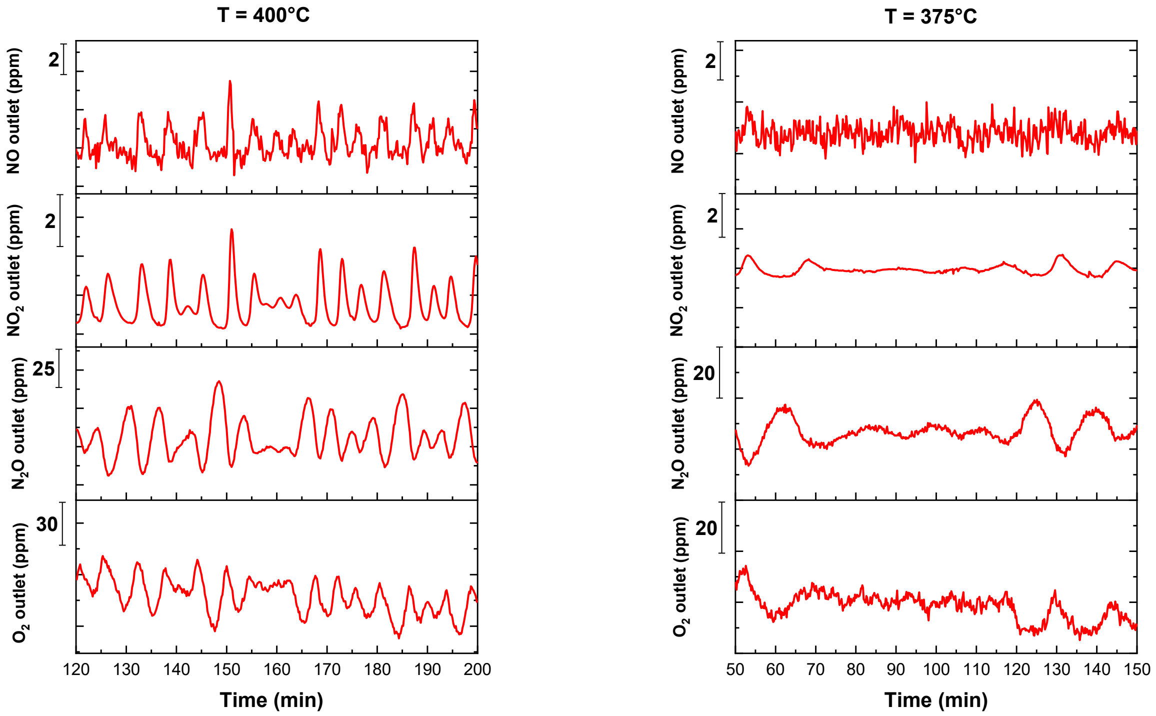

Figure 4.56 Composition of NO, NO_2, N_2O and O_2 at the reactor outlet during the catalytic testing of the sample Z25_IMS_Ac_0,05.

As it can be seen from ***Figure 4.55***, Z25_IMS_Ac_0,05 is the only sample who still exhibits an oscillatory behaviour at 400°C and 375°C. However, these oscillations exhibit a highly irregular pattern (***Figure 4.56***). ***Table 4.9*** reports the catalytic properties of the impregnated samples, synthetized with 0,05 g of copper acetate. Contrary to the previous cases, no amplitude or period have been calculated due to the irregular behaviour of the oscillations.

Table 4.9 Catalytic properties of the impregnated samples, synthetized with 0,05 g of precursor.

SAMPLE	Temperature (°C)	Conversion (%)	Residence time (min)
Z40_IMS_Ac_0,05	400	18	∞
	375	8	∞
	350	0,8	∞
Z25_IMS_Ac_0,05	400	22	18
	375	10	63
	350	0,7	∞

As always, the conversion decreases with temperature while the residence time increases significantly. However, in this case, the two samples exhibit similar conversion values, therefore the only difference between them relies in the presence of oscillations for the sample Z25_IMS_Ac_0,05.

The following figures compare the impregnated catalyst synthetized from the same parent zeolite but with different quantities of precursor. The comparison is shown at 400°C, since it's the highest temperature used, and it's therefore characterized by the highest conversion values.

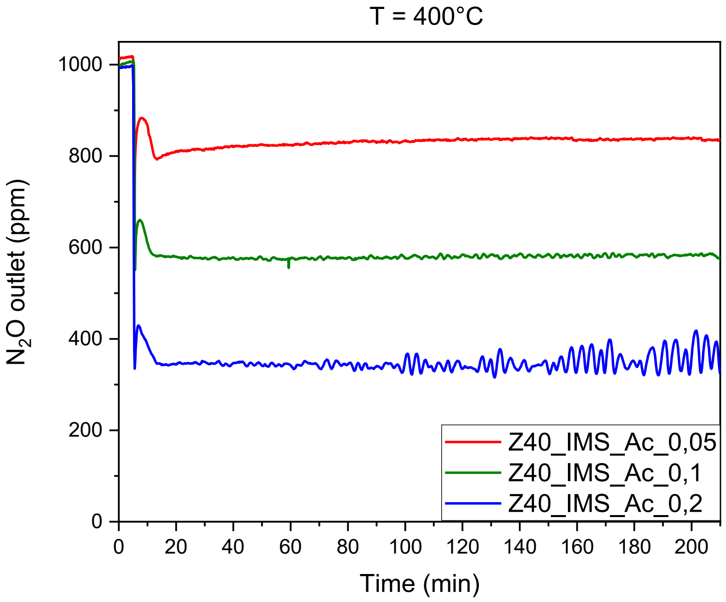

Figure 4.57 Comparison between the samples synthetized from the zeolite with Si/Al ratio equal to 40.

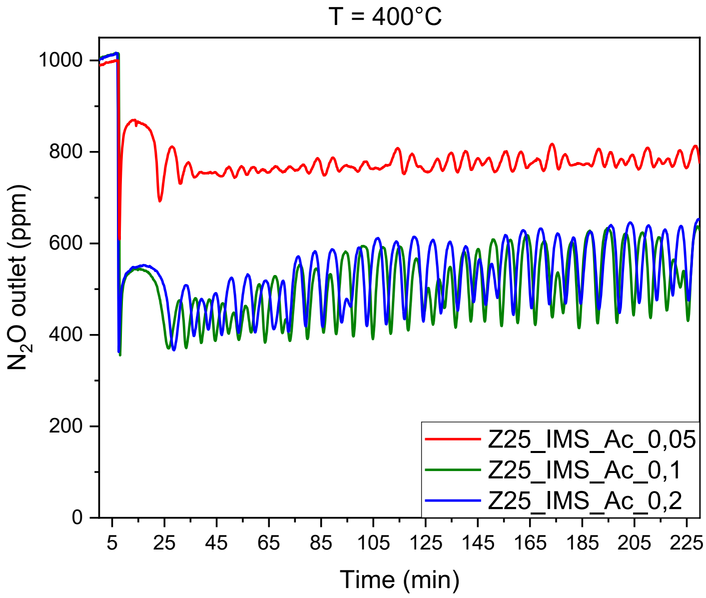

Figure 4.58 Comparison between the samples synthetized from the zeolite with Si/Al ratio equal to 25.

As it can be seen from ***Figure 4.58***, the impregnated samples with Si/Al ratio equal to 25 constitute the only group which exhibits oscillations for any quantity of precursor used in the synthesis. From both the figures it's possible to see how the residence time is similar for the samples prepared from the same parent zeolite, no matter how much precursor has been used in the synthesis. Therefore, the residence time and the peak in the transitory phase due to the reducing pre-treatment could be correlated to the properties of the parent zeolite. In ***Figure 4.57***, the conversion of the zeolites having the Si/Al ratio equal to 40 decreases with the quantity of precursor. This can't be said for the samples synthetized from the parent zeolite with Si/Al ratio equal to 25 (***Figure 4.58***). As a matter of fact, Z25_IMS_Ac_0,2 and Z25_IMS_Ac_0,1 exhibits a very similar catalytic activity, even though the latter has been synthetized with half quantity of copper precursor with respect to the former.

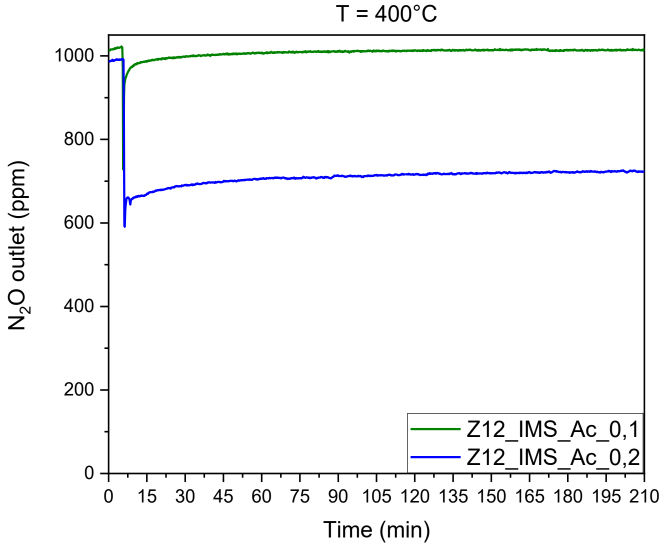

Figure 4.59 Comparison between the samples synthetized from the zeolite with Si/Al ratio equal to 12.

Finally, the conversion of the samples with the lowest Si/Al ratio in ***Figure 4.59*** decreases significantly with the temperature, reaching 1% at 375°C. Moreover, the samples don't exhibit any oscillations, not even at the highest nominal quantity of precursor.

4.2.3 NS1_IMS_Ac_0,2 and Z25_IMS_Nt_0,2

The Z25_IMS_Nt_0,2 has been tested as well, to investigate better the effect of the copper precursor.

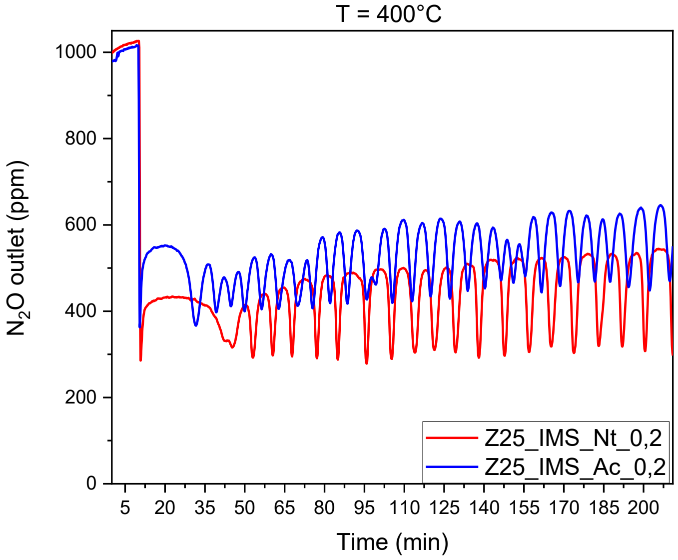

Figure 4.60 Outlet concentration of N_2O during the catalytic activity testing of Z25_IMS_Nt_0,2 compared to Z25_IMS_Ac_0,2.

The two samples differ only because of the type of precursor used, while the quantity of the precursor, the type of synthesis and the parent zeolite are the same. The parent zeolite with Si/Al ratio equal to 25 has been chosen since the samples deriving from it are the one who exhibits oscillations most of the cases, as it was observed from the results in the previous section. ***Figure 4.60*** shows how the sample prepared with copper nitrate exhibits regular oscillations, and a higher conversion value compared to Z25_IMS_Ac_0,2.

NS1_IMS_Ac_0,2 was synthetized in order to investigate the effect of the parent zeolite on the catalytic activity. As it was described in ***Chapter 3.1***, the original framework of this sample is silicate-1 microporous zeolite with MFI framework type and Si/Al ratio = infinity, which has been impregnated with 0,2 g of copper acetate.
This analysis has been performed on specifically synthetized zeolite with the structure identical to ZSM-5, however where the structural units are made from silanol nests and therefore in the absence of any Al sites, on which Cu could be exchanged. As a result, all the introduced copper is deposited as CuO particles, and none of it is exchanged because of the absence of Al sites. As it can be seen from ***Figure 4.61***, in addition to not exhibiting oscillations, the sample doesn't convert any of the inlet gas. As opposed to this case, it can be observed that the zeolites with the lowest Si/Al ratio (=12) are the ones characterized by the greatest number of Al sites, which allow these samples to exchange more copper species than the other zeolites. However, none of these zeolites exhibited any oscillations pattern, not even at the highest temperature. Therefore, it can be concluded that in order to observe oscillations, it's necessary to have both CuO particles and exchanged copper ions in the structure, which is the case of the zeolites having the intermediate Si/Al ratio, equal to 25.

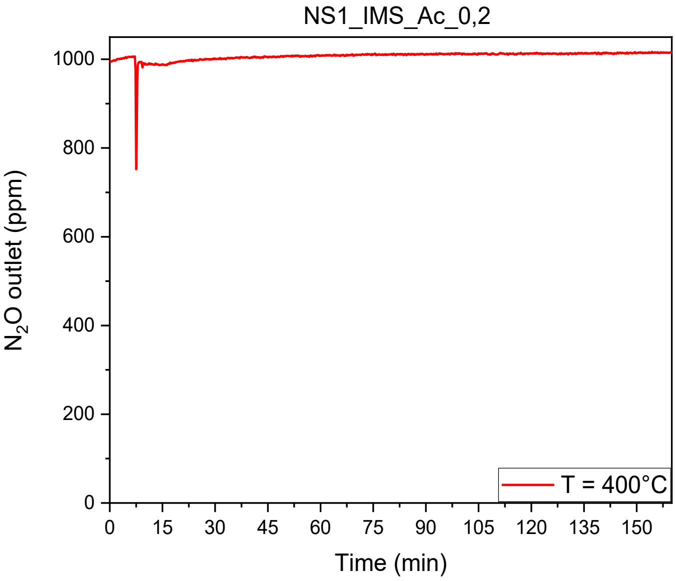

Figure 4.61 Outlet concentration of N_2O during the catalytic activity testing of NS1_IMS_Ac_0,2.

As it can be seen from ***Table 4.10***, even the oscillations exhibit different patterns. In fact, Z25_IMS_Nt_0,2 is characterized by higher period, residence time and amplitude values as opposed to the other sample. Moreover, contrary to what it was observed in ***Figure 4.59***, the residence time is different for the two zeolites, even though they both have the same Si/Al ratio. Therefore, this parameter can be affected by the type of precursor used, independently of the Si/Al ratio.

Table 4.10 Comparison between the catalytic properties of Z25_IMS_Ac_0,2 and Z25_IMS_Nt_0,2.

SAMPLE	Temperature (°C)	Conversion (%)	Period (min)	Residence time (min)	Amplitude (ppm)
Z25_IMS_Ac_0,2	400	47	7	28	174
Z25_IMS_Nt_0,2	400	59	9	45	212

5. Conclusions and future perspectives

This Master Thesis work has been dedicated to the study of the catalytic activity and the oscillatory behaviour regarding the decomposition of N_2O over Cu-ZSM-5 zeolites. Several catalysts have been synthetized though the ion-exchange or the impregnation method, starting from zeolites with three different Si/Al ratios, and using copper acetate as precursor.

The catalytic tests have revealed that the ion-exchanged samples exhibited a low catalytic activity and no oscillatory behaviour, as opposed to the impregnated ones. In addition to exhibiting a good catalytic activity (reaching 65% of conversion with Z40_IMS_Ac_0,2), the impregnated samples presented an oscillatory behaviour only for the zeolites with the two highest Si/Al ratio (equal to 40 and 25), at 400 and 375°C. In particular, only the impregnated zeolites with the intermediate Si/Al ratio showed an oscillatory behaviour in any of the conditions tested. The same can't be said for the zeolites with the Si/Al ratio equal to 40, which exhibited irregular oscillation when 0,1 g of precursor were used (***Figure 4.49***) and no oscillations at all when 0,05 g of precursor were employed in the synthesis (***Figure 4.54***). Finally, none of the impregnated samples with the lowest Si/Al ratio exhibited any oscillatory behaviour.

The characterization tests helped to shed more light on the differences between the impregnated and the ion-exchanged samples. First, both EDX and XRF showed that the impregnated samples presented a significantly higher copper content that the ion-exchanged ones (***Table 4.1***). This is because during the synthesis of the impregnated samples, most of the precursor is introduced in the zeolite, thanks to the evaporation of the solution, as opposed to the ion-exchanged ones, where the excess of the precursor is eliminated through centrifugation. Moreover, the zeolites with the lowest Si/Al ratio contained more copper, since they are characterized by more Al sites.

Another difference between the ion-exchanged and the impregnated ones is the presence of copper oxide (CuO) clusters. The H_2-TPR analysis revealed the presence of sharp peaks in the 250-270°C range only for the impregnated samples, which were attributed to the reduction of CuO clusters. The presence of such species is also supported by the scientific literature, which demonstrated that in the impregnated samples there is usually present a substantial amount of aggregation in the copper-containing clusters, which are preferentially located at the external surface of the material. [38] These peaks are absent in the ion-exchanged samples, which however exhibited a higher number of peaks attributed to the reduction of the various copper species introduced in the zeolitic framework. Additionally, the XRD analysis revealed the presence of a peak attributed to the CuO clusters only for the impregnated samples with 0,2 of precursor. In the ones synthesise with 0,1 g of precursor this peak was not recorded because the CuO particles were finely dispersed on the surface. The combination of the EDX and the TPR results allowed the calculation of the H_2/Cu ratio, which was closer to 1 for the impregnated samples, meaning that most of the copper has been reduced in the process.

The FTIR revealed the presence of dicarbonyl and monocarbonyl species for all the samples. However, only the impregnated samples with the highest Si/Al ratio (i.e the ones who exhibited the oscillations) presented a shoulder correspondent to the CuO particles (***Figure 4.26***), while none of the zeolite with Si/Al were characterized by this feature.

In conclusion, the zeolites with the intermediate Si/Al ratio, which always exhibited the oscillatory behaviour, are characterized by the following characteristics:

- An optimal Si/Al ratio which allowed the introduction of copper ions and species in the structure. A decrease of the zeolite Si/Al ratio leads to an increase of the number of ion-exchange sites, reaching the maximum concentration of isolated Cu^{2+} ions for the zeolite with the Si/Al ratio equal to 12.

- The abundance of CuO clusters present on the zeolites, which were proved by the TPR, the XRD and the FTIR analysis.
- The FTIR spectra presented a well-defined isosbestic point, which could indicate the homogeneity of the copper species in the structure.
- These samples were characterized by the higher exchanged percentage of the Brønsted sites (%EX), calculated in ***Table 4.4***.

As it was explained earlier, the Si/Al is an important factor which could determine the occurrence of the oscillatory phenomenon. The fact that the zeolites with the intermediate Si/Al ratio exhibited such evident oscillation can be due to the synergy and the coexistence of the copper species and the CuO clusters, which could favour the occurrence of the oscillatory phenomena. As a matter of fact, Armandi et al. suggested that the oscillatory phenomenon could be associated with the presence of oligomeric Cu_xO_y species with extra-lattice oxygen (ELO), which are able to undergo reduction/oxidation cycles. Such species are mostly present in excessively exchanged samples prepared through impregnation. [8] On the other hand, the structure of the zeolites with the lower Si/Al ratio (which never exhibited any oscillations) is mostly characterized by the presence of copper ions, thanks to the significant amount of Al sites.

There are several fields in which the future development of this Master Theis can be done. First, a different precursor could be used in the synthesis, to investigate its effect on the oscillatory behaviour and on the catalytic activity. In this thesis, copper nitrate has been used as precursor to synthetize an impregnated sample, instead of copper acetate. When compared with its homologous synthetized with copper acetate, it can be observed that the catalytic activity was better, and the oscillatory behaviour was more pronounced (***Figure 4.60***). Therefore, this aspect should be investigated for the ion-exchanged samples as well.

Moreover, for the ion-exchanged samples it would be interested to explore better the effect of temperature during the synthesis procedure. As it can be seen from ***Table 4.6***, that the sample Z25_SI50°C_Ac_0,2 exhibited a slightly higher conversion that its homologous synthetized at RT. Therefore, the same could be done for other zeolites by synthetizing them at 50°C or at slightly higher temperatures, without reaching the boiling point of the solution.

Finally, as opposed to what was done in this study, the ion-exchanged samples could be synthetized by repeating the synthesis at least twice (repetitive ion-exchange), in order to allow a better introduction of the copper into the zeolite's structure.

6. List of symbols

BASs: Bronsted acid sites

BET: Brunauer-Emmett-Teller

CBUs: composite building units

Ea: activation energy (kcal/mol)

ELO: extra-lattice oxygen

EX : exchange percentage of the Bronsted sites (%)

GHG: Green House Gas

GWP: Global warming potential

LASs: Lewis acid sites

M: molarity (mmol/L)

NSCR: non-selective catalytic reduction

N_T: active site concentration (mol/g_{cat})

ODP: Ozone Depleting Potential (Kt/yr)

P/P_0 : relative pressure

PBUs: primary building units

r_{N2O}: conversion rate of N_2O ($mol/s\ g_{cat}$)

RT: room temperature (°C)

SBUs: secondary building units

SCR: selective catalytic reduction

SSA: specific surface area (m^2/g)

Teragrams N_2O-N/yr: teragrams of N_2O in equivalent nitrogen units per year (Tg N/yr)

TWC: three-way catalytic converter

$\Delta_r H^0$: standard heat of reaction (kJ/mol)

θ : half of the diffraction angle (°)

7. References

[1] G. Randhawa and A. Bodenham, "The increasing recreational use of nitrous oxide: History revisited," *Br J Anaesth*, vol. 116, no. 3, pp. 321–324, Mar. 2016, doi: 10.1093/BJA/AEV297.

[2] F. Lin, T. Andana, Y. Wu, J. Szanyi, Y. Wang, and F. Gao, "Catalytic site requirements for N2O decomposition on Cu-, Co-, and Fe-SSZ-13 zeolites," *J Catal*, vol. 401, pp. 70–80, Sep. 2021, doi: 10.1016/j.jcat.2021.07.012.

[3] A. F. Bouwman and United Nations Environment Programme, *Drawing down N_2O to protect climate and the ozone layer : a UNEP synthesis report*.

[4] "Nitrogen Oxides (NOx), Why and How They Are Controlled," 1999. [Online]. Available: http://www.epa.gov/ttn/catc

[5] T. Boningari and P. G. Smirniotis, "Impact of nitrogen oxides on the environment and human health: Mn-based materials for the NOx abatement," *Current Opinion in Chemical Engineering*, vol. 13. Elsevier Ltd, pp. 133–141, Aug. 01, 2016. doi: 10.1016/j.coche.2016.09.004.

[6] R. W. Portmann, J. S. Daniel, and A. R. Ravishankara, "Stratospheric ozone depletion due to nitrous oxide: Influences of other gases," *Philosophical Transactions of the Royal Society B: Biological Sciences*, vol. 367, no. 1593, pp. 1256–1264, 2012, doi: 10.1098/rstb.2011.0377.

[7] A. R. Ravishankara, J. S. Daniel, and R. W. Portmann, "Nitrous oxide (N2O): The dominant ozone-depleting substance emitted in the 21st century," *Science (1979)*, vol. 326, no. 5949, pp. 123–125, 2009, doi: 10.1126/science.1176985.

[8] M. Armandi, T. Andana, S. Bensaid, M. Piumetti, B. Bonelli, and R. Pirone, "Effect of the preparation technique of Cu-ZSM-5 catalysts on the isothermal oscillatory behavior of nitrous oxide decomposition," *Catal Today*, vol. 345, pp. 59–70, Apr. 2020, doi: 10.1016/j.cattod.2019.10.018.

[9] "Overview of Greenhouse Gases | US EPA." https://www.epa.gov/ghgemissions/overview-greenhouse-gases (accessed Jan. 10, 2023).

[10] D. Chen *et al.*, "SPM 147 1 Framing, Context, and Methods Coordinating Lead Authors: Lead Authors: Contributing Authors", doi: 10.1017/9781009157896.003.

[11] H. Tian *et al.*, "A comprehensive quantification of global nitrous oxide sources and sinks," *Nature*, vol. 586, no. 7828, pp. 248–256, Oct. 2020, doi: 10.1038/s41586-020-2780-0.

[12] A. J. Thomson, G. Giannopoulos, J. Pretty, E. M. Baggs, and D. J. Richardson, "Biological sources and sinks of nitrous oxide and strategies to mitigate emissions," *Philosophical Transactions of the Royal Society B: Biological Sciences*, vol. 367, no. 1593. Royal Society, pp. 1157–1168, 2012. doi: 10.1098/rstb.2011.0415.

[13] M. Konsolakis, "Recent Advances on Nitrous Oxide (N2O) Decomposition over Non-Noble-Metal Oxide Catalysts: Catalytic Performance, Mechanistic Considerations, and Surface Chemistry Aspects," *ACS Catalysis*, vol. 5, no. 11. American Chemical Society, pp. 6397–6421, Nov. 06, 2015. doi: 10.1021/acscatal.5b01605.

[14] "COM(2013) 683 final REPORT FROM THE COMMISSION TO THE COUNCIL AND THE EUROPEAN PARLIAMENT on the implementation of Council Directive 91/676/EEC concerning the protection of waters against

pollution caused by nitrates from agricultural sources based on Member State reports for the period 2008-2011 {SWD(2013) 405 final}," 2013.

[15] "U.S. Energy Information Administration - EIA - Independent Statistics and Analysis." https://www.eia.gov/environment/emissions/ghg_report/ (accessed Jan. 12, 2023).

[16] C. J. Rhodes, "Properties and applications of zeolites," *Sci Prog*, vol. 93, no. 3, pp. 223–284, 2010, doi: 10.3184/003685010X12800828155007.

[17] J. Chen and J. Wiley, "Chemistry of Zeolites and Related Porous Materials: Synthesis and Structure."

[18] K. Na, M. Choi, and R. Ryoo, "Recent advances in the synthesis of hierarchically nanoporous zeolites," *Microporous and Mesoporous Materials*, vol. 166, pp. 3–19, Jan. 2013, doi: 10.1016/J.MICROMESO.2012.03.054.

[19] P. C. Martínez Sánchez and J. Pérez Pariente, *Zeolites and ordered porous solids : fundamentals and applications*. Editorial Universitat Politècnica de València, 2011.

[20] M. Granda Valdés, A. I. Pérez-Cordoves, and M. E. Díaz-García, "Zeolites and zeolite-based materials in analytical chemistry", doi: 10.1016/j.trac.2005.04.016.

[21] G. Book, "IUPAC Gold Book".

[22] E. G. Derouane *et al.*, "The acidity of zeolites: Concepts, measurements and relation to catalysis: A review on experimental and theoretical methods for the study of zeolite acidity," *Catal Rev Sci Eng*, vol. 55, no. 4, pp. 454–515, Sep. 2013, doi: 10.1080/01614940.2013.822266.

[23] A. Edited by JiříJiříˇJiříČejka, A. Corma, and S. Zones, "Zeolites and Catalysis."

[24] L. Lisi, R. Pirone, G. Russo, N. Santamaria, and V. Stanzione, "Nitrates and nitrous oxide formation during the interaction of nitrogen oxides with Cu-ZSM-5 at low temperature," *Appl Catal A Gen*, vol. 413–414, pp. 117–131, Jan. 2012, doi: 10.1016/j.apcata.2011.10.049.

[25] M. L. Tsai, R. G. Hadt, P. Vanelderen, B. F. Sels, R. A. Schoonheydt, and E. I. Solomon, "2+ Active site formation in Cu-ZSM-5: Geometric and electronic structure requirements for N2O activation," *J Am Chem Soc*, vol. 136, no. 9, pp. 3522–3529, Mar. 2014, doi: 10.1021/ja4113808.

[26] F. Kapteijn, J. Rodriguez-Mirasol ', and J. A. Moulijn, "Heterogeneous catalytic decomposition of nitrous oxide," 1996.

[27] F. Kapteijn, G. Marbán, M. Marbán, J. Jos´, J. Rodriguez-Mirasol, and J. A. Moulijn, "Kinetic Analysis of the Decomposition of Nitrous Oxide over ZSM-5 Catalysts," 1997.

[28] P. Ciambelli, A. di Benedetto, E. Garufi, R. Pirone, and G. Russo, "Spontaneous Isothermal Oscillations in N 2 O Decomposition over a Cu-ZSM5 Catalyst Spontaneous isothermal oscillations of N 2 O and O 2 outlet con-centrations are observed in N 2 O decomposition," 1998.

[29] T. Ochs and T. Turek, "The mechanism of kinetic oscillations in the catalytic N O decomposition over Cu-ZSM-5," 1999.

[30] H.-G. Lintz and T. Turek, "Isothermal oscillations in the catalytic decomposition of nitrous oxide over Cu-ZSM-5," 1995.

[31] P. Ciambelli, E. Garufi, R. Pirone ', G. Russo ', and F. Santagata ', "Oscillatory behaviour in nitrous oxide decomposition on over-exchanged Cu-ZSM-5 zeolite," 1996.

[32] T. Turek, "Kinetic oscillations during the catalytic decomposition of nitrous oxide," *Catal Today*, vol. 105, no. 2, pp. 275–282, Jul. 2005, doi: 10.1016/j.cattod.2005.01.016.

[33] G. Turnes Palomino, P. Fisicaro, S. Bordiga, A. Zecchina, E. Giamello, and C. Lamberti, “Oxidation States of Copper Ions in ZSM-5 Zeolites. A Multitechnique Investigation,” *Journal of Physical Chemistry B*, vol. 104, no. 17, pp. 4064–4073, May 2000, doi: 10.1021/jp993893u.

[34] V. L. Sushkevich, A. v. Smirnov, and J. A. van Bokhoven, “Autoreduction of Copper in Zeolites: Role of Topology, Si/Al Ratio, and Copper Loading,” *Journal of Physical Chemistry C*, vol. 123, no. 15, pp. 9926–9934, Apr. 2019, doi: 10.1021/acs.jpcc.9b00986.

[35] P. E. Fanning and M. A. Vannice, “A drifts study of Cu-ZSM-5 prior to and during its use for N2O decomposition,” *J Catal*, vol. 207, no. 2, pp. 166–182, 2002, doi: 10.1006/JCAT.2002.3518.

[36] S. A. Yashnik, Z. R. Ismagilov, and V. F. Anufrienko, “Catalytic properties and electronic structure of copper ions in Cu-ZSM-5,” in *Catalysis Today*, Dec. 2005, vol. 110, no. 3–4, pp. 310–322. doi: 10.1016/j.cattod.2005.09.029.

[37] M. H. Groothaert, J. A. van Bokhoven, A. A. Battiston, B. M. Weckhuysen, and R. A. Schoonheydt, “Bis(μ-oxo)dicopper in Cu-ZSM-5 and its role in the decomposition of NO: A combined in situ XAFS, UV-vis-near-IR, and kinetic study,” *J Am Chem Soc*, vol. 125, no. 25, pp. 7629–7640, Jun. 2003, doi: 10.1021/ja029684w.

[38] W. Griinert *et al.*, “Structure, Chemistry, and Activity of Cu-ZSM-5 Catalysts for the Selective Reduction of NO* * in the Presence of Oxygen,” 1994. [Online]. Available: https://pubs.acs.org/sharingguidelines

[39] F. Pinna, “Supported metal catalysts preparation,” *Catal Today*, vol. 41, no. 1–3, pp. 129–137, 1998, doi: 10.1016/S0920-5861(98)00043-1.

[40] C. Perego and P. Villa, “Catalyst preparation methods,” 1997.

[41] S. P. B. Kremer *et al.*, “Zeotile-2: A microporous analogue of MCM-48,” *Solid State Sci*, vol. 7, no. 7, pp. 861–867, Jul. 2005, doi: 10.1016/j.solidstatesciences.2005.01.021.

[42] K. Hadjiivanov, K. I. Hadjiivanov, and D. G. Klissurski, “USE OF CARBON MONOXIDE AS AN IR PROBE MOLECULE FOR TESTING METAL OXIDE SURFACES WITHOUT SAMPLE ACTIVATION Low Carbon Energy for Transport and Doemstic Use (EPLUS) View project Low-carbon Energy for the Transport and Domestic Use-EPLUS View project USE OF CARBON MONOXIDE AS AN IR PROBE MOLECULE FOR TESTING METAL OXIDE SURFACES WITHOUT SAMPLE ACTIVATION,” 1998. [Online]. Available: https://www.researchgate.net/publication/325698082

[43] M. Thommes *et al.*, “Physisorption of gases, with special reference to the evaluation of surface area and pore size distribution (IUPAC Technical Report),” *Pure and Applied Chemistry*, vol. 87, no. 9–10, pp. 1051–1069, Oct. 2015, doi: 10.1515/pac-2014-1117.

[44] J. R. H. Ross, “Some Catalytic Reactions,” in *Heterogeneous Catalysis*, Elsevier, 2012, pp. 171–217. doi: 10.1016/b978-0-444-53363-0.10008-8.

[45] F. Ambroz, T. J. Macdonald, V. Martis, and I. P. Parkin, “Evaluation of the BET theory for the characterization of meso and microporous MOFs,” *Small Methods*, vol. 2, no. 11. John Wiley and Sons Inc, 2018. doi: 10.1002/smtd.201800173.

[46] M. M. J. Treacy and J. B. Higgins, “Collection of Simulated XRD Powder Patterns for Zeolites Editors”, Accessed: Feb. 14, 2023. [Online]. Available: http://www.iza-structure.org/databases/

[47] B. M. Abu-Zied, W. Schwieger, and A. Unger, “Nitrous oxide decomposition over transition metal exchanged ZSM-5 zeolites prepared by the solid-state ion-exchange method,” *Appl Catal B*, vol. 84, no. 1–2, pp. 277–288, Oct. 2008, doi: 10.1016/j.apcatb.2008.04.004.

[48] P. da Costa, B. Modén, G. D. Meitzner, D. K. Lee, and E. Iglesia, “Spectroscopic and chemical characterization of active and inactive Cu species in NO decomposition catalysts based on Cu-ZSM5,” *Physical Chemistry Chemical Physics*, vol. 4, no. 18, pp. 4590–4601, 2002, doi: 10.1039/b203700a.

[49] R. Bulánek, B. Wichterlová, Z. Sobalík, and J. Tichý, “Reducibility and oxidation activity of Cu ions in zeolites Effect of Cu ion coordination and zeolite framework composition,” 2001.

[50] D. S. Cruz-Navarro, M. Torres-Rodríguez, M. Gutiérrez-Arzaluz, V. Mugica-álvarez, and S. B. Pergher, “Comparative Study of Cu/ZSM-5 Catalysts Synthesized by Two Ion-Exchange Methods,” *Crystals (Basel)*, vol. 12, no. 4, Apr. 2022, doi: 10.3390/cryst12040545.

[51] L. Martins, R. Pablo, S. Peguin, and E. Antonio Urquieta-González, “Cu AND Co EXCHANGED ZSM-5 ZEOLITES-ACTIVITY TOWARDS NO REDUCTION AND HYDROCARBON OXIDATION,” 2006.

[52] G. C. Bond, S. N. Namijo, and J. S. Wakeman, “Thermal analysis of catalyst precursors. Part 2. Influence of support and metal precursor on the reducibility of copper catalysts,” *Journal of Molecular Catalysis*, vol. 64, no. 3, pp. 305–319, Feb. 1991, doi: 10.1016/0304-5102(91)85140-W.

[53] J. Y. Yan, G.-D. Lei, W. M. H. Sachtler, and H. H. Kung, “Deactivation of Cu/ZSM-5 Catalysts for Lean NO x Reduction: Characterization of Changes of Cu State and Zeolite Support,” 1996.

[54] S. Bordiga, C. Lamberti, F. Bonino, A. Travert, and F. Thibault-Starzyk, “Probing zeolites by vibrational spectroscopies,” *Chemical Society Reviews*, vol. 44, no. 20. Royal Society of Chemistry, pp. 7262–7341, Oct. 21, 2015. doi: 10.1039/c5cs00396b.

[55] K. I. Hadjiivanov, M. M. Kantcheva, and D. G. Klissurski, “IR study of CO adsorption on Cu-ZSM-5 and CuO/SiO, catalysts: CF and n: components of the Cu+-CO bond.”

[56] P. A. Georgiev, N. Drenchev, K. I. Hadjiivanov, J. Ollivier, T. Unruh, and A. Albinati, “Dynamics of bound states of dihydrogen at Cu(I) and Cu(II) species coordinated near one and two zeolite framework aluminium atoms: A combined sorption, INS, IR and DFT study,” *Int J Hydrogen Energy*, vol. 46, no. 53, pp. 26897–26914, Aug. 2021, doi: 10.1016/j.ijhydene.2021.05.166.

[57] K. Rodponthukwaji *et al.*, “Catalytic upgrading of carboxylic acids as bio-oil models over hierarchical ZSM-5 obtained: Via an organosilane approach,” *RSC Adv*, vol. 7, no. 57, pp. 35581–35589, 2017, doi: 10.1039/c7ra03890a.

[58] P. T. Fanson, M. W. Stradt, W. N. Delgass, and J. Lauterbach, “Infrared evidence for the existence of nitrate species on Cu-ZSM5 during isothermal rate oscillations in the decomposition of N 2 O,” *Catal Letters*, vol. 77, no. 3, 2001.

Acknowledgments

Thank you Allah for the strength and the blessings that You gave me through my life and this academic path.

Thank you mom and dad for raising me in the best environment and allowing me to pursue my dreams and aspirations. You’ve been showing me since an early age what hard work and dedication really are; you will always have my utmost respect and admiration. Thanks to my brothers Hamza, Iliass and Rayan for showing me how important brotherhood and sharing are.

I thank my supervisor prof. Samir Bensaid for giving me the opportunity to work on such an interesting matter, I learned much more than what I could have imagined. I also thank my co-tutors prof. Raffaele Pirone and prof. Marco Piumetti for helping me during the realization of this work. A special thanks goes to PhD student Khrystyna and prof. Marco Armandi, for supporting me constantly during the whole period.

To my friends in Turin, thank you for making these years unforgettable and easier. I consider myself very lucky to have found people like you. A special thanks goes to Caterina, for being my rock and my guidance during the first year, allowing me to get in touch with so many wonderful people. I’ll always remember you for your generosity and your kindness.

To my friends and ex-roommates Valentina and Janka, thank you for making my Erasmus much more special and enriching. You’ve been like sisters to me during that time, and I hope we can reunite soon.

A special thanks goes to Antonio, Can, Mahdi and Masha for the unforgettable moments we spent together in the residence. Thank you for keeping me company during those days and showing me how beautifully we can all get along, no matter what our origin is. I’ll never forget our evening teas, the Turkish breakfasts, and the Iranian dishes.

Maha Maimi